EVALUATING THE UTILITY OF AN ATMOSPHERIC PRESSURE CHEMICAL IONIZATION MASS SPECTROMETER FOR DETECTING ORGANIC PEROXIDES DURING BETA-PINENE OZONOLYSIS EXPERIMENTS

Amanda Jameer

A THESIS SUBMITTED TO

THE FACULTY OF GRADUATE STUDIES

IN PARTIAL FULFILLMENT OF THE REQUIREMENTS

FOR THE DEGREE OF

MASTER OF SCIENCE

GRADUATE PROGRAM IN CHEMISTRY

YORK UNIVERSITY

TORONTO, ONTARIO

OCTOBER 2014

Acknowledgements

I would like to express my great appreciation to Dr. Donald R. Hastie for his guidance and support during the planning and development of this project. I am grateful for his patience and understanding through the progression of this project. I would also like to thank Dr. Jochen Rudolph and Dr. Robert McLaren for being on my supervisory committee. I appreciate the valuable feedback they provided me throughout this project. Additionally, I would like to extend my thanks to Dr. Mark Gordon for being on my exam committee.

I wish to acknowledge help from past and current members from Dr. Donald R. Hastie's group (Zoya Dobrusin and Merhnaz Sarrafzadeh). Their willingness to help me in the lab was much appreciated. My grateful thanks are also extended to members of Dr. Jochen Rudolph's group (Christine Facca, Marina Saccon, Anna Kornilova and Yasamin Hassani) and Dr. Robert McLaren's group (Zoe Davis and Ibraheem Nuaaman) for their advice and support. Additionally, I would like to thank Dr. John Kinrade for mentoring me while doing my project and Greg Koyanagi for his help and guidance while working in the lab. I am especially thankful for the assistance and valuable support from Carol Weldon from Center for Atmospheric Chemistry. I wish to acknowledge NSERC, Enbridge Inc., the Charles Hantho and Harold Schiff foundations for providing financial support during my studies at York University.

Finally, I would like to thank my family and friends for their understanding, support and encouragement throughout my study.

Abstract

The intent of this study was to use a positive-ion atmospheric pressure chemical ionization mass spectrometer ((+) APCI-MS/MS) to detect organic peroxide products formed during β-pinene ozonolysis experiments. Detection was based on utilizing the neutral-loss scan (NLS) analysis mode of the APCI-MS/MS to observe ion signals exhibiting unique mass losses of 34 u. This mass loss was considered exclusive to protonated organic peroxides containing a hydroperoxy moiety. Given this observation, the NLS analysis mode was used to selectively detect organic peroxides formed during β-pinene ozonolysis experiments. Overall, six organic peroxide structures were proposed. Further product-ion scan analysis on the six proposed structures revealed additional unique mass losses of 32 u and 62 u that could be use in combination with 34 u NLS analysis to selectively detect organic peroxides. The results from this study can assist in ascertaining organic peroxide contribution to secondary organic aerosol for future ozonolysis experiments.

Table of Contents

List of Tables

List of Figures

List of Abbreviations and Acronyms

APCI	Atmospheric pressure chemical ionization
CBI	Criegee biradical intermediate
CE	Collision energy
CEM	Channel electron multiplier
CH$_4$	Methane
CH$_3$OH	Methanol
CI	Chemical ionization
CID	Collision induced dissociation
CIMS	Chemical ionization mass spectrometry
CO	Carbon monoxide
CO$_2$	Carbon dioxide
DC	Direct current
EI	Electron ionization
eV	Electron volt
g	Grams
ΔG	Change in free energy
GB	Gas phase basicity
ΔH	Change in enthalpy
H$^+$	Proton
HO	Hydroxy radicals
HO$_2$	Hydroperoxyl radicals
H$_2$O	Water

H_2O_2	Hydrogen peroxide
HPLC	High performance liquid chromatography
kJ	Kilojoules
ln	Natural logarithm
M	Neutral molecule
M^+	Molecular ion
MFC	Mass flow controller
MFM	Mass flow meter
MHP	Methyl hydroperoxide
MS/MS	Tandem mass spectrometry
m/z	mass to charge ratio
N_2	Nitrogen
NLS	Neutral loss scan
nm	Nanometer
NO	Nitrogen monoxide
NO_x	Summation of NO and NO_2
NO_2	Nitrogen dioxide
NO_3	Nitrate radicals
O_2	Oxygen
O_3	Ozone
PA	Proton affinity
Pa	Pascals
PAA	Peroxyacetic acid
ppm	part-per-million
q	Radio frequency only quadrupole

Q   Quadrupole

RF   Radio frequency

RO$_2$ Peroxy radicals

ΔS$^\circ$ Standard change in entropy

SCI   Stable Criegee intermediate

SIM   Selected ion monitoring

SO$_2$ Sulphur dioxide

SOA   Secondary organic aerosol

SRM   Selected reaction monitoring

T   Temperature

τ   Effective residence time

TDLAS   Tunable diode laser absorption spectroscopy

TIC   Total ion count

u   Atomic mass units

VOC   Volatile organic compounds

1. Introduction to Organic Peroxides

This study focused on detecting organic peroxides (mainly organic hydroperoxides and peroxy acids) since they are important compounds in the natural atmosphere. These compounds have an impact on the radical chemistry of the atmosphere and may play a role in secondary organic aerosol formation. Considering this, several methods have been employed for organic peroxide detection. A review of these detection methods reveals the complications associated with organic peroxide detection. For this reason, this study looked into using mass spectrometric analysis for organic peroxide detection.

1.1. Introduction to Organic Peroxide Formation

It is of great interest to study how both biogenic (originating from plants) and anthropogenic (originating from human activities) disturbance affects the troposphere. Of particular importance in atmospheric research is the resultant chemical composition of the troposphere after biogenic or anthropogenic perturbation. Moreover, the chemical composition at the trace level is largely controlled by the presence of various oxidants in the troposphere (Reeves and Penkett, 2003). These oxidants include nitrate (NO_3), hydroxyl (HO), hydroperoxyl (HO_2) and peroxy (RO_2) radicals and ozone (O_3) (Lee et al., 2000). The presence of these oxidants help determine the lifetime of many biogenic and anthropogenic pollutants such as methane (CH_4) (Lee et al., 2000 and Reeves and Penkett, 2003). In the troposphere, HO radicals are the most important oxidant arising from the photolysis of O_3 (Lee et al., 2000). Aside from photolysis, HO radicals are regenerated through the photolysis of hydrogen

peroxide (H_2O_2) and organic hydroperoxide (ROOH) (Reaction 1.1 to 1.2) (Jacobs, 1999 and Lee et al., 2000).

$$H_2O_2 + h\nu \rightarrow 2\ HO \qquad\qquad\qquad \text{Reaction 1.1}$$

$$ROOH + h\nu \rightarrow RO + HO \qquad\qquad\qquad \text{Reaction 1.2}$$

H_2O_2 is the main gas-phase hydroperoxide produced through the self-reaction of HO_2 radicals in the atmosphere (Reaction 1.3) (Lee et al., 2000 and Crounse et al., 2006). However, organic hydroperoxides are generally formed in the atmosphere through the oxidation of volatile organic compounds (VOC) with either O_3 or HO radicals. Reaction 1.4 to 1.6 shows the general reaction for organic hydroperoxide formation from HO radicals with VOC (represented by RH), while O_3-initiated organic hydroperoxide formation is discussed in greater detail in Section 3.3.

$$HO_2 + HO_2 \rightarrow H_2O_2 + O_2 \qquad\qquad\qquad \text{Reaction 1.3}$$

$$RH + HO \rightarrow R + H_2O \qquad\qquad\qquad \text{Reaction 1.4}$$

$$R + O_2 + M \rightarrow RO_2 + M \qquad\qquad\qquad \text{Reaction 1.5}$$

$$RO_2 + HO_2 \rightarrow ROOH + O_2 \qquad\qquad\qquad \text{Reaction 1.6}$$

The most dominant organic hydroperoxide in the atmosphere is methyl hydroperoxide (MHP) primarily produced by the oxidation of CH_4 with HO radicals (Jackson and Hewitt, 1999 and Lee et al., 2000). However, higher order organic hydroperoxides can form through reactions 1.4 to 1.6 if VOC in the atmosphere contain more than one carbon. Table 1.1 adopted from Jackson and Hewitt (1999) and Lee et al., (2000) lists other organic hydroperoxides

identified in the atmosphere, that are formed from VOC containing more than one carbon within its structure. For instance, ethyl hydroperoxide is formed from HO-initiated oxidation of ethane (Lee et al., 2000). Organic peroxy acids (RC(O)OOH) like peroxyacetic acid, forms by HO_2 radicals reacting with acylperoxy radicals (RC(O)O$_2$) as oppose to peroxy radicals (Kroll and Seinfeld, 2008). The formation of acylperoxy radicals originates from HO-inititated oxidation of hydrocarbons containing a carbonyl functional group like acetone or acetaldehyde (Jacobs, 1999 and Lee et al., 2000). Reactions 1.7 to 1.9 illustrate how the oxidation of acetaldehyde can form the acylperoxy radical and peroxyacetic acid.

Table 1.1: Organic peroxides identified in the atmosphere

Peroxide	Chemical Formula
Hydroxymethyl hydroperoxide	$HOCH_2OOH$
Ethyl hydroperoxide	CH_3CH_2OOH
Hydroxyethyl hydroperoxide	$CH_3CH(OH)OOH$
Hydroxypropyl hydroperoxide	$CH_3CH(OH)CH_2OOH$
Peroxyacetic acid	$CH_3C(O)OOH$

$$CH_3CH(O) + HO \rightarrow CH_3C(O) + H_2O \qquad\qquad \text{Reaction 1.7}$$

$$CH_3C(O) + O_2 + M \rightarrow CH_3C(O)OO + M \qquad\qquad \text{Reaction 1.8}$$

$$CH_3C(O)OO + HO_2 \rightarrow CH_3C(O)OOH + O_2 \qquad\qquad \text{Reaction 1.9}$$
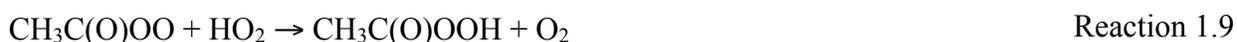
The peroxides shown in Table 1.1 originate from hydrocarbons containing 2 to 3 carbons within its structure. However, studies have shown that additional sources of organic hydroperoxides can arise from biogenic hydrocarbon oxidation (Docherty et al., 2005, Heaton et al., 2007, and Reinnig et al., 2009). This is pivotal since it is estimated that biogenic hydrocarbon emissions dominate over anthropogenic emissions (Yu et al., 1999). An important class of biogenic hydrocarbons capable of forming organic hydroperoxides and peroxy acids are monoterpenes ($C_{10}H_{16}$). According to Lee and coworkers (2006), these compounds are emitted from conifers as well as broad-leaved trees. Moreover, Docherty and coworkers (2005) stated that monoterpene emissions account for approximately 10 % of the total global biogenic hydrocarbon emissions. A great detail of research has focused on α- and β- pinene since these two monoterpenes constitutes a large portion of global monoterpene emissions (Jenkin et al., 2000 and Jenkin, 2004).

1.2. Relation to Secondary Organic Aerosol

Aside from being a reservoir for HO, HO_2 and RO_2 radicals, organic hydroperoxides may play role in secondary organic aerosol formation (SOA) (Heaton et al., 2007 and Reinnig et al., 2008). Studies on SOA formation and composition are widely found in the atmospheric science literature owing to its potential impacts on human health and global climate (Heaton et al., 2007 and Kroll and Seinfeld 2008). A precursor to SOA formation is the gas-phase

oxidation of VOC in the atmosphere. Generally, VOC oxidation can lead to products with sufficiently low vapour pressure. As a result, lower vapour pressure products can contribute to SOA by forming new particles or by condensing onto existing particles (Kroll and Seinfeld, 2008 and Reinning et al., 2009). Despite the abundance of atmospheric literature, SOA formation and composition continues to be poorly understood (Kroll and Seinfeld, 2008). However, recent modelling studies have estimated that organic peroxides (organic hydroperoxides and peroxy hemiacetals) might be a major component of SOA (Jenkin, 2004 and Reinnig et al., 2008 and 2009). For example, during α- and β- pinene ozonolysis experiments, bulk peroxide analysis showed that organic peroxides contributed to approximately 47 and 85 % of SOA mass formed respectively for each reaction (Docherty et al., 2005). Furthermore, Heaton and coworkers (2007) have suggested that further reactions of organic peroxides can form higher molecular weight dimers and oligomers. These compounds are suspected to be better candidates for new particle formation in comparison to other commonly found oxidative species like carboxylic acids during monoterpene oxidation experiments (Heaton et al., 2007).

2. Methods for Hydrogen Peroxide and Organic Peroxide Detection

2.1. Previous Detection Methods

Several techniques have been used to detect these compounds in ambient air samples. A majority of these methods either employ spectrometric techniques or extensive sample treatment coupled with chromatography. Earlier methods looked at measuring hydrogen peroxide (H_2O_2) using a colorimetric technique. For example Bufalini and coworkers (1975) measured H_2O_2, a resultant product from formaldehyde photo-oxidation, by forming a coloured complex using titanium (IV) and 8-quinilinol as colorimetric reagents. This paper expanded on Purcell and Cohen (1967) original work on H_2O_2 detection using kinetic colorimetry. However, this technique suffered from both chemical and physical interferences. For instance, compounds like peroxyacetic acid (PAA) and O_3 produce a coloured complex similar to that produced by H_2O_2 under the same experimental conditions. Moreover, other compounds like MHP, ethyl hydroperoxide, n-butyl hydroperoxide, $tert$-butyl hydroperoxide and peroxyacetylnitrate also produced a coloured complex similar to H_2O_2 even though the response time was slower than that of H_2O_2 under the same experimental conditions. Similarly, Bufalini et al., (1975) found that O_3 produced from the presence of part-per-billion levels of NO_x, produced a coloured complex similar to that of H_2O_2. Consequently, the chemical interference caused by compounds other than H_2O_2 inhibited the selective detection of H_2O_2. Although a total oxidant concentration could be obtained by this method, there would be no way to distinguish each compound from each other. Further compounding this problem was the rate at which the coloured complex formed. Purcell and Cohen (1967) observed colour complexes forming at different rates under the same experimental conditions. For instance, Purcell and Cohen (1967)

calculated the colorimetric half-life for different oxidants. Under the same experimental conditions, H_2O_2 formed a coloured complex immediately yielding a short half-life while ethyl hydroperoxide had a colorimetric half-life time of 50 minutes. Aside from chemical interferences, colorimetric techniques generally suffer from issues like visible light scattering especially in the presence of atmospheric particulates (Lee et al., 2000).

Spectrometric methods continued to improve detection by employing chemiluminescence techniques. One of the first chemiluminescence methods reported by Kok et al., (1978) utilized adsorbing coils and impingers to extract and concentrate H_2O_2 into aqueous phase during ambient sampling. Subsequently, H_2O_2 in the aqueous phase oxidized luminol in the presence of copper (II) to produce a complex that emitted at a wavelength of 450 nanometers (nm). Another chemiluminescence method described by Jacob and Klockow (1992) used peroxyoxylate to measure H_2O_2 in a marine atmosphere. Unlike the previous method, this method used a cool glass tube to trap H_2O_2 and water in the ice phase before melting and reacting with peroxyoxylate. This prevented analytical issues such as inlet loss and production of H_2O_2 by O_3 on the surface of impingers (Lee et al., 2000). However, both chemiluminescence methods only identified and quantified H_2O_2.

Conversely, early fluorometric analysis was able to detect and measure both H_2O_2 and organic hydroperoxides simultaneously. For instance, Lazrus et al., (1986) utilized an automated two-channel set-up where one channel measured H_2O_2 and organic hydroperoxides and the second channel measured just organic hydroperoxides. To accomplish this, both channels were treated with the enzyme peroxidase to produce a fluorescent dimer detected at an excitation wavelength of 400 nm; the second channel was pre-treated with catalase, an enzyme that selectively destroyed H_2O_2. However, it was determined that catalase was not as selective

since additional experiments with selected organic hydroperoxides revealed a slight reaction to MHP (Lazrus et al., 1986). Circumventing this analytical issue required Lazrus and coworkers (1986) to add sufficient catalase to react all but 3% of H_2O_2 within an aqueous sample. Consequently, this results in a level of uncertainty in determining H_2O_2 especially if organic hydroperoxide concentration is higher than H_2O_2 concentration (Lee et al., 2000)

Eventually, fluorometry was used in conjunction with chromatographic techniques. Kok et al. (1995) successfully detected and measured H_2O_2, hydroxymethyl hydroperoxide, peroxyformic acid, MHP, and PAA in aqueous solution. Compounds were successfully separated using high performance liquid chromatography (HPLC) then derivitized with peroxidase. The resultant fluorescent dimers were detected using a fluorescence detector. Identification of each compound was based on a comparison of elution times between previously analyzed standards and aqueous samples under the same conditions. Since there are only a handful of commercially available organic peroxide standards, some standards had to be synthesized, purified and standardized for quantitative use (Kok et al., 1995).

Additionally, tunable diode laser absorption spectroscopy (TDLAS) has been used to provide on-line determination of H_2O_2. Unlike previous methods described above, measurements are performed in the gas-phase and do not require pre-treatment. For example, Mackay et al. (1990) used this method to obtain a diurnal profile for H_2O_2. However, instrument calibration was achieved by utilizing permeation devices, which proved to be problematic because of temperature variations (Mackay et al., 1990). Despite a shift to an on-line approach, this method was specific to H_2O_2 and provided no information regarding organic peroxides.

Alternatively, mass spectrometry is a technique that could provide fast on-line analysis for organic peroxides. Generally, it provides information regarding the molecular weight of species and depending on the type of mass spectrometer, can provide structural information of a compound. Unlike colorimetric and fluorometric methods, samples to be analyzed do not need to be extracted into solution and treated with colorimetric or derivitizing reagents for detection. Furthermore, mass spectrometry is not affected by organic peroxide solubility in different solvents or the ability to separate a mixture of different organic peroxides whereas HPLC analysis relies heavily on these attributes. Lastly, TDLAS is only capable of measuring H_2O_2 and at best can discriminate between H_2O_2 and organic hydroperoxides when paired with a similar experimental set-up as the one described by Lazrus et al., (1986) (Weinstein-Lloyd et al., 1998). On the other hand, mass spectrometry can detect a wide range of products depending on the type of mass spectrometer utilized. Mass spectrometry simply requires samples to be ionized before subsequent analysis and detection. An array of ionization techniques is available in mass spectrometry and is normally selected based on the physio-chemical properties of the sample to be analyzed.

Mass spectrometry techniques have already been employed to detect organic peroxides during ambient or laboratory studies. For example Crounse et al., (2006) used chemical ionization mass spectrometry (CIMS) to detect H_2O_2 and PAA during airborne observations. Detection was accomplished by chemically ionizing both compounds with CF_3O^- ions to form a cluster. Similarly, CIMS was used by Reinnig et al., (2009) to identify and characterize organic hydroperoxide and peroxy acid structures generated by gas-phase ozonolysis of both monoterpenes and sesquiterpenes. Their detection was achieved by chemically ionizing formed products with protonated water ions (H_3O^+) (Reinnig et al., 2009). Collectively, these methods

show that mass spectrometry can provide fast on-line analysis for identification and characterization of unknown organic peroxides.

2.2. The Current Project

The aim of this project is to expand on chemical ionization methods published in the scientific literature (Baker et al., 2001, Rondeau et al., 2003, Crounse et al., 2006, Heaton et al. 2007, and Reinnig et al., 2009) to develop a technique for organic peroxide detection. Specifically, a positive-ion atmospheric pressure chemical ionization mass spectrometer ((+) APCI-MS/MS)) is utilized to evaluate its ability to detect organic peroxides formed during gas-phase ozonolysis experiments of β-pinene inside York University's smog chamber. Establishing a technique requires an understanding of the ion-molecule chemistry occurring inside the instrument during on-line analysis and evaluating various operational modes for the (+) APCI-MS/MS. Subsequently, knowledge gained will be applied to smog chamber ozonolysis experiments to selectively detect organic peroxides. Selective detection is beneficial since instrument responses relating to organic peroxides can be isolated from other isobaric compounds to aid in structure elucidation. As a result, structure elucidation can assist in understanding chemical transformations of monoterpenes in the atmosphere.

3. Sample Ionization for Mass Spectrometry

3.1. Ionization Techniques for Mass Spectrometry

Mass spectrometry analysis requires samples to be ionized before detection. A variety of ionization techniques can be employed to ionize samples. Ionization techniques are generally based on the amount of internal energy transferred during the ionization process and the physico-chemical properties of the sample (de Hoffmann and Stroobant, 2007). For example, electron ionization (EI) is a commonly used ionization technique in organic chemistry where a neutral sample absorbs energy after interacting with an ionizing electron (70 eV). When enough energy is absorbed, an electron is ejected from the analyte to produce a molecular ion ($M^{+\cdot}$) in the mass spectrum. Since most organic molecules require approximately 10 eV for ionization (de Hoffmann and Stroobant, 2007), the excess energy can induce excessive fragmentation in the ion source. As a result, the EI technique can fail to produce intact molecular ions. Furthermore, the mass spectrum will predominately display fragments of the molecular ion making it difficult to elucidate the molecular structure. Since organic compounds like organic peroxides contain a weak peroxy bond (O-O), EI is generally an inadequate ionization technique for its ionization and subsequent identification.

3.1.1. Chemical Ionization

Alternatively, chemical ionization (CI) is a "softer" ionization technique compared to EI, where analyte ions are produced with little excess energy. As a result, the mass spectrum displays less fragmentation in comparison to EI and the analyte ion can be detected. In CI, target neutral molecules (M) are ionized through a series of collisions with reagent ions present

in the ion source. These ion-molecule collisions can result in a series of reactions that include proton transfer, hydride abstraction, adduct formation and charge transfer. Proton transfer is the most common ion-molecule reaction to occur in the ion source resulting in the formation of a protonated analyte molecule having the form $[M + H]^+$ (Reaction 3.1.1).

$$M + RH^+ \rightarrow [M + H]^+ + R \quad \Delta H_{rxn}° = - \Delta PA \quad GB = -\Delta G_{rxn}° \qquad \text{Reaction 3.1.1}$$

During a proton transfer reaction, reagent ion RH^+ donates a proton to a neutral molecule (M), forming a $[M + H]^+$ ion. This reaction is analogous to an acid-base reaction where reagent ions (RH^+) and the neutral molecule (M) are considered a Brönstead acid (proton donor) and Brönstead base (proton acceptor), respectively. Furthermore, the ability for Reaction 3.1.1 to proceed as written is dependent on the proton affinity (PA) and gas-phase basicity (GB) for both species. PA is defined as the negative enthalpy change for the protonation reaction described by Reaction 3.1.1. On the other hand, GB is defined as the negative change in Gibbs free energy for Reaction 3.1.1. While PA indicates whether heat is released (exothermic) or absorbed (endothermic) during a reaction, GB indicates whether the reaction can be spontaneous under specific conditions. Ultimately, these two thermochemical parameters are related through the expressions shown in Equations 3.1.1 and 3.1.2 (Gal et al., 2001). Proton transfer will occur as long as the PA and GB of the target neutral molecule (M) are higher than the PA and GB of the reagent ion (RH^+).

$$\Delta G_{rxn}° = \Delta H_{rxn}° - T \Delta S° \qquad \text{Equation 3.1.1}$$

GB = PA - T $\Delta S°$ Equation 3.1.2

In the event that the PA of a neutral molecule (M) and the reagent ion (RH^+) are similar, adduct formation occurs as opposed to proton transfer (Reaction 3.1.2) (de Hoffmann and Stroobant, 2007). As a result, an adduct ion $[M + RH]^+$ will be observed in the mass spectrum instead of a protonated molecule $[M + H]^+$. This association reaction is also commonly considered as a form of gas-phase solvation (de Hoffmann and Stroobant, 2007).
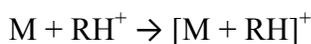
M + RH^+ → $[M + RH]^+$ Reaction 3.1.2

3.1.2. Protonation of Target Neutral Molecules

The previous section discussed thermochemical quantities governing the gas-phase protonation described by Reaction 3.1.1. However, it is noteworthy to discuss parts of the target neutral molecule (M) where a proton can attach. Although the focus is not to discuss this subject in great detail, general knowledge of target neutral molecule's basic sites for proton attachment is useful for this project. According to Bouchoux (2007), proton transfer reactions can result in changes like bond weakening or strengthening depending on the attachment site. Therefore knowledge of basic sites on target neutral molecules will assist in the interpretation of mass spectra acquired in this project. Since organic peroxides are the primary focus of this project, proton transfer to these target neutral molecules are only considered in this section.

Organic peroxides contain numerous basic sites for proton attachment depending on the chemical structure. Using the general structure of organic peroxide shown in Figure 3.1, the peroxy bond (-O – O-) provides a basic site for proton attachment. The two oxygen atoms

comprising the peroxy bond contain two lone electron pairs not shared by any atom within the organic peroxide structure. This results in an electron rich area within the organic peroxide structure susceptible to chemical reactions like proton transfer. During proton transfer, an electron is transferred from the lone pair on either oxygen atom to the incoming proton to form a chemical bond (Bouchoux 2007).
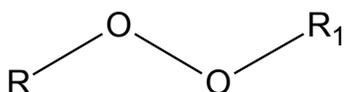
Figure 3.1: General structure for an organic peroxide. R and R_1 represent carbon chains which may contain other functional groups.

Aside from the peroxy bond, organic peroxides can contain additional basic sites for proton attachment depending on the nature of R and R_1 shown in Figure 3.1. For example, R and R_1 structures containing carbonyl (-C=O) or alcohol (-OH) groups are basic sites for proton attachment. Similar to the peroxy bond, the C=O and OH groups are electron rich due to the presence of two lone electron pairs on the oxygen atom. However, the presence of a double bond (two bonding electron pairs) between the carbon and oxygen of a carbonyl group, contributes to the electron rich region surrounding the carbonyl group. Additionally, R and R_1 can contain a phenyl ring group (-C_6H_5). Phenyl ring groups do not contain true double bonds since electrons are delocalized. Given this, electrons cannot be transferred to the incoming proton to form a chemical bond. However, theoretical and experimental studies done by Rondeau et al., (2008) showed that organic peroxides containing a phenyl group can protonate within the phenyl ring. Considering this study, the presence of a phenyl group is considered an additional basic site for proton attachment during this project.

3.1.3. Atmospheric Pressure Chemical Ionization (APCI)

Since the resultant analyte ion from CI is dependent on the collisions between reagent ions RH^+ and neutral molecules M, the pressure inside the source must be sufficiently high to promote collisions. For this reason, CI is normally conducted under higher pressure conditions in comparison to EI. In EI, ionization is normally performed at 10^{-2} Pa while CI is performed at more than 100 Pa (de Hoffmann and Stroobant, 2007). APCI is an example of a CI method where the ionization is achieved under atmospheric pressure conditions to promote collisions between the reagent ions RH^+ and the neutral molecules M. Ionization is initiated by low-energy thermal electrons from either a beta source or a corona discharge (de Hoffmann and Stroobant, 2007 and Watson and Sparkman, 2007). The low-energy thermal electrons ionize the major components of the neutral reagent gas, which can in turn ionize the analyte through a series of ion-molecule reactions. As a result, these reactions produce both positive and negative ions. These reactions are discussed in detail in latter sections.

3.1.4. Ionization Reagent Selection for APCI

To promote ion-molecule reactions like proton transfer or adduct formation, an appropriate ionization reagent must be selected. The selection of an ionization reagent will depend on the nature of the ionization reagent and sample being analyzed. In APCI, the appropriate selection of an ionization reagent would result in the production of proton-rich ions from a neutral sample molecule through ion-molecule reactions. For example ammonia (NH_3) has a relatively high PA (Table 3.1) making it a good Brönstead base. To detect this neutral molecule in the positive-ion APCI mode, the ionization reagent selected must have a lower PA (strong Brönstead acid) to donate the proton to ammonia to form the ion NH_4^+ ($[M + H]^+$ ion).

Using Table 3.1 methane (CH_4), water (H_2O), and methanol (CH_3OH) can be used as an ionization reagent.

Additionally, the ionization reagent selected will affect the appearance of the acquired mass spectrum. The difference in mass spectrum appearance derives from the amount of excess energy transferred during the ionization process of the neutral molecule. In general, the amount of excess energy available is related to the difference in the proton affinity (ΔPA) between the neutral molecule and the ionization reagent **(Watson and Sparkman, 2007).** The greater the ΔPA, the more excess energy is available during the formation of the protonated molecule ([M + H]$^+$) **(Watson and Sparkman, 2007).** Consequently, the excess energy available can cause extensive fragmentation of the protonated molecule [M + H]$^+$. Since the ΔPA can influence the stability of the [M + H]$^+$ ion, this value along with PA must be taken into consideration when selecting an ionization reagent.

Table 3.1: Characteristics of selected ionization reagents for CI

Ionization Reagent	Proton Affinity of Ionization Reagent (kJ mol^{-1})
CH$_4$	551
H$_2$O	697
CH$_3$OH	762
NH$_3$	854
(CH$_3$)$_2$NH	921

[Watson and Sparkman, 2007]

4. Operation Mode for the APCI-MS/MS

4.1. Description of the APCI-MS/MS

The APCI-MS/MS used in this project consists of three main parts: (i) the ion source operated at atmospheric pressure that generates sample ions; (ii) a vacuum interface that allows the transfer of ions from the ion source to the mass spectrometer; and (iii) a high vacuum chamber that houses a quadruple ion guide (q_o), two mass analyzers (Q_1 and Q_3), a collision induced dissociation cell (CID) (q_2), and lastly a channel electron multiplier detector (CEM). Figure 4.1.shows a general schematic of the APCI-MS/MS design used in this project.
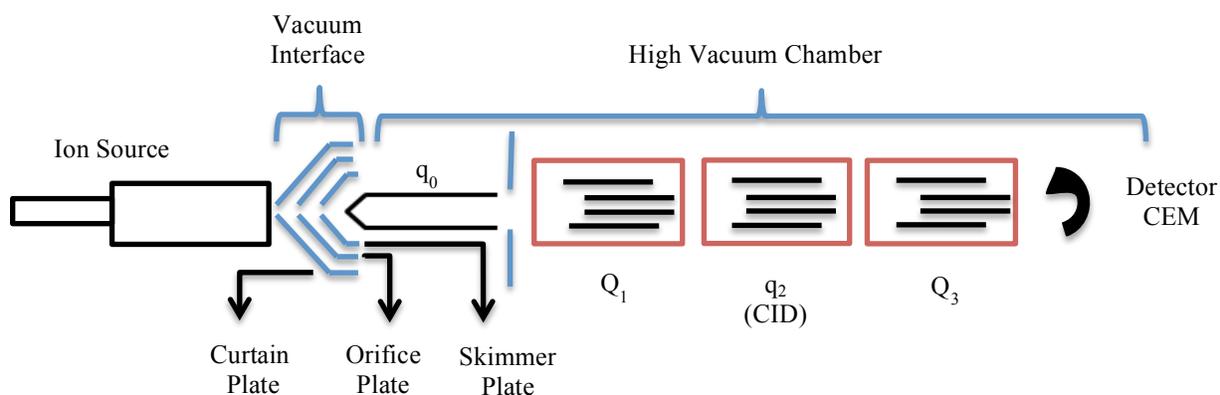
Figure 4.1: Detailed schematic of APCI-MS/MS

4.1.1. The APCI-MS/MS Ion Source

Figure 4.2 outlines the principle for the APCI ion source. The corona discharge needle emits a cloud of electrons ionizing the components of air surrounding the needle (N_2, O_2, H_2O, etc.). The initial ionization forms primary ions through the sequence of reactions (Proctor and Todd, 1983):

17

$$N_2 + e^- \rightarrow N_2^+ + 2e^- \hspace{4cm} \text{Reaction 4.1}$$

$$N_2^+ + 2N_2 \rightarrow N_4^+ + N_2 \hspace{4cm} \text{Reaction 4.2}$$

$$N_4^+ + H_2O \rightarrow H_2O^+ + 2N_2 \hspace{3.5cm} \text{Reaction 4.3}$$

$$H_2O^+ + H_2O \rightarrow H_3O^+ + OH \hspace{3.5cm} \text{Reaction 4.4}$$
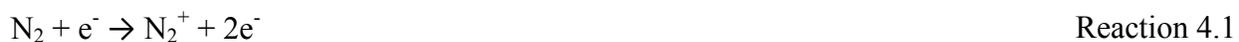
Since water (H_2O) is found in trace amounts of air and has the highest PA of all gases found in ambient conditions, the ions formed in the APCI ion source are predominately H_3O^+ and $(H_2O)_nH^+$ (if n is greater than 1) (Watson and Sparkman, 2007). Additional secondary ions can form if the analyte matrix is present in the gas phase. The secondary ions formed in the ion source act as the ionization reagent, which, in the positive ion mode, reacts further with neutral analyte through proton transfer or addition. Operating the ion source at atmospheric pressure ensures a large number of ion-molecule and molecule-molecule collisions that thermalizes the ions and ensures high reaction rates. The resultant gas-phase ions are then transferred to the mass analyzer through the use of differential pumping.

Analyte (M)
Flow

Curtain Plate

Skimmer

Ions

Purified Air

Corona Discharge

Orifice

(a)

Air

H_2O
N_2
O_2

H_2O H_3O^+

N_2^+ H_2O

N_{2}^{+} N_2

H_2O N_2

N_4^+

N_4^+ H_3O^+

To mass analyzer

Positively Charged

Plasma Region of Corona
discharge

(b)
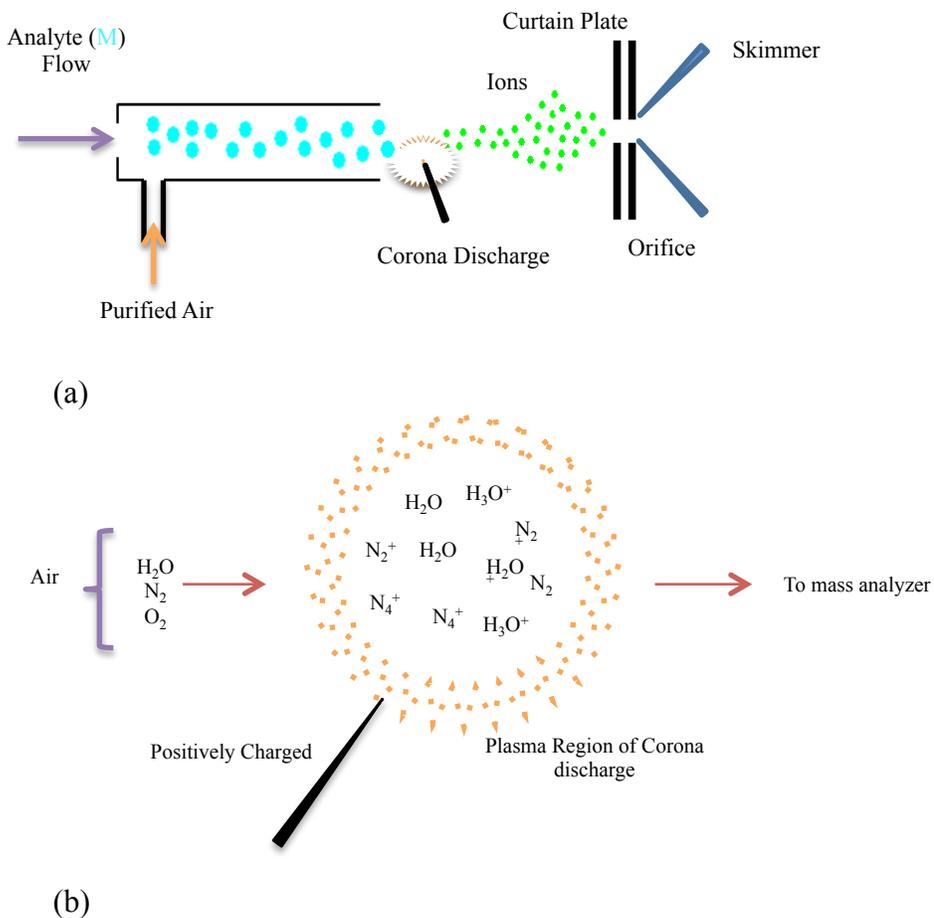
Figure 4.2: Diagram for the APCI-MS/MS ion source. (a) Shows an overall view while (b) shows a more detailed diagram of ionization within the plasma region of the corona discharge in the absence of sample. The components of air are ionized at atmospheric pressure

4.1.2. Vacuum Interface Region

After ionization, generated ions are drawn into the vacuum interface region by a potential gradient formed across the interface region. In addition to allowing sample ion transfer, the vacuum interface region separates the high pressure region of the ion source from the low pressure region of the vacuum chamber. The vacuum interface region is comprised of two regions known as the gas curtain interface and differentially pumped interface region. Figure 4.3 depicts a detailed diagram of the vacuum interface region. Ions entering into the gas

curtain interface encounter a flow of curtain gas (usually purified nitrogen). This curtain gas prevents sample, solvent and ambient air from entering the mass spectrometer. Additionally, gas phase ions collision with the curtain gas can effectively fragment weakly associated ions, commonly known as de-clustering. This region is at atmospheric pressure to help retain the stable ion-molecule products formed in the ion source.

After ion de-clustering, sample ions are transferred towards the differentially pumped interface by the pressure differential across the orifice plate. Additionally ion transmission is favoured by a voltage difference applied between the orifice plate and skimmer. This is the first low pressure region the sample ions encounter before they enter the high vacuum chamber containing the quadruples. This region is normally around 2.2 Torr and is maintained by a mechanical pump located outside the instrument. Sample ions enter the high vacuum chamber through an aperture in the skimmer cone.
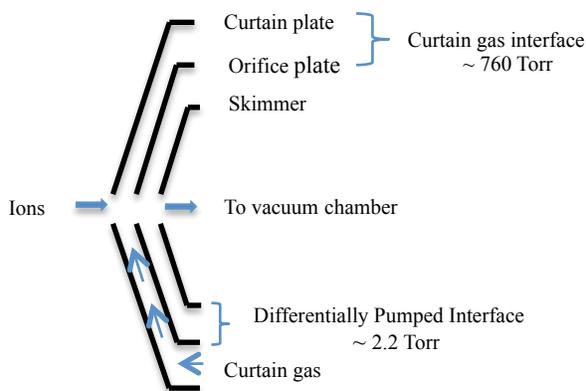
Figure 4.3: Detailed diagram of vacuum interface region

4.1.3. High Vacuum Chamber

After ion de-clustering in the vacuum interface, gas-phase ions enter the high vacuum chamber housing the quadrupoles. However, gas-phase ions have a tendency to disperse after leaving the ion source. This can result in a loss of ions between the ion source and the mass spectrometer. The APCI-MS/MS used in this experiment combats this issue by using a radio frequency (RF) ion guide quadrupole (q_0). The following sections outline the theory behind quadrupole operation. After passing through q_0, gas-phase ions encounter three sequential quadrupoles, Q_1, q_2, and Q_3. Q_1 and Q_3 are mass filters while q_2 is another ion guide. In addition to being an ion guide, q_2 can be used as a collision cell where target gas-phase ions are fragmented and analyzed by tandem mass spectrometry. Ultimately, the fate of gas-phase ions through each quadrupole will depend on the operation mode of the APCI-MS/MS.

4.1.4. Description of the Quadrupoles

The quadrupoles used in mass spectrometry are composed of four preferably hyperbolic but usually circular parallel metal rods, which, can be used to set up an electric field to control gas-phase ions. Figure 4.4 (a) and (b) depicts the geometry for the four quadrupoles along a X-Y and X-Z plane. This geometry can be used to make an ion guide, if radio frequency (RF) voltage is applied to the rods, and a mass filter if a RF and direct current (DC) voltage is applied.
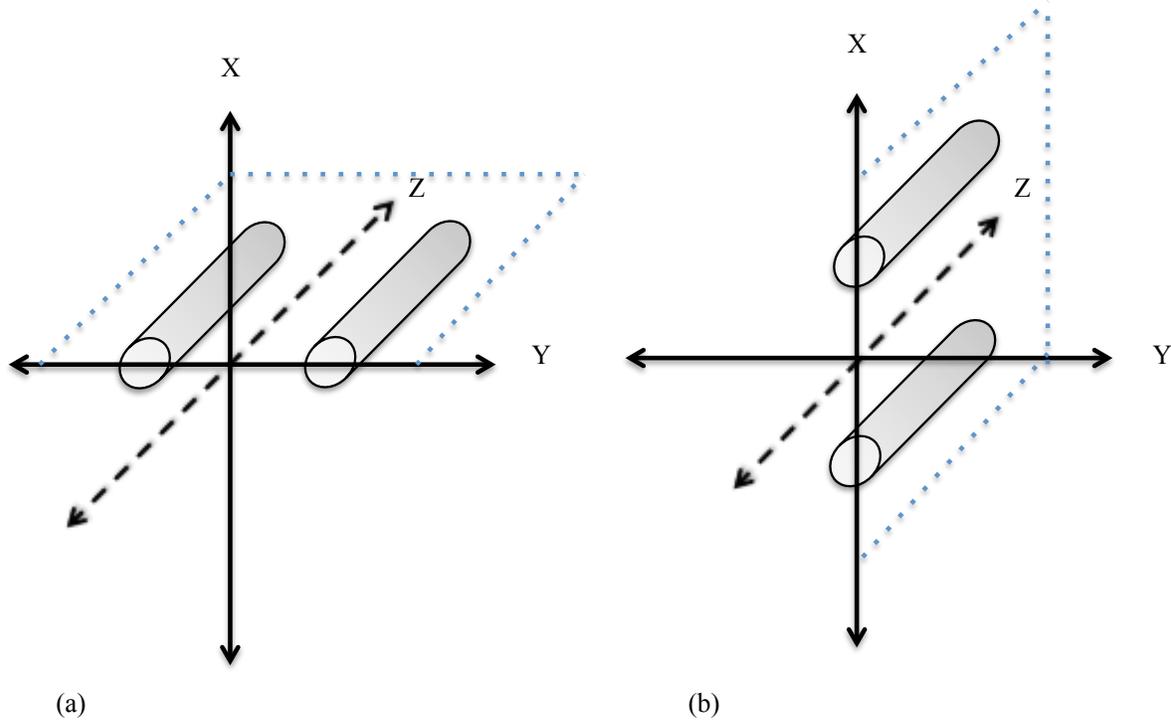
Figure 4.4: Diagram illustrating the position of the rods in three-dimensional space. Gas phase ions travel along the z-axis

4.1.4.1. Ion Guides

Consider first applying only an RF voltage to the rods depicted in Figure 4.4 (a) and (b). Using description presented by Miller and Denton (1986), the operation of ion guides (q_0 and q_2) is best visualized by describing the motion of gas-phase ions traveling along the z-axis in the X-Z and Y-Z plane as RF voltage is applied to each rod. The equations governing the motion of gas-phase ion through the ion guides is discussed in later sections.

When RF is applied to the rods, the rods along the x-axis will obtain a positive potential for half a cycle then acquire a negative potential for the other half of the cycle. When the two rods shown in Figure 4.4 (a) are positive, positively charged gas-phase ions will accelerate and focus towards the center of the two rods due to repulsion. On the other hand, a negative

potential acquired during the second half of the cycle results in positively charge gas-phase ions accelerating towards the rods and away from the center due to attraction. The rod potentials alternate to prevent the positive gas-phase ions from discharging itself on the rods. Although this describes gas-phase ion motion for the X-Z plane, this rationale can be applied to the rods along the y-axis and ion pathway along the Y-Z plane (Figure 4.4 (b)). Ultimately, the alternating rod potentials create an oscillating field to reduce the amount of dispersion while gas-phase ions travel through the ion guide quadrupoles (Watson and Sparkman, 2007).

4.1.4.2. Mass Filters

For the mass filter, each pair of rods in Q_1 and Q_3 has a DC potential supplied to it in addition to the applied RF voltage needed. Using Figure 4.4 (a) and (b), rods along the x-axis are subjected to a positive DC potential while rods along the y-axis are subjected to a negative potential. Figure 4.5 shows the superposing RF and DC potentials on opposing rod pairs.

When rod pairs lying along the x-axis are subjected to a positive DC voltage, heavier gas-phase positive ions traveling along the X-Z plane will move towards the z-axis while traveling through the quadrupole. Although rods along the x-axis experience negative potential due to the changing RF voltage, this change has a negligible affect on heavier gas-phase ions. On the other hand, RF voltages effects lighter gas-phase ions. Lighter ions experiencing a negative voltage will accelerate, collide with the rods, discharge, and become neutral. As a result, the rods along the x-axis as shown in Figure 4.4 (a) act as a high mass pass filter, allowing masses above a certain critical *m/z* value to pass (de Hoffman and Stroobant, 2007). Masses below that critical value will be filtered out. The same logic can be applied for rod pairs along the y-axis (Figure 4.4 (b)). Unlike the rod pairs shown in Figure 4.4 (a), rod pairs along

the y-axis have a negative DC voltage applied to each rod. Positive heavier gas-phase ions will move away from the z-axis and travel towards the negative rods without being effected by the RF voltage. Contrastingly, lighter gas-phase ions are focused towards z-axis especially when the positive cycle of the RF voltage is larger than the negative DC voltage. As a result, rod pairs lying along y-axis will act as a low mass pass filter, allowing certain masses below a critical m/z value to pass. For gas-phase ions to pass through both Q_1 and Q_3, the ions must be stable along both X-Z and Y-Z planes. This forms the basis of the quadrupole mass filter.

X rod pairs = + (U + V(cosωt)
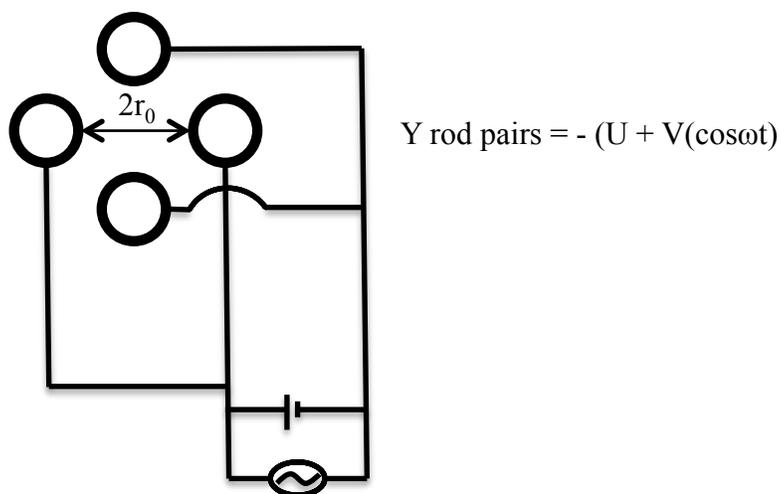
Y rod pairs = - (U + V(cosωt)

Figure 4.5: Illustration showing the superposing RF and DC potentials to opposing APCI-MS/MS rods. U and V are the magnitude of the DC and RF potential, respectively; r_0 is the distance from the z-axis; ω is the angular frequency for the RF potential; and t is time.

4.1.4.3. Equations of Motion for Mass Filters

As ions are travelling along the z-axis, the ion's motion through the quadrupoles can be described using a combination of Paul and Mathieu's equation described by Miller and Denton

(1986). These equations of motions can be found in Appendix A since the focus of this project was not to derive or solve these equations. However, these equations help establish a relationship between the x and y positions of gas-phase ions and time as ions travel along the z-axis. Essentially, as long as the x and y positions of gas-phase ions are less than r_0 (Figure 4.5), gas-phase ions can pass through the quadrupole without discharging against the rods. Using Paul and Mathieu's equation (Appendix A), x and y can be determined for any ion mass as a function of U (DC) and V (RF).

A diagram representing the stability areas for gas-phase ions along the x- and y-axis is shown in Appendix A along with a brief explanation. An enlarged diagram showing stability region in Figure A.3 is given in Figure 4.6. Changing from one *m/z* value to another causes a proportional multiplication of Equation A.3 and A.4 in Appendix A. Therefore, the triangular area shown in Figure A.3, will change from one mass to the other producing multiple proportional triangles as shown in Figure 4.6. Figure 4.6 is of great importance since it quantitatively shows how quadrupoles operate as mass filters and ion guides. This diagram shows values of *a* and *q* for which mass m_1, m_2, and m_3 are stable and will transmit through mass filter quadrupoles. Stable values of *a* and *q*, are represented by the area inside their respective triangle. Moreover, *a* and *q* values falling outside the portrayed triangles in Figure 4.6 are unstable areas and will result in an ion discharging itself against the rods.
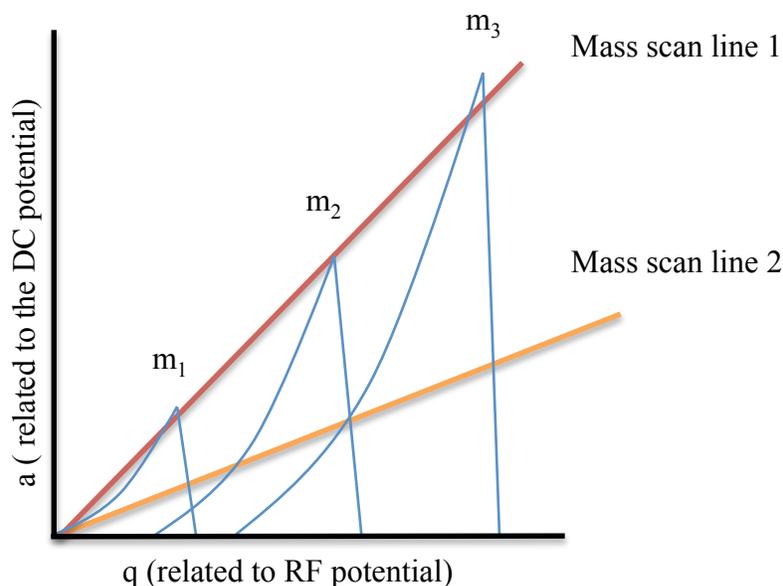
Figure 4.6: Schematic illustrating the stability for ions inside a quadrupole. The stability areas are a function of a (DC) and q (RF). Values of a and q where ions with mass m_1, m_2 and m_3 are stable inside a quadrupole, are represented by the area inside the triangle for each mass. Mass scan lines are obtained by changing the ratio of DC/RF by a fixed value.

Although different combinations of RF (q) and DC (a) will allow certain masses to be stable and transmit through the quadrupole, the APCI-MS/MS operates by changing RF and DC at a fixed ratio. Using Figure 4.6, changing the DC/RF by a fixed ratio restricts the instrument to a set of points along a straight line (mass scan line) (de Hoffmann and Stroobant, 2007). As a result, gas-phase ions where m_1, m_2, and m_3 have a and q values located on the mass scan line, will be stable and transmit through the quadrupole. Additionally, Figure 4.6 shows that lowering the DC/RF ratio can lower the quadrupoles' ability to separate gas-phase ions. This can be visualized hypothetically by considering mass scan line 1 and 2 in Figure 4.6. Using these two mass scan lines, it can be seen a quadrupole operating along mass scan line 1 can separate and transmit m_2 and m_3 gas-phase ions efficiently as opposed to mass scan line 2

where quadrupole operation eventually reaches a point where m_2 and m_3 can not be separated. This aspect is known as the resolving power for the quadrupoles. Overall, the APCI-MS/MS operates by changing the DC/RF at a fixed ratio and can detect sequentially a range of masses to ultimately generate a mass spectrum.

Additionally it is important to note that Figure 4.6 can be used to explain why all gas-phase ions are transmitted through an ion guide quadrupole. In the previous section, the RF-only mode for ion guides was discussed. Since there is no DC component ($a = 0$ in Figure 4.6 and Equation A.8), the mass scan line lies horizontally along the x-axis representing values of q (de Hoffmann and Stroobant, 2007). Therefore theoretically, all ions are stable and will transmit through the ion guide. However, this is not necessarily true since the horizontal line representing values of q in Figure 4.6 show that smaller ions become unstable as the RF increases.

4.1.4.4. Collision Cell

In addition to being an ion guide, q_2 can be used as a collision cell to perform tandem mass spectrometry analysis (MS/MS). During MS/MS experiments, precursor ions are selected in Q_1 and are allowed to fragment into smaller fragment ions (product ions) in q2. This is accomplished by introducing an inert gas (nitrogen or argon) into q_2 at a high enough pressure such that gas-phase ions entering q_2 will undergo collisions with the inert gas. The pressure introduced into q_2 of the APCI-MS/MS used in this experiment is approximately 8 mTorr. Since collisions with inert gas can cause product ions to scatter away from the z-axis, RF voltages applied to q_2 quadrupole help focus ions back towards the center of the quadrupole minimizing product-ion losses.

27

Similar to the previous discussion regarding gas-phase ion motion inside the quadrupoles, the focus of this project is not to describe the physical principals behind gas-phase fragmentation upon collision with an inert gas in detail. However, it is understood that during collision events, a portion of the gas-phase ion kinetic energy ($\frac{1}{2}\ m\mathrm{v}^2$) is converted to internal energy (Shukla and Futrell, 2000 and de Hoffmann and Stroobant, 2007). The amount of kinetic energy that can be converted to internal energy in a single collision event is described briefly in Appendix B. It is this conversion that drives the fragmentation of precursor ions to product ions. Additionally, the kinetic energy gained by gas-phase ions is related to the potential energy (zeV) available in the electric fields in the mass spectrometer (Watson and Sparkman, 2007). The equation describing this relationship can be found in Appendix B (Equation B.1). Essentially, Equation B.1 shows that increasing the potential difference causes an increase in gas-phase ion kinetic energy. As a result, more kinetic energy is available to convert to internal energy during collision events, which ultimately affects the degree of fragmentation of precursor ions.

Additionally, the degree of fragmentation depends on the potential energy (collision energy) experienced by the precursor ion before it enters q_2. Collision energy (CE) is expressed in electron volts (eV) units and can be adjusted on the APCI-MS/MS. The APCI-MS/MS can supply 5 to 40 eV to a precursor ion during MS/MS experiments. Appendix B briefly describes the relationship between CE and the amount of energy that can be converted to internal energy. Chiefly, increasing the CE voltage setting on the APCI-MS/MS causes an increase in gas-phase ion kinetic energy and increase in the amount of internal energy.

In this project, MS/MS experiments were carried out using a CE setting of 10 eV. This setting was selected since intact protonated molecules or adducts could not be identified in full

scan mass spectra due to extensive fragmentation. Since 1 eV is equal to 96.48 kJ mol^{-1}, an APCI-MS/MS setting of 10 CE may not be sufficient at fragmenting a precursor-ion after a single collision. This notion is valid when considering the center of mass equation (Equation B.2) in Appendix B and the energy required to break carbon – carbon bonds (bond energy ~ 350 kJ mol^{-1}), carbon – oxygen bonds (bond energy ~ 350 kJ mol^{-1}) and oxygen – oxygen bonds (bond energy ~ 188 kJ mol^{-1}) (Bach et al., 1996). In this case, multiple collisions can increase the internal energy and further drive precursor-ion fragmentation (Douglas, 1998). The RF capability of q_2 can promote multiple collisions within q_2 by reducing the dispersion of precursor-ions caused by collision events and focusing the ions towards the center of the quadrupoles.

4.1.5. Full and Tandem Mass Spectrometry Scan Modes

Tandem mass spectrometry (MS/MS) helps provide structural information for a precursor ion of interest. There are numerous different MS/MS experimental modes for the APCI-MS/MS. Table 4.1 summarizes the different MS/MS modes while Figure 4.7 provides a conceptual diagram for MS/MS experiments.

Table 4.1: Summary of APCI-MS/MS analysis modes used in the experiment

Analysis mode	Function of Q_1	Function of q_2	Function of Q_3	
Full Scan	Mass analyzer	Stabilize ions	Stabilizes ions	Overall scan without any collisions
Product-ion scan	Selects ion	Fragments selected ion	Mass analyzer	Fragmentation pattern for a specific ion
Neutral-loss scan (NLS)	Mass analyzer	Fragments selected ion	Mass analyzer Offset by a specific value from Q_1	Searching for molecules with specific mass loss
Selected reaction monitoring (SRM)	Selects precursor ion(s)	Fragments precursor ion(s)	Selects product ion(s)	Monitoring a selected ion pair
Selected ion monitoring (SIM)	Selects precursor ion(s)	Stabilizes ion(s)	Stabilizes ion(s)	Monitoring a selected ion

[Watson and Sparkman, 2007]
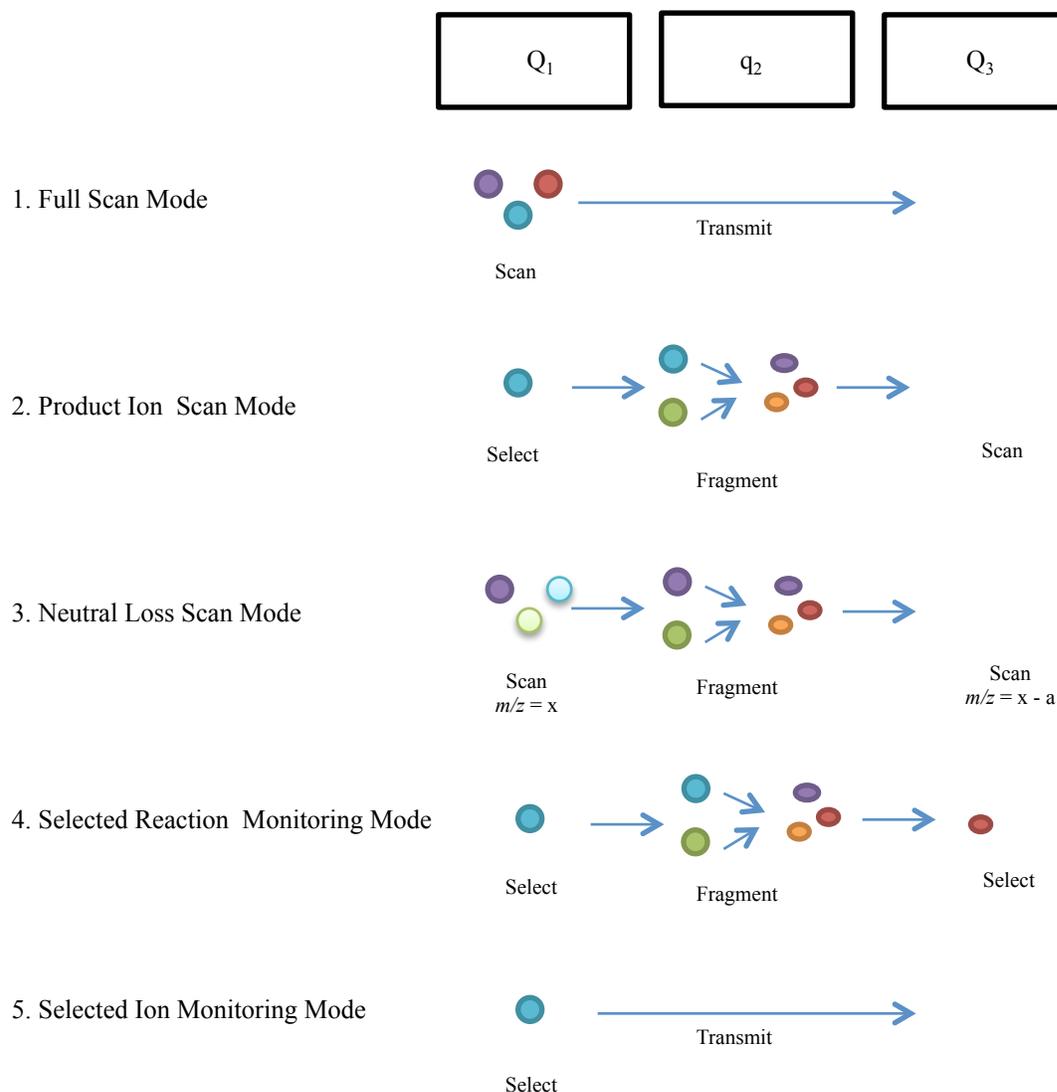
Figure 4.7: Conceptual diagram of different MS/MS experimental modes for the APCI-MS/MS

Full scan mode analysis is used to acquire an overall qualitative scan for a given range of m/z values. In general this spectrum produces intact ions since there are minimal collisions with neutral gas molecules to induce fragmentation. Once gas-phase ions are transmitted through q_0, Q_1 is set to scan a range of m/z ions ($10 - 300$) while q_2 and Q_3 are used as ion guides to stabilize gas-phase ion motion as they are transferred to and counted by the detector (CEM).

The full scan analysis mode can serve as a screening tool to determine ionization schemes and determine what ions to focus on for future mass spectrometry analysis. Figure 4.8 (a) shows an example of a spectrum acquired in the full scan analysis mode.
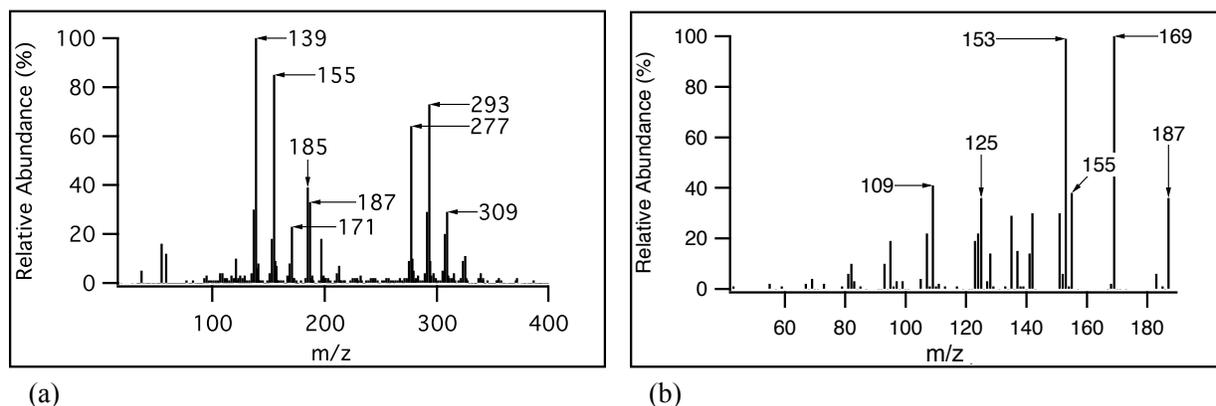
Figure 4.8: Example of spectra acquired using (+) APCI-MS/MS. Figure (a) represents a full scan mass spectrum acquired by setting the APCI-MS/MS to scan *m/z* ranges 10 – 300 while (b) represents a MS/MS spectrum illustrating the fragment ions of *m/z* 187 during a product-ion scan.

In contrast to full scan mode analysis, product-ion scan mode analysis is an MS/MS analysis mode where structural diagnostic information for a precursor ion can be obtained. As opposed to the full scan mode analysis only an ion with a specific *m/z* ratio is selected in Q_1. The precursor ion is allowed to pass into q_2, which act as a collision cell. In q_2 of the APCI-MS/MS used in this project, the precursor ion collides with nitrogen molecules to produce smaller product ions. The resultant product ions are then analyzed by Q_3, which is set to scan over a specific range (de Hoffmann, 1996). Structural information on the precursor ion may be obtained by examining the product ions produced in the collision cell. Figure 4.8 (b) depicts an example of a product-ion scan mass spectrum obtained during this project.

Comparatively, the neutral-loss scan (NLS) mode analysis can be used as a diagnostic tool like the product-ion scan mode analysis. However, this mode provides a convenient way to detect precursor ions that expel a common neutral fragment during collision events in the collision cell. To acquire a spectrum in this analysis mode, Q_1 and Q_3 are scanned at the same rate (de Hoffmann and Stroobant, 2007, and Watson and Sparkman, 2007). However, Q_3 is offset by some fixed m/z ($m/z = x - a$) value in comparison to Q_1 ($m/z = x$). Detection only occurs if a precursor ion exhibits a specific mass loss in the collision cell. For example, alcohols can be detected by a neutral loss of water (18 u). This analysis mode can offer a high degree of selectivity in comparison to a full scan mode analysis since only precursor ions with a specified mass loss will be detected and recorded.

Selected reaction monitoring (SRM) analysis mode is one of the most widely used modes in tandem mass spectrometry. This technique monitors the ion signal associated with the transition between a specific precursor and product ion (ion pair) during collision studies. This technique is usually performed after a product-ion scan since knowledge of product ions formed from a particular precursor ion is needed. During this analysis mode, a precursor ion is selected by Q_1, allowed to fragment in q_2, and the corresponding product ion is selected by Q_3. Ions selected by Q_1 are only detected if it produces a product ion selected by Q_3. Unlike the other tandem mass spectrometry analysis modes discussed above, both Q1 and Q_3 are not used for scanning although Q_3 can be set for multiple ions. Additionally, the absence of scanning allows for users to focus on a precursor and product ion over longer time intervals (de Hoffmann and Stroobant, 2007). As a result, increased sensitivity is achieved. The benefits of this type of analysis stem from the fact that multiple ion pairs can be analyzed simultaneously for long periods of time.

Lastly, selected ion monitoring (SIM) analysis mode is analogous to SRM analysis mode with the exception that SIM analysis mode detects target precursor ions. Precursor ions are selected in Q_1 and allowed to transmit through q_2 and Q_3. Similar to SRM analysis mode, sensitivity is achieved since the instrument can focus on select precursor ions as opposed to an array of precursor ions like full scan analysis mode. Additionally, multiple precursor ions can be selected by Q_1 and monitored simultaneously for longer durations.

4.1.6. Utility of Neutral Loss Scan Analysis (NLS)

One of the most useful methods for organic peroxide detection involved observing losses of 34 u (H_2O_2) during product-ion scan analysis. This loss was observed for organic peroxide compounds containing a hydroperoxy (organic hydroperoxide) or peroxy acid (organic peroxy acid) functional group. Since this loss was indicated as being characteristic for organic hydroperoxides and peroxy acids (Baker et al., 2001, Reinnig et al., 2008 and Reinnig et al., 2009), it was expected that selected detection for these compounds could be achieved by utilizing the NLS analysis mode of the (+) APCI-MS/MS. This analysis mode could be used as a "pre-screening" tool to isolate *m/z* ion signals representing organic hydroperoxides and peroxy acids.

Expected benefits of this analysis mode include a reduction in instrumental analysis time provided that there is prior knowledge about the types of functional groups present during the project. Prior knowledge circumvents performing product-ion scan analyses on all observed ion signals in the full scan mass spectrum. This would be imperative during ozonolysis experiments given the diverse types of oxidation products (i.e. carboxylic acids, ketones, aldehydes, etc.) formed during β-pinene/ozonolysis experiments.

Despite these expected benefits, a review of scientific literature showed that this mode was mainly used for qualitatively screening biological compounds (de Hoffmann and Stroobant, 2007). In the atmospheric science literature, only a few studies capitalized on the benefits of the NLS analysis mode. Dron et al., (2007) described using NLS analyses to screen for carboxylic acids in complex SOA by searching for neutral losses of methanol (32 u) after derivatization with boron trifluoride in a 14% methanol solution. Additionally, Williams and Perreault (2000) utilized NLS analysis to probe for neutral losses of nitrogen oxide (30 u) to selectively detect nitrated polycyclic aromatic compounds in a laboratory mixture of poly aromatic compounds.

Aside from these two studies, no other mass spectrometry application for SOA characterization has taken advantage of this analysis mode. However, it was apparent during this project that there could be wider applications for this analysis mode in atmospheric chemistry research as it was found to be useful for selective organic peroxide detection.

5. Ozonolysis Mechanism and Reaction Pathways

Since the primary focus was to observe organic peroxide formation during oxidation experiments, this project was designed to follow the chemistry facilitated by reactions with O_3. This chemistry allowed for reactions in the York University smog chamber to be conducted in a NO_x (NO and NO_2) free environment. The general schematic of alkene-ozonolysis is portrayed in Figure 5.1 (Finlayson-Pitts and Pitts Jr., 1999).
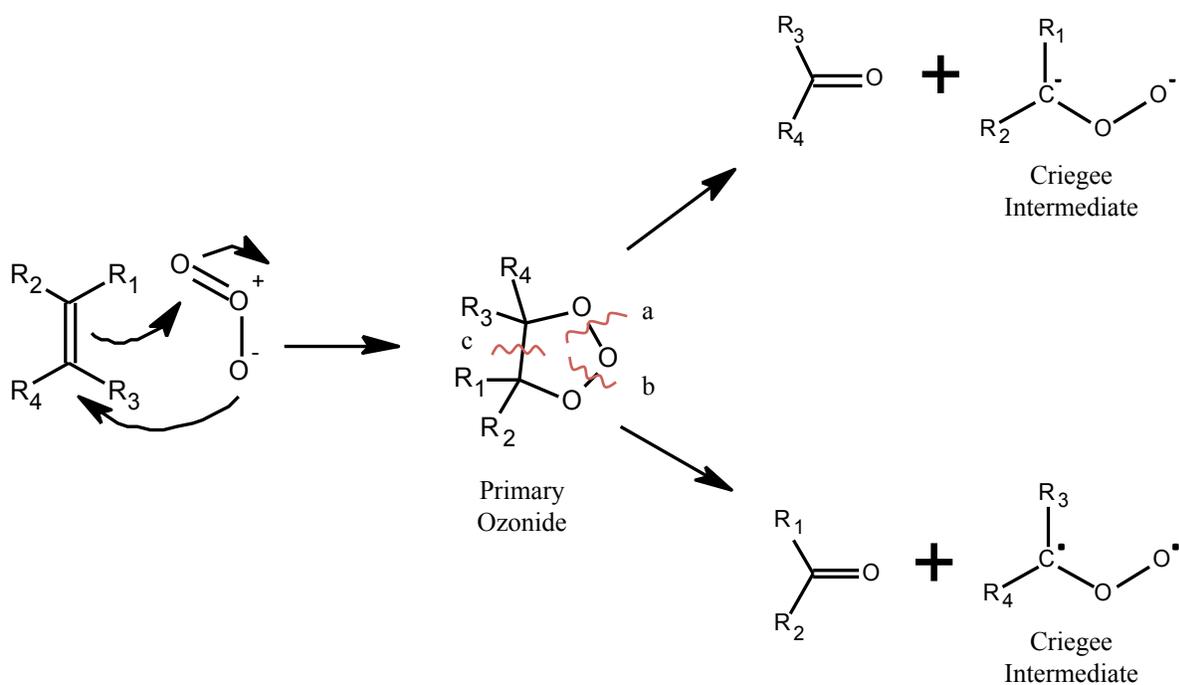
Figure 5.1: General Schematic of alkene-ozonolysis adopted from Finlayson-Pitts and Pitts Jr. (1999)

The ozonolysis mechanism described by Finlayson-Pitts and Pitts Jr. (1999) is a summary of the work done by Criegee (1975). The primary step for ozonolysis is to add across the double bond of an alkene to form an energy-rich primary ozonide. The resultant complex is unstable and will decompose by cleaving one of the peroxy bonds (O – O) and the carbon-

carbon (C – C) bond. Figure 5.1 shows, that there are two locations, position *a* and *b*, where bond cleavage can occur. For symmetrical alkenes like ethylene, cleavage of either peroxy bond gives the same products. Contrastingly, the peroxy bonds for unsymmetrical alkenes like β-pinene will preferentially cleave to produce a more substituted intermediate (Finlayson-Pitts and Pitts Jr., 1999). Regardless of symmetry, the breakage of the peroxy and carbon-carbon bond will yield what is known as a Criegee biradical intermediate (CBI). For endocyclic monoterpenes like α-pinene, primary ozonide decomposition produces a CBI with a carbonyl oxide moiety and carbonyl functional group (Docherty et al., 2005). On the other hand, exocyclic monoterpenes like β-pinene produces a CBI possessing a carbonyl oxide and a separate carbonyl. As a result, ozonolysis of exocyclic monoterpenes will produce a CBI with one less carbon than the original structure. This can be properly observed in Figure 5.2 (a) and (b).
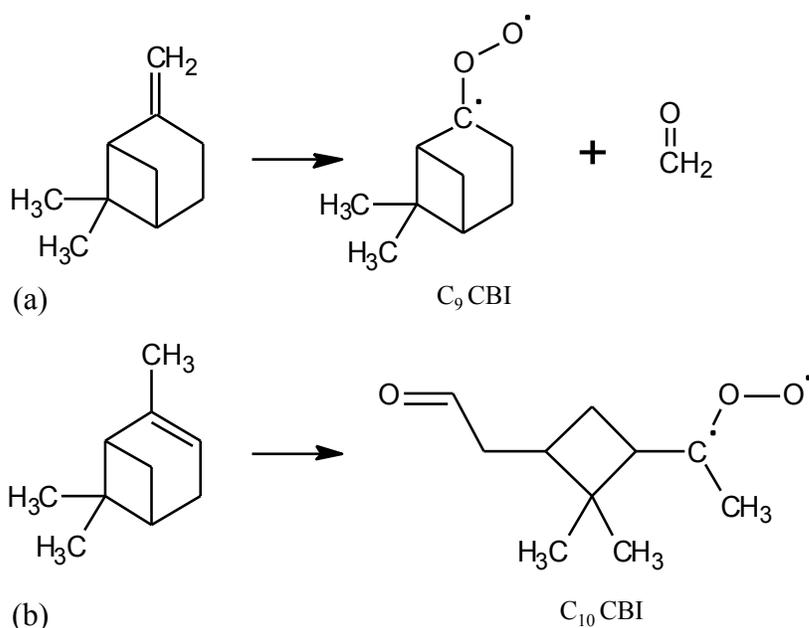
Figure 5.2: Formation of Criegee biradical intermediate (CBI) for (a) β- pinene and (b) α-pinene

Like the primary ozonide, the CBI formed also possesses excess energy. As a result, the CBI will undergo two different reaction pathways; stabilization (stable Criegee intermediate channel (SCI)) or decomposition (hydroperoxide channel). A simplified mechanism is depicted in Figure 5.3. In general, stabilization during monoterpene ozonolysis occurs by colliding with components of air such as oxygen (O_2) and nitrogen (N_2). The resultant complex can react with a variety of components such as carbonyls, acids, water and alcohols to form different classes of organic peroxides (α-hydroxy, α-alkoxy, and α-acyloxy hydroperoxides) (Docherty et al., 2005). However, under atmospheric conditions, the stabilized CBI is often dominated by reactions with water vapour forming the α-hydroxyhydroperoxide (Kroll and Seinfeld. 2008). This source of hydroperoxide formation is of great interest since its formation occurs without involving HO_2 radicals (Lee et al., 2000).
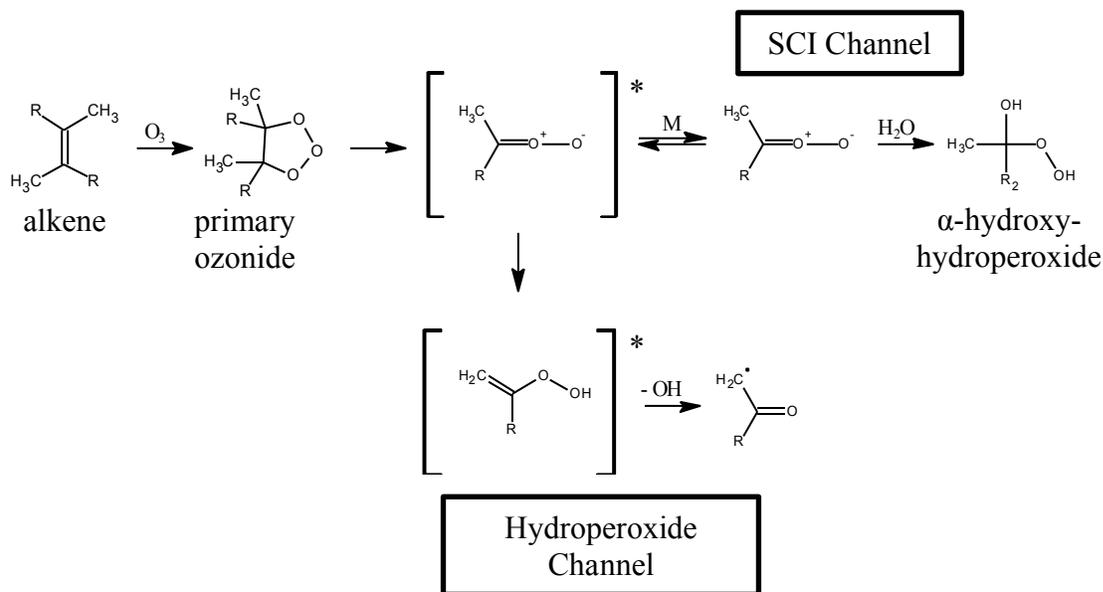
Figure 5.3: General schematic outlining the two reaction pathways for the excited criegee biradical intermediate (denoted by *).

On the other hand, the hydroperoxide channel results in the production of an unstable vinyl hydroperoxide that decomposes to form HO and an alkyl radical (R) (Kroll and Seinfeld, 2008). Reasonably, the unstable vinyl hydroperoxide should stabilize by reacting with components of air (similar to SCI channel). However, there is no evidence to suggest that this pathway exists. Notably, the resultant alkyl radical from the hydroperoxide channel can undergo reactions with O_2 to form an alkyl peroxy radical (RO_2) and a hydroperoxide after reacting with HO_2 radicals. Although organic peroxides can be produced by further reactions of the RO_2 radical, its production will depend on NO_x levels. The competing reactions are shown in Reactions 5.1 to 5.3 (Kroll and Seinfeld, 2008).

$$RO_2 + HO_2 \rightarrow ROOH + O_2 \hspace{4cm} \text{Reaction 5.1}$$

$$RO_2 + NO \rightarrow RO + NO_2 \hspace{4cm} \text{Reaction 5.2a}$$

$$RO_2 + NO + M \rightarrow RONO_2 + M \hspace{3cm} \text{Reaction 5.2b}$$

$$RO_2 + NO_2 + M \leftrightarrow ROONO_2 + M \hspace{3cm} \text{Reaction 5.3}$$

Hydroperoxide formation occurs through Reaction 5.1. However, a NO_x concentration greater than 100 parts-per-trillion suppresses hydroperoxide (Lee et al., 2000). The RO_2 radical reacts through Reaction 5.2(a), 5.2(b), and 5.3 forming an alkoxy radical (RO), organic nitrate or peroxynitrates, respectively. Of the two reactions, Reaction 5.2(a) is believed to dominate forming an RO radical, whereas Reaction 5.2(b) accounts for < 25% of Reaction 5.2 (Kroll and Seinfeld, 2008). Although Reaction 5.3 forms peroxynitrates, these compounds thermally dissociate in the particle phase forming back the RO_2 radical, which can form hydroperoxides

through reactions with HO_2 (Kroll and Seinfeld, 2008). A modified diagram adopted from Kroll and Seinfeld (2008) portrays a simplified mechanism for the fate of RO_2 radicals starting with VOC oxidation (Figure 5.4). Regardless of the reaction pathway for the formed CBI, organic peroxides are expected to be a product during alkene-ozonolysis.
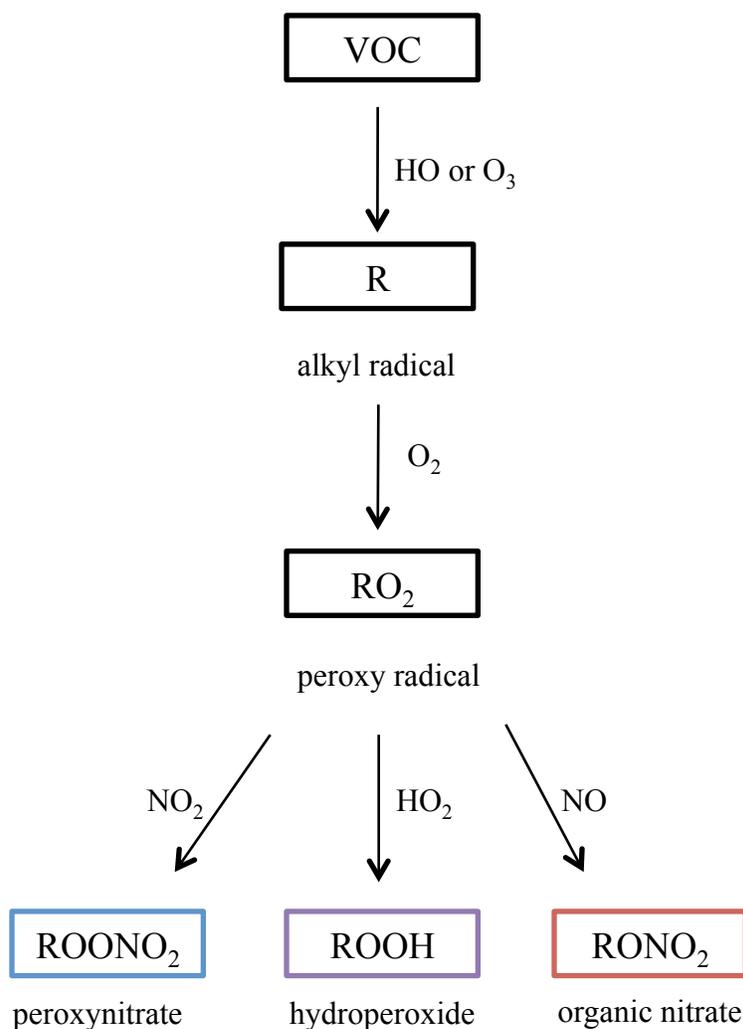
Figure 5.4: Simplified schematic illustrating the pathways for forming peroxynitrate, hydroperoxide and organic nitrate products through the oxidation of VOC by HO radicals and O_3. Diagram was adopted and modified from Kroll and Seinfeld (2008).

6. Experimental Design for Organic Peroxide Standard Analysis and β-Pinene Ozonolysis Experiments

6.1. Organic Peroxide Standard Introduction

Simple organic peroxides were purchased (Sigma-Aldrich) to observe the gas-phase ion-molecule chemistry of the organic peroxide when protonated water or methanol clusters were used as an ionization reagent. The organic peroxides used in this experiment can be found in Table 6.1 and their chemical structures can be found in Figure 6.1. These peroxides were selected, as much as possible, to represent different classes of organic peroxides.

Table 6.1: Organic peroxides analyzed by the APCI-MS/MS

Name of Compound	Molecular Formula	Molar Mass (g mol^{-1})	Organic Peroxide class
tert-butyl hydroperoxide	(CH$_3$)$_3$COOH	90	hydroperoxide
tert-butyl peroxyacetate	(CH3)$_3$COOC(O)CH$_3$	132	peroxy ester
Cumene hydroperoxide	C$_6$H$_5$C(CH$_3$)$_2$OOH	152	hydroperoxide
Peroxyacetic acid	CH$_3$C(O)OOH	76	peroxy acid
di-*tert*-butyl peroxide	(CH3)$_3$COOC(CH$_3$)$_3$	146	dialkylperoxide
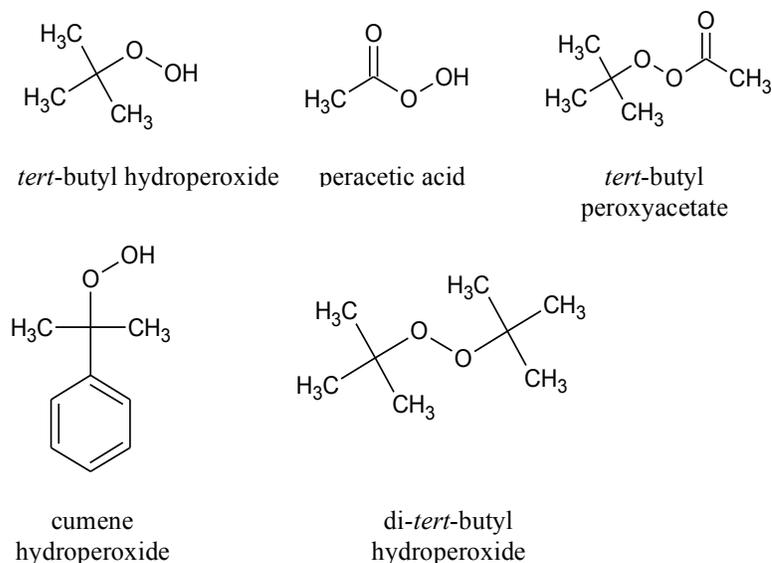
Figure 6.1: Chemical structure for organic peroxides analyzed by (+) APCI-MS/MS

Organic peroxides were analyzed neat or a 10% volume/volume (v/v) was prepared using either distilled water or methanol (Sigma-Aldrich) as a solvent. Each type of standard preparation was continuously introduced to the APCI-MS/MS through the use of a 50 microliter (μL) syringe needle (Hamilton Company) mounted onto a syringe pump (Harvard Apparatus, Model 11 Plus) operating at 0.5 microliter per minute (μL min^{-1}). Standard preparation entered into the APCI-MS/MS with the aid of a purified air stream (Aadco Instruments Inc.). Purified air stream's flow was set to 5 Liter per minute (L min^{-1}) and was controlled through the use of a mass flow controller (MFC). An overall schematic showing standard preparation introduction is depicted in Figure 6.2. Since some of the standards were light sensitive, the standards and experimental set up were protected from light to prevent decomposition. The standards used had sufficient volatility for the output of the airflow to contain some of the standard in its gas form. Purified air containing the standard in its gas form was swept into a 5 L 3-neck round

bottom flask for continuous mixing. A magnetic stirrer was used to promote uniform mixing of the standards before chemical ionization. After mixing, standards were introduced to the ion source of the APCI-MS/MS where it underwent chemical ionization with either protonated water or methanol clusters. Ionization products were detected by the APCI-MS/MS operating in the positive-ion mode.

Aadco flow at 5 L/min

Syringe pump at
0.5µL/min

To dilution flask   To ion source

Stir plate
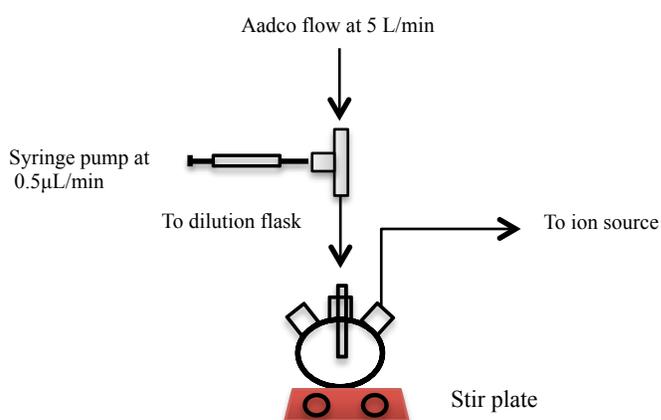
Figure 6.2: Experimental design for standard introduction

6.2. Introduction of Ionization Reagent to Ion Source

6.2.1. Selection of Ionization Reagent

Generally under ambient conditions (+) APCI-MS/MS utilizes protonated water cluster to chemically ionize neutral molecules. However, the APCI-MS/MS can easily be set-up to use other ionization reagents. Therefore, protonated methanol and its clusters were selected as an alternative ionization reagent. This reagent was selected based on the positive results obtained for the chemical ionization of selected organic peroxides by Rondeau et al., (2003).

6.2.2. A Comparison of Protonated Water and Methanol Clusters

Employing different ionization reagents can influence the ion-molecule chemistry occurring in the ion source. The formation of protonated water clusters from ambient air was discussed in Section 4.1.1. Protonated methanol clusters can form in the ion source through a proton transfer reaction occurring between protonated water clusters and neutral methanol molecules (Reaction 6.1). In Reaction 6.1 protonated water clusters act as Brönstead acids while the methanol clusters act as Brönstead bases. For this reaction to occur, the PA of methanol must be larger than the PA of water. A comparison for the PA of water and methanol clusters is shown in Table 6.2. Since the PA difference between methanol and water is almost 70 kJ mol^{-1}, this condition is met.

$$(H_2O)_mH^+ + (CH_3OH)_n \rightarrow ((CH_3OH)_nH)^+ + (H_2O)_m \qquad \text{Reaction 6.1}$$

Table 6.2: Proton affinities for n size clusters of water and methanol

Size (n)	Gas Phase Proton Affinity (kJ mol^{-1}) Water [a]	Gas Phase Proton Affinity (kJ mol^{-1}) Methanol [b]
1	696	766
2	828	879
3	884	937
4	915	962

[a] [Kawai et al., 2003]

[b] [Bernstein, E.R., 1996]

6.2.3. Introduction of the Ionization Reagent into the Ion Source

Different techniques were utilized to introduce either ionization reagent (water or methanol) into the ion source. Various approaches were performed to evaluate the impact of changing the location of the ionization reagent source on gas-phase proton transfer from the protonated reagent ions to the neutral standards.

6.2.3.1. Introduction of Ionization Reagent using a Direct Method

Figure 6.3 (a) shows a conceptual diagram for the introduction of purified air into the ion source. Purified air was used since it contained traces of water to use as an ionization reagent. However, introducing methanol into the ion source required injecting it into the purified air stream. This was accomplished by changing the experimental set-up depicted in Figure 6.3 (a) to include a syringe pump apparatus capable of dispensing 0.1 μL min^{-1} to 5.0 μL min^{-1} of methanol into the purified air stream (Figure 6.3 (b)). Since the experimental set-up for methanol differed in comparison to the experimental set-up depicted in Figure 6.3 (a), additional experiments were repeated by replacing methanol with distilled water for future comparative analysis.
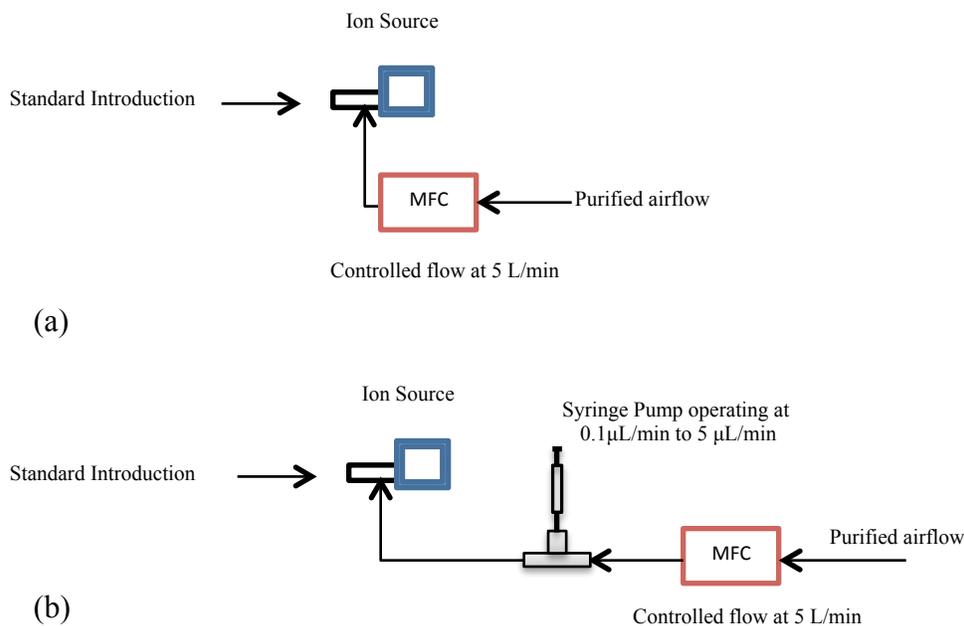
Figure 6.3: Experimental set-up for ionization reagent introduction. (a) Conceptual diagram where water vapour from purified air was introduced directly into the ion source. The experimental set-up depicted by (b) shows how methanol vapours were introduced into a stream of purified air before entering the ion source.

6.2.3.2. Introduction using the Double Syringe Pump Method

Since Figure 6.3 (a) and (b) portrayed an experimental set up where standard and ionization reagent introduction into the ion source were separate, an additional experimental set up was designed to allow ionization reagent and standards to mix before entering the ion source (Figure 6.4). This was accomplished by modifying the experimental set-up described by Figure 6.3 (b) to include two syringe pumps operating at a range of flow rates (0.1 μL min^{-1} to 5.0 μL min^{-1}) and a 5 L 3-neck round bottom flask. To ensure that the vapour pressure of the ionization reagent was not being exceeded, the calculation shown in Appendix C was used to determine the maximum syringe pump flow allowance.

Purified airflow at 5 L/min

MFC

Solute syringe pump at 0.5 µL/ min

To dilution flask

Solvent syringe pump at 0.1 µL/min – 5.0 µL/min

Ion Source
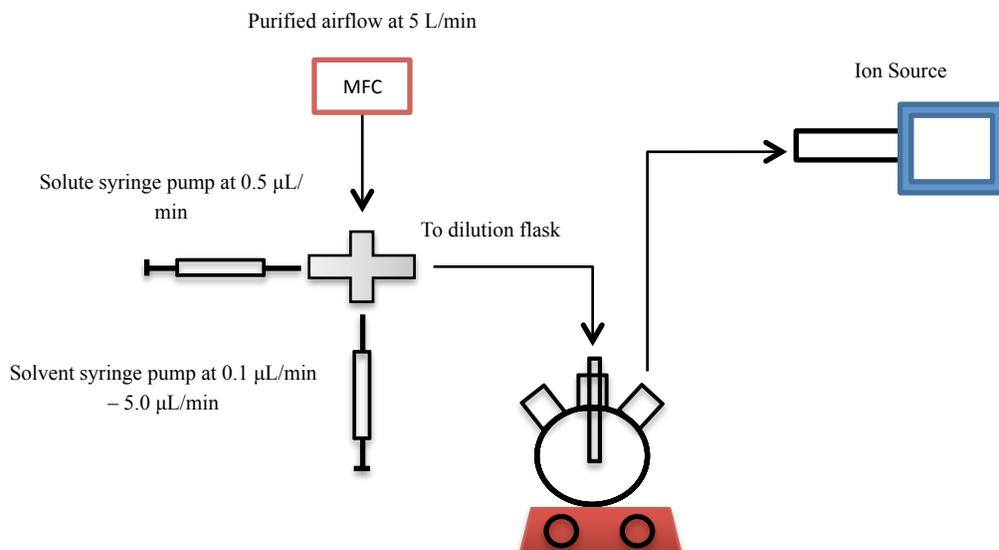
Figure 6.4: Experimental set-up for the double syringe pump method

6.3. Ionization of the Standards using Protonated Water Clusters

To evaluate the ability of (+) APCI-MS/MS to ionize organic peroxide standards with protonated water clusters, the standards were either injected neat or a 10% v/v diluted standard in water into a purified air stream or by injections of distilled water using the methods described in Section 6.3.3. For organic peroxide detection, the following reactions were hypothesized to occur in the ion source:

$$(H_2O)H^+ + R_1OOR_2 \rightarrow H^+ \bullet R_1OOR_2 + H_2O \qquad \text{Reaction 6.2}$$

$$(H_2O)H^+ + R_1OOR_2 \rightarrow (H_2O)H^+ \bullet R_1OOR_2 \qquad \text{Reaction 6.3}$$

$$(H_2O)_nH^+ + R_1OOR_2 \rightarrow (H_2O)_nH^+ \bullet R_1OOR_2 \qquad \text{Reaction 6.4}$$

Equations 6.2 to 6.4 appeared to be a reasonable ionization scheme since the PA of the selected organic peroxides were generally higher than the PA of water. Table 6.3 and Table 6.2 show the

47

PA of the selected organic peroxides and water and its clusters, respectively. PA values were not available for all organic peroxides used in this experiment. For those organic peroxides values were estimated from known organic compounds with similar structure.

Table 6.3: Proton affinities for organic peroxides used during the experiment

Molecule	Proton Affinity (kJ mol^{-1})
tert-butyl hydroperoxide	803[a]
tert-butyl peroxyacetate	783[b]
Cumene hydroperoxide	791[c]
Peroxyacetic acid	> 696[d]
di-*tert*-butyl peroxide	791[e]

[a] Estimated using *tert*-butyl alcohol as reference [Rondeau et al., 2003]

[b] [Hastie et al., 2010]

[c] Estimated using dialkyl peroxide as reference [Rondeau et al., 2003]

[d] Reasonably deduced to be larger than the PA of water based on reported PA values for benzene (750 kJ/mol), toluene (784 kJ/mol), benzoic acid (821 kJ/mol), phenylamine (882 kJ/mol) and phenol (817 kJ/mol) in the NIST Chemistry WebBook .

[e] [Rondeau et al., 2003]

6.4. Ionization with Protonated Methanol Clusters

In addition to water, methanol was selected as a possible ionization reagent for organic peroxides. The formation of protonated methanol clusters from neutral methanol molecules using protonated water clusters was discussed in Section 6.2.2. The ion-molecule chemistry of

organic peroxide standards with protonated methanol clusters was evaluated using the standards neat or a 10% v/v standard prepared in water or methanol. Standards were injected in the same manner discussed in Section 6.1. Methanol was introduced into the ion source through the methods discussed in Section 6.3.3. For organic peroxide detection, the following ionization scheme was believed to occur in the ion source:

$(CH_3OH)H^+ + R_1OOR_2 \rightarrow H^+ \bullet R_1OOR_2 + CH_3OH$ Reaction 6.6

$CH_3OH)H^+ + R_1OOR_2 \rightarrow (CH_3OH)H^+ \bullet R_1OOR_2$ Reaction 6.7

$(CH_3OH)_nH^+ + R_1OOR_2 \rightarrow (CH_3OH)_nH^+ \bullet R_1OOR_2$ Reaction 6.8

Similar to the ionization scheme described in Section 6.4, this ionization scheme was logical since the PA of methanol was lower than the PA of the organic peroxide standards used in this experiment. The PA of methanol and its clusters can be found in Table 6.2.

6.5. Smog Chamber Experiments

6.5.1. Smog Chamber Description

β-Pinene ozonolysis experiments were performed in an 8 m^3 cylindrical smog chamber at York University. The smog chamber consisted of a Teflon bag with two Teflon coated aluminum endplates. To promote mixing during ozonolysis experiments, a fan was located at the input end of the smog chamber. The Teflon bag and endplates were encased by a mobile frame covered with Mylar to prevent radiation from entering or leaving the smog chamber during experiments. Although the mobile frame was lined with 24 ultraviolet lights with a radiation output range of 350 to 400 nm (Philips F40L, 40 Watt), these lights were not used

during ozonolysis experiments. A humidity and temperature meter (Omegatte HH311) attached to the chamber was used to monitor the temperature and humidity during experiments. A general schematic of the smog chamber is depicted in Figure 6.5
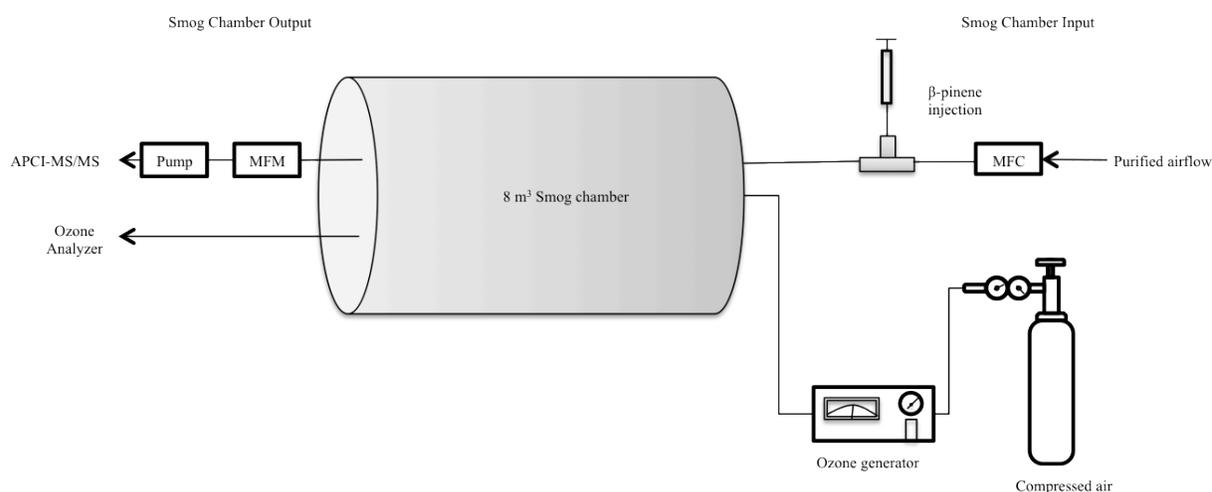
Figure 6.5: Schematic for the York University smog chamber

6.5.2. Smog Chamber Experimental Set-up

To ensure the smog chamber was free from organic products formed during previous experiments, background scans (shown in Figure 6.6) of the smog chamber were acquired using (+) APCI-MS/MS (operating parameters are listed in Appendix D). Before smog chamber experiments were conducted, the chamber was flushed for 24 hours with 30 L min^{-1} of purified air.

During experiments, smog chamber air was pulled into the ion source at a rate of 2 L min^{-1} using a pump and a mass flow meter (MFM). Additionally, an ozone (O$_3$) analyzer (UV Photometric, Thermo Environmental Inc.) was attached to the output end of the chamber to monitor the O$_3$ concentration. The removal of chamber air for APCI-MS/MS and ozone

concentration analysis was balanced with an input of purified air. Once the chamber was determined to be clean, 23 µL β-pinene was injected into the chamber using a 25 µL syringe (Hamilton Company) to achieve a concentration of 0.4 part-per-million (ppm). The calculation for β-pinene volume injection is outlined in Appendix E. After injection, β-pinene was allowed to mix for one hour. Following mixing, O_3 was injected into the chamber to achieve a concentration of 1 ppm. Calculations for O_3 concentration, operating parameters for the O_3 generator, and a summary of the experimental conditions for all smog chamber studies can be found in Appendix F. The contents of the chamber were allowed to mix until a stable total ion count (TIC) signal was observed by the APCI-MS/MS. A stable TIC signal was usually obtained after contents of the chamber were mixed for 40 minutes.
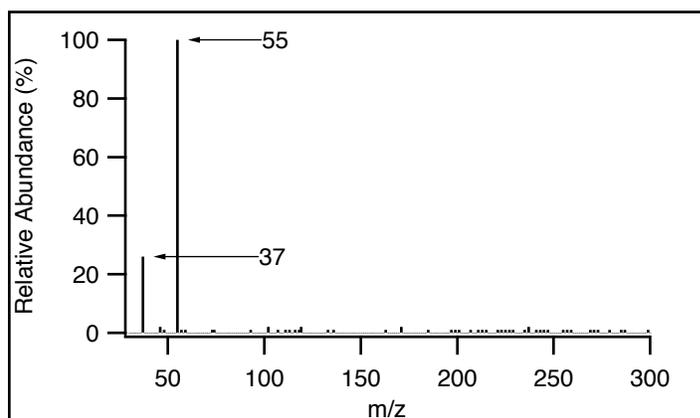
Figure 6.6: Example of a typical background spectrum acquired with (+) APCI-MS/MS. Ion signals *m/z* 37 and 55 represents $(H_2O)_2H^+$ and $(H_2O)_3H^+$, respectively.

During ozonolysis experiments, HO radical production was possible if the CBI formed decomposed through the hydroperoxide channel as described in Section 5.0. Since an HO scavenger was not used in this project to supress HO radical formation, it was assumed that β-pinene oxidation products were strictly formed from oxidation with ozone.

6.5.3. Data Acquisition

6.5.3.1. Ionization with Protonated Water Clusters

Smog chamber experiments were initially conducted using water vapour present in purified air as a reagent gas. The introduction of purified air into the ion source has been discussed in previous sections. Ozonolysis products formed in the chamber underwent chemical ionization with protonated water clusters in the ion source. The resultant oxidation products were analyzed firstly by acquiring full mass spectra for a range of m/z values (10 – 400). Subsequently, the acquired mass spectra were used to select m/z ions of interest for further MS/MS studies. Product-ion scans were acquired for selected ions to ascertain the possible identity. Moreover, the (+) APCI-MS/MS operated in the neutral-loss scan mode to observe the possibility of losing neutral fragments with masses of 18, 32, 34, 46, and 62 u from protonated oxidation products.

6.5.3.2. Ionization with Protonated Methanol Clusters

Similar to organic peroxide standard analysis using protonated water and its clusters, methanol was used as an ionization reagent to determine its ability to ionize oxidation products during smog chamber studies. Prior to ozonolysis experiments, a 50 μL syringe filled with methanol was mounted onto a syringe pump (Harvard Apparatus, Model 11 Plus) and allowed to pump methanol into the ion source at a rate of 0.2 μL min^{-1}. The set-up used was previously described by Figure 6.3 (b). Ozonolysis experiments commenced in a similar manner to the method described in the previous section. Full scan spectra were acquired for a range of m/z values (10 – 400) before and after the addition of methanol into the ion source for comparative analysis. Product-ion scans for selected precursor ions were acquired to determine if oxidation

products from the chamber were ionized with protonated methanol clusters. Additionally, NLS analyses were performed to observe which protonated oxidation products could lose neutral fragments of 18, 32, 34, 46 and 62 u.

7. Results and Discussion

7.1. Analysis of Commercially Available Organic Peroxide Standards

7.1.1. Ionization with Protonated Water Clusters

Prior to β-pinene ozonolysis experiments, commercially available organic peroxides were analyzed to observe their gas-phase reaction towards either water or methanol as an ionization reagent in the ion source of the (+) APCI-MS/MS. Table 7.1 lists expected *m/z* values based on the predicted ion-molecule chemistry described in Section 6.3 for organic peroxide standards ionized using protonated water and its clusters.

Table 7.1 List of expected *m/z* ion signals for organic peroxide standards chemically ionized using protonated water and its clusters

Name of Compound	Molar Mass (g mol^{-1})	Expected *m/z* Ion Signals	
		$[M + H]^+$	$[M + H_2O + H]^+$
tert-butyl hydroperoxide	90	91	109
tert-butyl peroxyacetate	132	133	151
Cumene hydroperoxide	152	153	171
Peroxyacetic acid	76	77	95
di-*tert*-butyl peroxide	146	147	165

Additionally, organic peroxide standards were used during MS/MS experiments to determine fragmentation pathways and confirm their respective structures. Ultimately, the intent of performing MS/MS experiments was to identify commonalities between the spectra of all acquired organic peroxides. Full scan mass spectra for all organic peroxides are depicted in Figure 7.1 (a) to (e). Most of the acquired full scan mass spectra were dominated by fragments ions with no intact $[M + H]^+$ ions observed in appreciable amounts. Using Table 7.1, no m/z values indicating ionization with protonated water and its clusters was observed as expected through Reaction 6.2 to 6.4. Instead, most of the organic peroxides analyzed experienced fragmentation at their peroxy bond (O – O). For example, the full scan mass spectrum of *tert*-butyl hydroperoxide (Figure 7.1 (a)) did not yield m/z 91 and 109 indicative of the $[M + H]^+$ and $[M + H_2O + H]^+$ ions but was dominated by the fragment ion m/z 73 ($(CH_3)_3CO^+$) likely resulting from a loss of water (H_2O) from the $[M + H]^+$ ion. Similarly, *tert*-butyl peroxyacetate and di-*tert*-butyl peroxide both fragmented at the peroxy bond to produce an ion signal at m/z 73. Additionally, fragmentation at the peroxy bond was also indicated in the full scan mass spectrum of cumene hydroperoxide by the presence of the m/z 135 ion ($(C_6H_5)(CH_3)_2CO^+$).
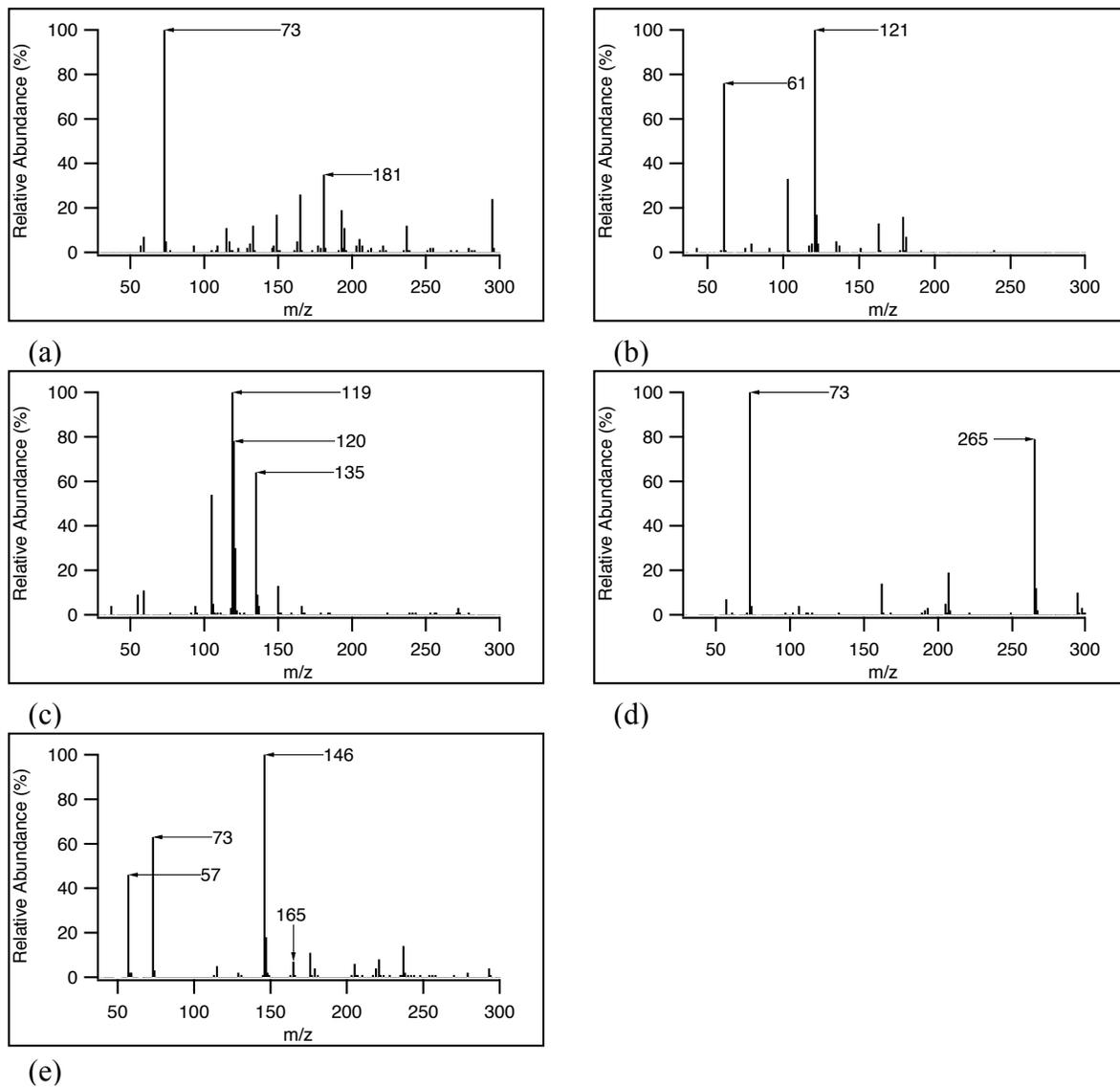
Figure 7.1: Full scan mass spectra for all organic peroxides acquired by (+) APCI-MS/MS. (a) *tert*-butyl hydroperoxide, (b) peracetic acid, (c) cumene hydroperoxide, (d) *tert*-butyl peroxyacetate, and (e) di-*tert*-butyl peroxide

In addition to the major features described above, most standards exhibited unique features in their full scan mass spectrum. For instance, a protonated dimer [M + M + H]$^+$ ion was observed for *tert*-butyl hydroperoxide (*m/z* 181) and *tert*-butyl peroxyacetate (*m/z* 265)

resulting from the high pressure conditions in the ion source of the APCI-MS/MS. Additionally, unlike the other standards analyzed di-*tert*-butyl peroxide was capable of ionizing in the ion source to form a molecular ion ($[M]^+$, *m/z* 146). This is possible because of its low ionization energy value 8.78 eV in comparison to the components of air (oxygen = 12.0697 eV and nitrogen = 15.581 eV) (NIST Chemistry WebBook). No information regarding the ionization of peracetic acid could be ascertained using the full scan mass spectrum since it was dominated by *m/z* ion signals that were attributed to acetic acid.

Lastly, cumene hydroperoxide exhibited a loss of 32 u likely resulting from a loss of molecular oxygen (O_2) from the $[M + H]^+$ ion. Since this type of loss was not expected, this standard was investigated further. Although there was no information for the PA of cumene hydroperoxide, it was assumed that protonation of this molecule would occur at the hydroperoxy (-OOH) functional group. This assumption was established based on the results of a similar experiment from Reinnig et al., (2009) where cumene hydroperoxide protonation was achieved using (+) APCI-MS/MS with an ion trap. Product-ion scans from this study revealed the loss of hydrogen peroxide (H_2O_2, 34 u), which was deemed only possible if protonation occurred at the hydroperoxy moiety. To rationalize the loss of 32 u, it was suggested that protonation must occur within the ring of the molecule as oppose to the hydroperoxy moiety (Rondeau et al., 2003). Figure 7.2 outlines the possible mechanism for rationalizing the loss of 32 u from the protonated cumene hydroperoxide ion (Rondeau et al., 2003).

m/z 153   *m/z* 121
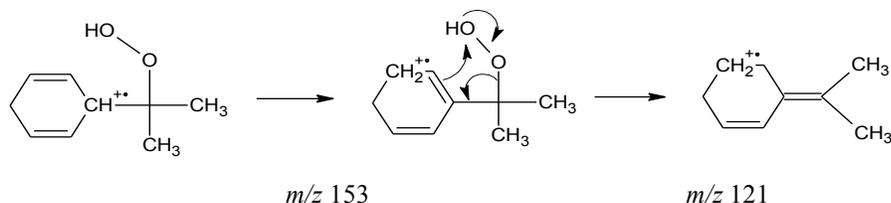
Figure 7.2: Mechanism proposed by Rondeau et al., (2003) for the elimination of O₂ from protonated cumene hydroperoxide

As shown by the results from this section, the main common feature from all organic peroxides analyzed by (+) APCI-MS/MS was that spectra were dominated by smaller fragment ions and lacked appreciable amounts of $[M + H]^+$ ions. It was apparent during this aspect of the experiment that ionizing organic peroxides with protonated water clusters was not a selective ionization technique. In short, minimal information about the neutral molecule was obtained by utilizing the full scan mode of the APCI-MS/MS under the given conditions.

7.1.1.1. Neutral-Loss Scan Analysis

This analysis mode was utilized since it provided a great deal of selectivity in comparison to the full scan mode analysis. The APCI-MS/MS was set to detect a range of *m/z* ions capable of losing a neutral mass of 34 u. Organic peroxides containing a hydroxyperoxy functional group are known to lose 34 u, attributed to a loss of hydrogen peroxide (H_2O_2) from the $[M + H]^+$ ion during MS/MS studies (Reinnig et al., 2009, Reinnig et al., 2008, and Baker et al., 2001). The resulting loss is possible as long as protonation occurs at the hydroperoxy functional group moiety of the peroxide. Figure 7.3 depicts the general structure for four classes of organic peroxides. Of the four structures, hydroperoxides and peroxy acids contain a

hydroperoxy moiety within its structure. A loss of H_2O_2 can be rationalized from these two

organic peroxide classes as long as protonation occurs at the hydroperoxy moiety.

Contrastingly, the general structure representing peroxy hemiacetals and peroxy esters cannot

explain a loss of H_2O_2 since their structure lacks a hydroperoxy moiety. Peroxy hemiacetals are

discussed in greater detail in Section 9.1.3. As a result, a loss of H_2O_2 is limited to organic

hydroperoxides and peroxy acids.
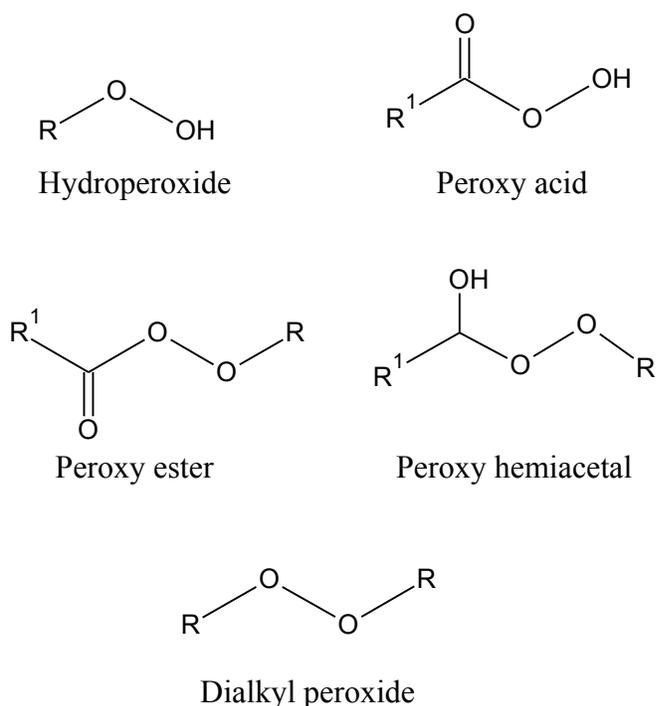
Figure 7.3: General structures for different classes of organic peroxides. While R^1 groups can indicate a hydrogen atom or organic constituent, R attached to oxygen can only indicate an organic constituent.

Out of the five selected organic peroxides standards used in this experiment, *tert*-butyl

hydroperoxide, peracetic acid and cumene hydroperoxide were the only standards that

possessed a hydroperoxy functional group within its structure (Figure 6.1). Therefore these

three standards were analyzed further using NLS analysis. Since NLS analysis produces a mass

spectrum of all precursor ions exhibiting a specified mass loss, the intent was to see if ion signals representing $[M + H]^+$ could be observed for the three organic peroxide standards possessing a hydroperoxy functional group based on a specified mass loss of 34 u from the $[M + H]^+$ ion. Figure 7.4 (a) to (c) represents the results for *tert*-butyl hydroperoxide, peracetic acid and cumene hydroperoxide using NLS analysis mode. The $[M + H]^+$ ion signal was present in all three NLS mass spectra. These ion signals were *m/z* 91 for *tert*-butyl hydroperoxide, *m/z* 77 for peracetic acid and *m/z* 153 for cumene hydroperoxide. This was different compared to the full scan mass spectra for *tert*-butyl hydroperoxide, peracetic acid and cumene hydroperoxide where $[M + H]^+$ ion signals were not observed (Figure 7.1 (a) to (c)). The $[M + H]^+$ ion was easily observed in NLS analysis mode compared to full scan mode because NLS analysis mode only displayed ion signals exhibiting a mass loss of 34 u during MS/MS experiments while full scan mode displayed all ions formed inside the ion source of the APCI. Given the increased sensitivity for $[M + H]^+$ ions, NLS analysis mode allowed for the confirmation of $[M + H]^+$ ions in the mass spectra for the three organic peroxide standards analyzed. Furthermore, this analysis mode confirmed the ion-molecule reaction previously mentioned in Section 6.4 describing the formation of $[M + H]^+$ ions using protonated water clusters as an ionization reagent.

Aside from observing $[M + H]^+$ ions in NLS mass spectrum, additional comments could be made regarding the acquired NLS mass spectra for *tert*-butyl hydroperoxide and cumene hydroperoxide. For instance, the NLS mass spectra for *tert*-butyl hydroperoxide and cumene hydroperoxide were dominated by precursor ions that were smaller than the molecular weight of the standard. *Tert*-butyl hydroperoxide had *m/z* ion signals less than 80 while cumene hydroperoxide had *m/z* ion signals less than 143, which were capable of losing 34 u during

MS/MS experiments. This most likely indicated that aside from [M + H]$^+$ ions, smaller fragmented ions formed in the APCI ion source could lose 34 u during MS/MS experiments.

Altogether, there was an advantage to using NLS analysis mode over the full scan analysis mode since [M + H]$^+$ ions could easily be observed for organic peroxide standards containing a hydroperoxy functional group. Given the higher degree of sensitivity and ability of [M + H]$^+$ ions for organic hydroperoxides and organic peroxy acids to lose 34 u during MS/MS experiments, NLS analysis mode was established as a potentially valuable "fingerprinting" technique to target compounds containing a hydroperoxy functional group during future smog chamber experiments.
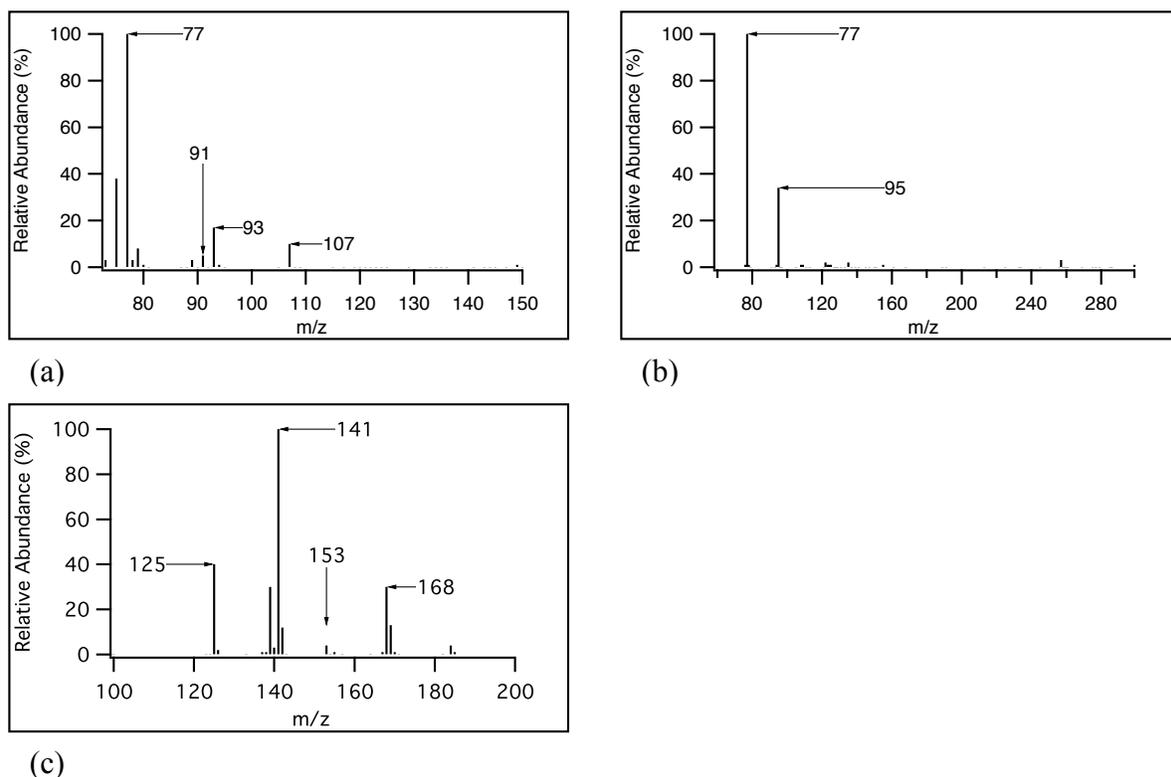
Figure 7.4: NLS for (a) *tert*-butyl hydroperoxide, (b) peracetic acid and (c) cumene hydroperoxide using protonated water and its cluster as an ionization reagent

7.1.1.2. Analysis of 10% v/v Standards

Reaction 7.1 describes the formation of protonated dimers. Since protonated dimers ([M + M + H]$^+$) were apparent for *tert*-butyl hydroperoxide (*m/z* 181) and di-*tert* butyl peroxyacetate (*m/z* 265) (Figure 7.1 (a) and (d)) these standards were analyzed once more by preparing a 10% v/v standard in water or methanol. This was done to reduce the dimer signal during full scan analysis. The remaining organic peroxide standards were diluted in the same manner for consistency and comparative analysis despite the lack of [M + M + H]$^+$ ions in their respective full scan mass spectra (Figure 7.1 (b), (c) and (e)). Nevertheless, the dimer signal was deemed not useful in this experiment since self-reactions would not be appreciable at atmospheric concentrations.

$$MH^+ + M \rightarrow (2M + H)^+ \hspace{4cm} \text{Reaction 7.1}$$

Although the results are not displayed, the full scan mass spectra for organic peroxide standards diluted with water were similar to the full scan mass spectra obtained when the standards were injected neat (Figure 7.1 (a) to (e)). The full scan mass spectra for standards diluted with water were dominated by fragmented ions. However, a difference in the [M + M + H]$^+$/ [M + H]$^+$ ratio for *tert*-butyl hydroperoxide and *tert*-butyl peroxyacetate was observed when comparing the full scan mass spectrum of neat and 10% v/v standards diluted in water. Table 7.2 summarizes the calculated [M + M + H]$^+$/ [M + H]$^+$ ratio for *tert*-butyl hydroperoxide and *tert*-butyl peroxyacetate. A decrease in the [M + M + H]$^+$/ [M + H]$^+$ ratio observed for the diluted *tert*-butyl hydroperoxide and *tert*-butyl peroxyacetate standards indicated that dimer formation in the APCI ion source was reduced.

Table 7.2: A comparison of $[M + M + H]^+ / [M + H]^+$ ratios for select organic peroxide standards

Name of Compound	Neat Standard Injection $[M + M + H]^+ / [M + H]^+$	10% v/v Standard Injection $[M + M + H]^+ / [M + H]^+$
tert-butyl hydroperoxide	326.6	5.7
tert-butyl peroxyacetate	494.1	81.7

Additionally, methanol was used as a diluent to try and reduce the formation of protonated dimers inside the APCI ion source during analysis of *tert*-butyl hydroperoxide and di-*tert* butyl peroxyacetate. Aside from being a commonly used solvent in analytical chemistry, the selection of this diluent was previously described in Section 6.3.1. Since methanol has a higher PA than water in the gas-phase, protonated methanol and its clusters formed inside the ion source as described by Reaction 6.1. As a result, organic peroxide standards analyzed underwent ion-molecule reactions with protonated methanol and its clusters as described by Reactions 6.6 to 6.8. Full scan mass spectra for organic peroxides dissolved in methanol are portrayed in Figure 7.5 (a) to (e) while Table 7.3 displays a list of expected *m/z* ion signals based on chemical ionization with protonated methanol and its clusters. To distinguish results in this project, mass spectra acquired using water as an ionization reagent are shown in black while mass spectra acquired using methanol as an ionization reagent are shown in blue. Although the aspect of this experiment was to remedy the formation of protonated dimers ($[M + M + H]^+$), the formation of protonated methanol dimers (($[2(CH_3OH) + H]^+$), *m/z* 65) was apparent in all full scan mass spectra except *tert*-butyl peroxyacetate (Figure 7.5 (c)) when methanol was used as a diluent. Its prominence indicated that the concentration of methanol

was high inside the APCI ion source. This suggested that methanol concentrations needed to be

reduced in the ion source. Additional experiments varying the concentration of methanol were

performed and described in Section 7.1.5.

Table 7.3 List of expected *m/z* ion signals for organic peroxide standards chemically ionized using protonated methanol and its clusters

Name of Compound	Molar Mass (g mol^{-1})	Expected *m/z* Ion Signals	
		$[M + H]^+$	$[M + CH_3OH + H]^+$
tert-butyl hydroperoxide	90	91	123
tert-butyl peroxyacetate	132	133	165
Cumene hydroperoxide	152	153	185
Peroxyacetic acid	76	77	109
di-*tert*-butyl peroxide	146	147	179
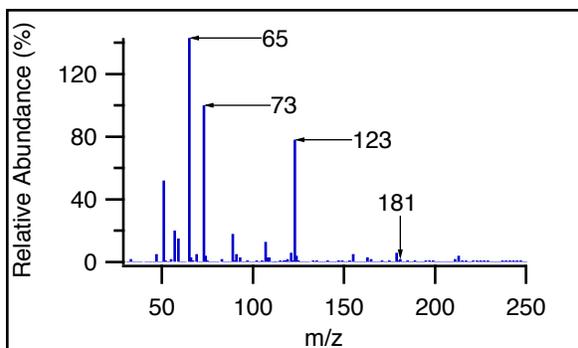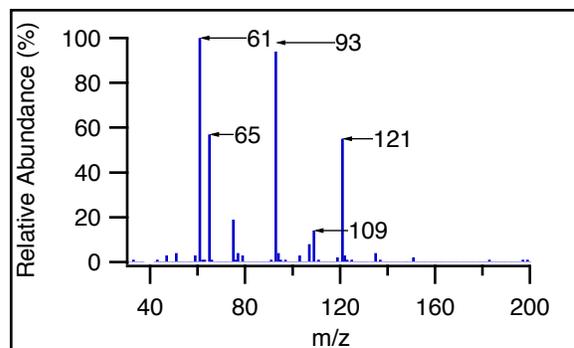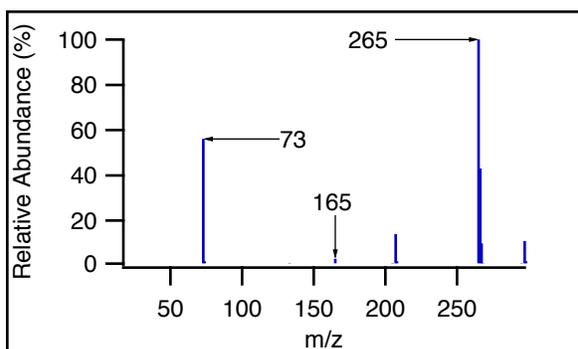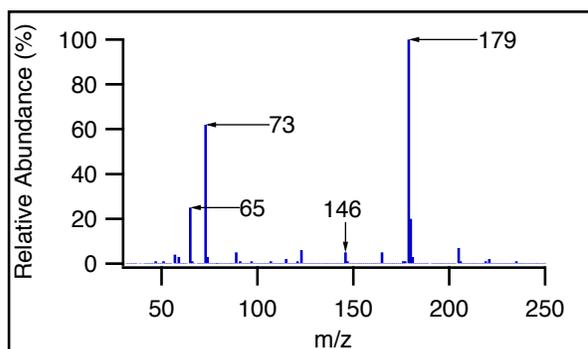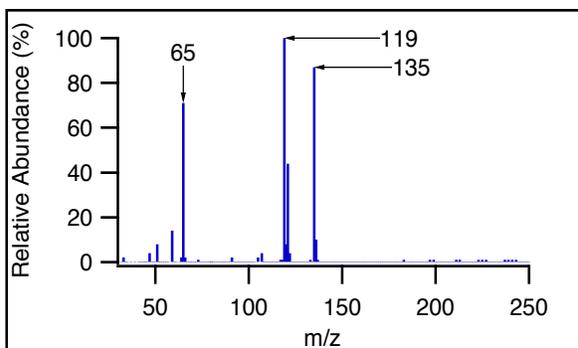
Figure 7.5: Full scan mass spectra for 10% v/v organic peroxide standards in methanol. (a) *tert*-butyl hydroperoxide, (b) peracetic acid, (c) *tert*-butyl peroxyacetate, (d) di-*tert*-butyl peroxide and (e) cumene hydroperoxide

Aside from observing protonated methanol dimers, the protonated dimer ion signal (m/z 181) was no longer visible in appreciable amounts in the full scan mass spectrum for *tert*-butyl

hydroperoxide in methanol (Figure 7.5 (a)), the protonated dimer ion signal (*m/z* 265) still dominated the full scan mass spectrum for *tert*-butyl peroxyacetate in methanol (Figure 7.5 (c)). The difference observed was most likely attributed to the PA of each species formed in the APCI ion source. In the ion source, neutral molecules compete for protons. The neutral molecule with the highest PA will undergo proton transfer. The full scan mass spectrum displayed in Figure 7.5 (a) showed that the introduction of 10 %v/v *tert*-butyl hydroperoxide in methanol into the APCI ion source yielded ion signals *m/z* 73, *m/z* 65 and *m/z* 123. Ion signal *m/z* 73 came from a loss of water (H_2O) from the $[M + H]^+$ ion as discussed in Section 7.1.1. However, the appearance of *m/z* 65 and *m/z* 123 indicated the formation of protonated methanol dimers ($[2(CH_3OH) + H]^+$) and adducts ($[M + CH_3OH + H]^+$), respectively. The reduced relative contribution of *m/z* 181 ($[M + M + H]^+$) was most likely due to competition for protons inside the ion source. Although the PAs for all species were not known, the reduction of *m/z* 181 ($[M + M + H]^+$) and appearance of ($[2(CH_3OH) + H]^+$) and ($[M + CH_3OH + H]^+$) in the full scan mass spectrum indicated that the PA for the two latter species were higher than the PA for the *tert*-butyl hydroperoxide dimer.

Contrastingly, the protonated dimer ion signal (*m/z* 265) was still prominent in the full scan mass spectrum for *tert*-butyl peroxyacetate (Figure 7.5 (c)). Unlike the full scan mass spectrum for *tert*-butyl hydroperoxide (Figure 7.5 (a)), the full scan mass spectrum shown in Figure 7.5 (c) contained *m/z* 165 ion signals representing the formation of $[M + CH_3OH + H]^+$ ions and was deficient in ion signals representing protonated methanol dimers *(m/z* 65, $[2(CH_3OH) + H]^+$). The continued prominence of ion signal *m/z* 265 suggested that tert-butyl peroxyacetate dimers had a higher PA than methanol dimers.

7.1.2. Ionization with Protonated Methanol Clusters

While diluting organic peroxide standards with methanol to reduce dimer formation, the resultant full scan mass spectra displayed in Figure 7.5 (a) to (d) showed m/z ion signals with a mass difference of + 33 u from each standard's molecular weight. This suggested the formation of adduct ions ($[M + CH_3OH + H]^+$) and inferred that the ion-molecule reaction described by Reaction 6.7 occurred in the APCI ion source. The ion signal representing $[M + CH_3OH + H]^+$ ions were apparent for *tert*-butyl hydroperoxide (m/z 123) and di-*tert*-butyl peroxide (m/z 179) whereas peracetic acid (m/z 109) and *tert*-butyl peroxyacetate (m/z 165) had $[M + CH_3OH + H]^+$ ion signals that were detected in small abundances. Unlike the full scan mass spectra for organic peroxide standards analyzed neat using water as an ionization reagent (Figure 7.1 (a) to (e)), the formation of an adduct ion was a common feature for four out of five organic peroxide standards diluted with methanol. Furthermore, diluting organic peroxide standards with water yielded full scan mass spectra similar to those presented in Figure 7.1 (a) to (e). It appeared that the use of methanol as a diluent yielded m/z ion signals that were intact and could be used to identify standards in a full scan mass spectrum.

In light of this observation, the ion-molecule chemistry of methanol with organic peroxide standards was investigated further. Product-ion scans were required to validate the formation of the adduct ion $[M + CH_3OH + H]^+$ in the ion source. These results are discussed in Section 7.1.2.1 in greater detail. Initially, methanol and organic peroxide standards were introduced into the ion source of the APCI-MS/MS using the double syringe pump method described in Section 6.3.3.2. Before standard introduction into the APCI ion source, methanol was introduced into the ion source to obtain a full scan mass spectrum. This is shown in Figure 7.6. The acquired full scan mass spectrum was dominated by protonated methanol dimers

$[2(CH_3OH) + H]^+$ at m/z 65. Additionally, the observed ion signals at m/z 33 and m/z 51 represented protonated methanol $[CH_3OH + H]^+$ and protonated methanol water cluster $[CH_3OH + H_2O + H]^+$, respectively. The absence of protonated water cluster ions $([(H_2O)_n + H]^+$ where n = 1, 2, 3, 4) despite the presence of water vapour in the purified air source, validated the occurrence of Reaction 6.1 in the ion source. Clearly, the gas-phase proton transfer reaction between water and methanol was responsible for the observed predominance of protonated methanol dimer, protonated methanol and its water cluster in the full scan mass spectrum.
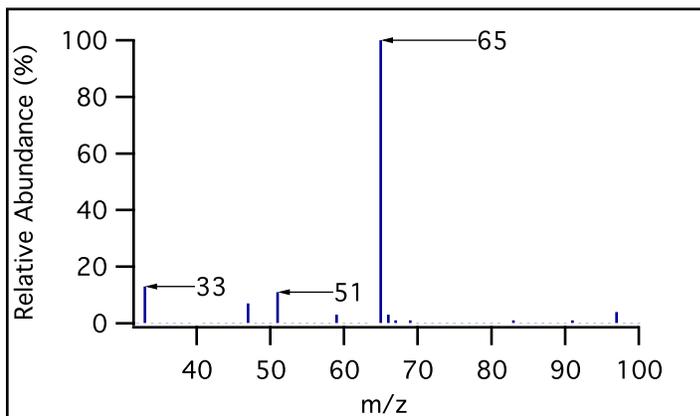
Figure 7.6: Full scan mass spectrum for pure methanol in the APCI ion source. Ion signal m/z 33, 51 and 65 represent $(CH_3OH)H^+$, $(CH_3OH)(H_2O)H^+$, and $(CH_3OH)_2H^+$, respectively.

To further investigate the ion-molecule chemistry of organic peroxide chemical ionization with protonated methanol, full scan mass spectra were acquired utilizing the double syringe pump method. Figure 7.7 to 7.10 depict the results for four out of five of organic peroxide standards. The larger traces illustrated in Figure 7.7 to 7.10 show the total ion count (TIC) (the sum of all m/z ion signals) plotted against time. The smaller full scan mass spectra for each figure shows the ion count for each detected m/z ion signal averaged over a 2.5 minute

time frame. Full scan mass spectra for cumene hydroperoxide were not acquired since the 10% v/v standard did not exhibit any ion signals indicating chemical ionization using protonated methanol.

During the experiment, the methanol syringe pump was allowed to operate for only half of the data acquisition time so the impact of the methanol could be more clearly observed. Since the total acquisition time was 5 minutes, the methanol syringe pump was allowed to operate during the last 2.5 minutes of the experiment. For the first 2.5 minutes of the experiment, the full scan mass spectra shown in black for Figures 7.7 to 7.10 are similar to the full scan mass spectra for neat organic peroxide standard analysis shown in Figure 7.1 (a) to (e). However, when the methanol pump was operating during the last 2.5 minutes of the experiment, the full scan mass spectra appearance for all organic peroxide standards shown in black in Figures 7.7 to 7.10 changed in response to the presence of protonated methanol and its clusters in the ion source. This change is portrayed by the full scan mass spectra shown in blue for Figures 7.7 to 7.10. Notably, the appearance of a $[M + 33]^+$ ion signal was observed for all four organic peroxide standards analyzed. Overall, Figure 7.7 to 7.10 showed that the presence of protonated methanol and its clusters in the APCI ion source was responsible for the resultant ion signals *m/z* 123 for *tert*-butyl hydroperoxide, *m/z* 179 for di-*tert*-butyl peroxide, *m/z* 165 for *tert*-butyl peroxyacetate and *m/z* 109 for peracetic acid.
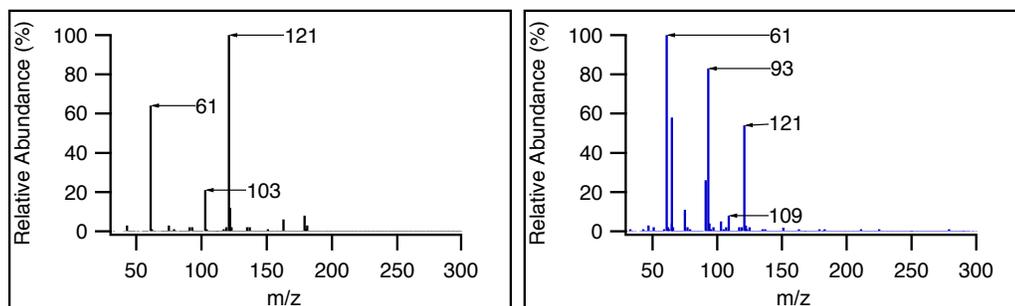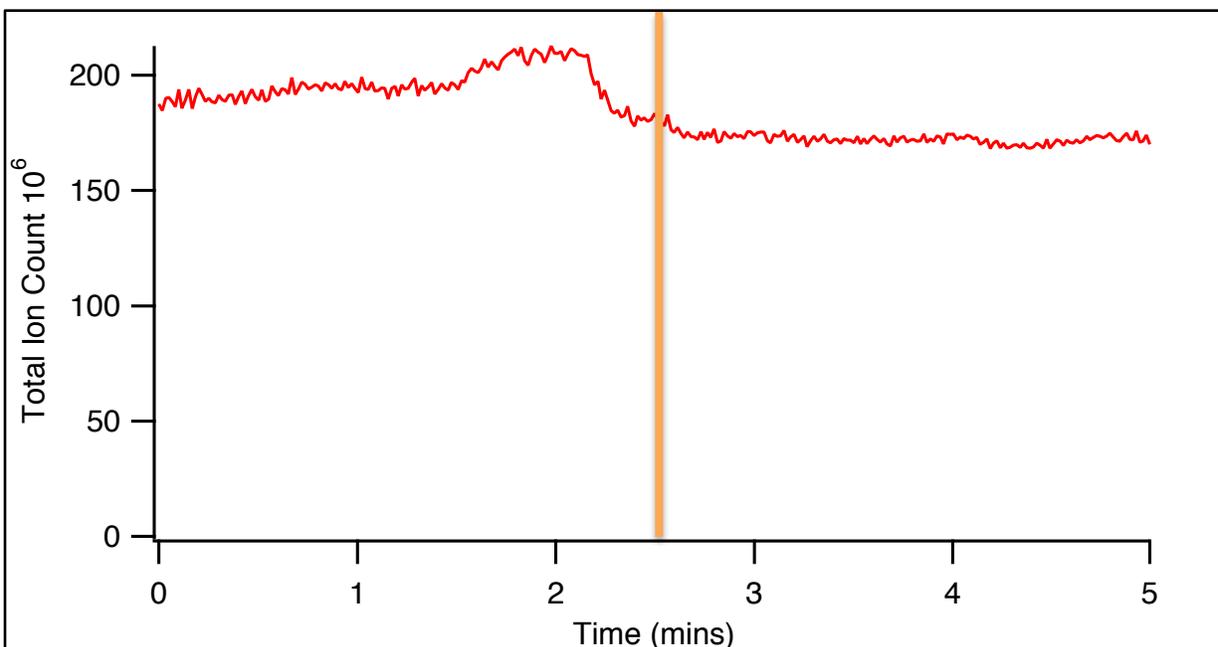
Figure 7.7: Chemical ionization of peracetic acid with and without methanol inside the ion source. The total ion count chromatogram is outlined in red while the vertical orange line indicates when the methanol pump was allowed to operate. Full scan mass spectra outlined in blue and black represent chemical ionization with and without methanol present inside the ion source, respectively.
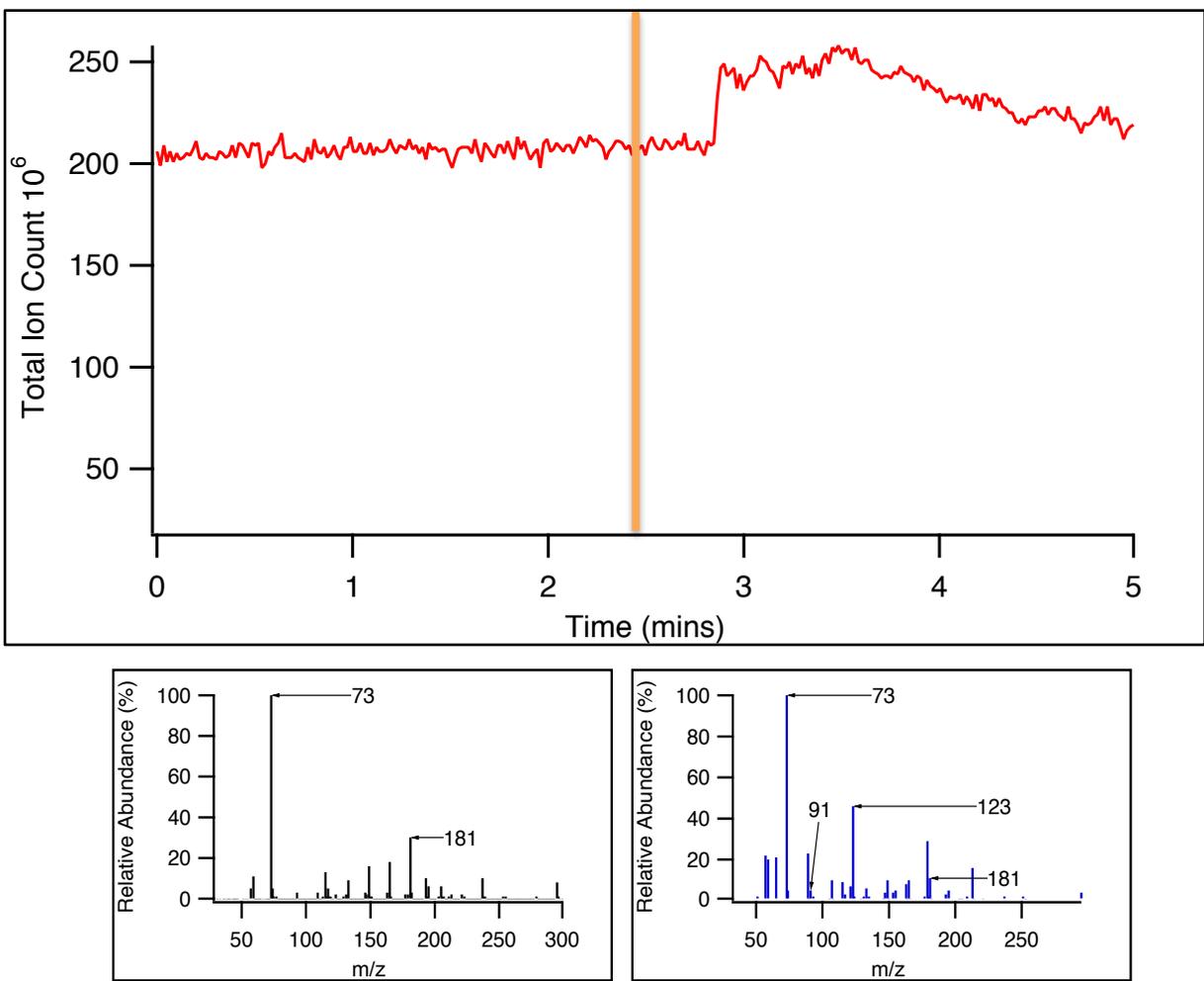
Figure 7.8: Chemical ionization of *tert*-butyl hydroperoxide with and without methanol inside the ion source. The total ion count chromatogram is outlined in red while the vertical orange line indicates when the methanol pump was allowed to operate. Full scan mass spectra outlined in blue and black represent chemical ionization with and without methanol present inside the ion source, respectively.
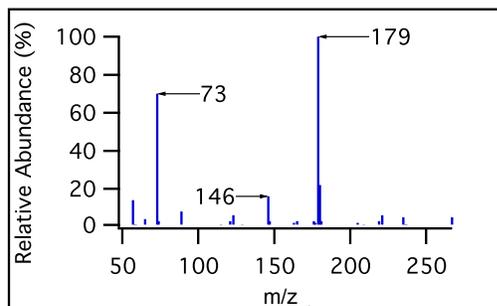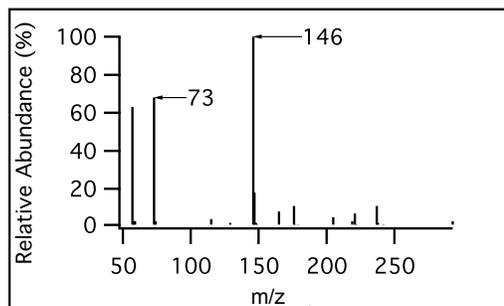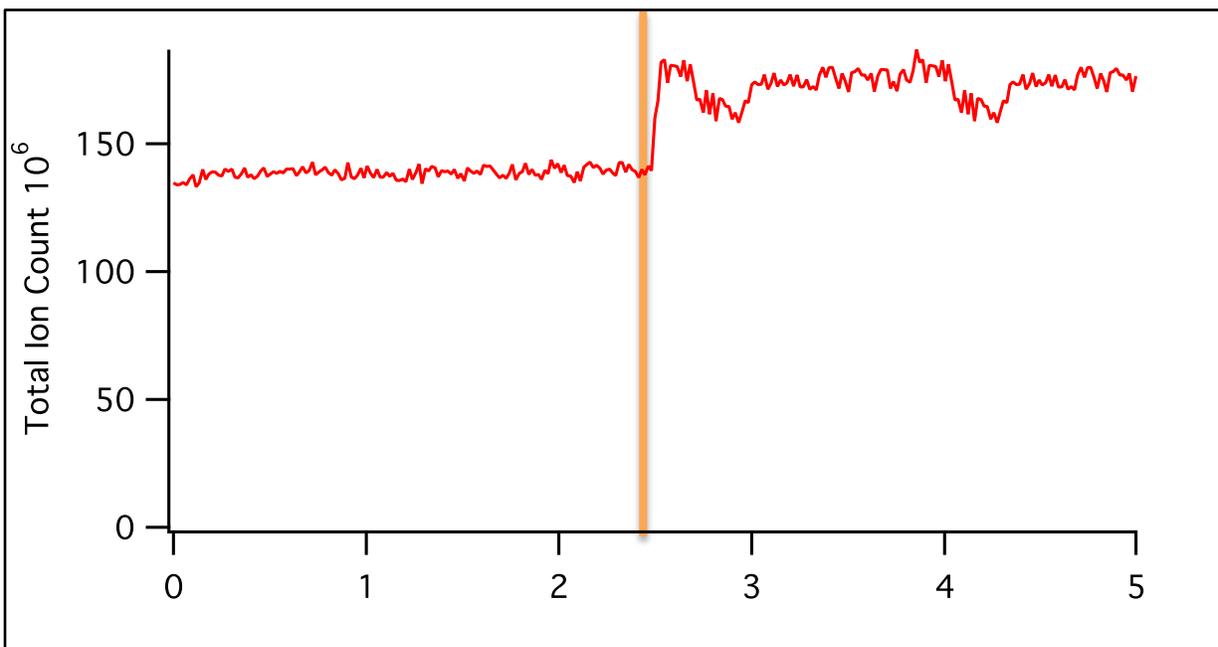
Figure 7.9: Chemical ionization of di-*tert*-butyl peroxide with and without methanol inside the ion source. The total ion count chromatogram is outlined in red while the vertical orange line indicates when the methanol pump was allowed to operate. Full scan mass spectra outlined in blue and black represent chemical ionization with and without methanol present inside the ion source, respectively.
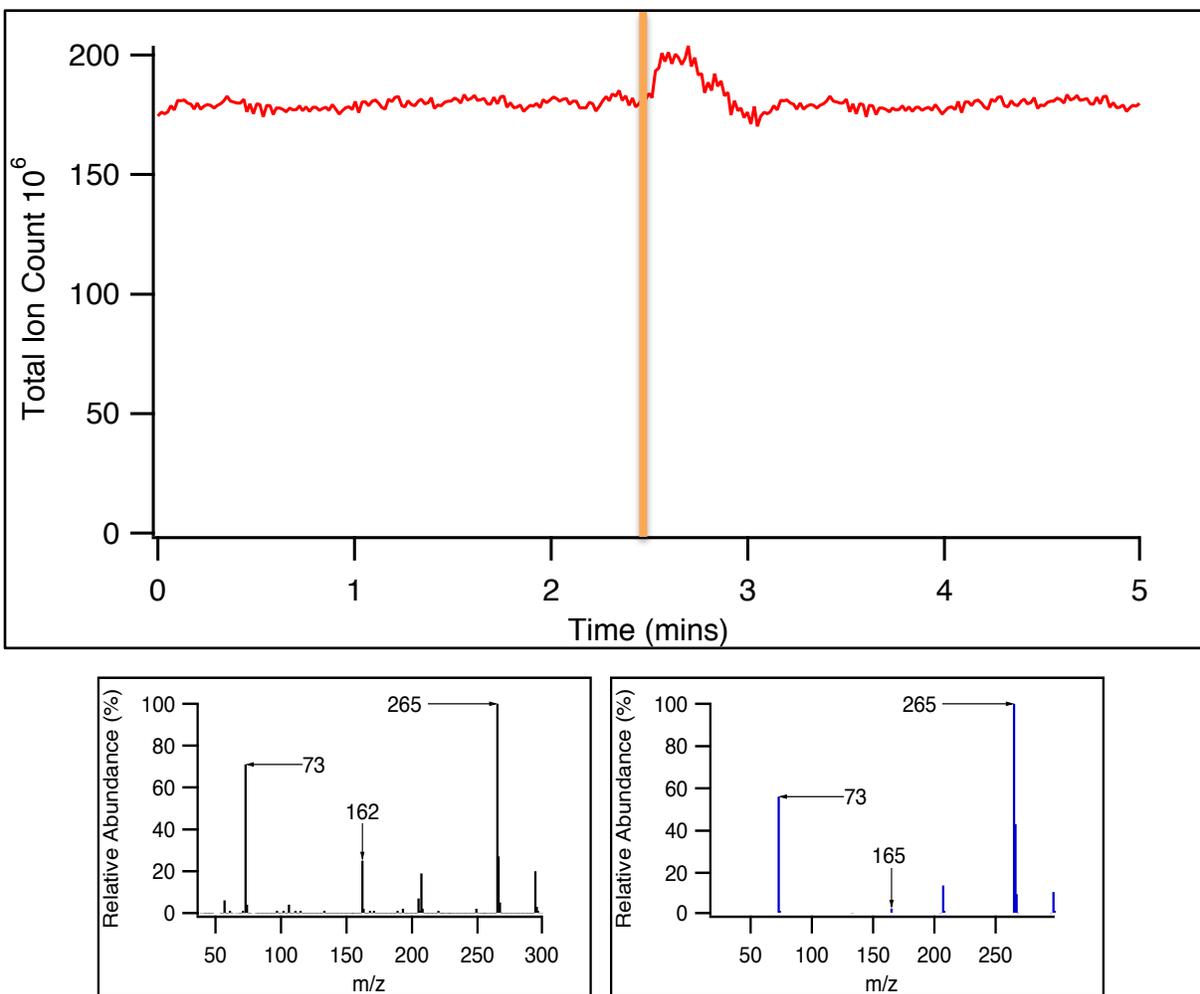
**Figure 7.10:** Chemical ionization of *tert*-butyl peroxyacetate with and without methanol inside the ion source. The total ion count chromatogram is outlined in red while the vertical orange line indicates when the methanol pump was allowed to operate. Full scan mass spectra outlined in blue and black represent chemical ionization with and without methanol present inside the ion source, respectively.

7.1.2.1. Product-Ion Scans

Product-ion scans were acquired to confirm the identity of the products of ionization when methanol was introduced into the APCI ion source. Results are portrayed in Figure 7.11 (a) to (d). All product-ion scans were acquired at a collision energy of 10 eV. During MS/MS studies, a neutral mass loss of 32 u (CH_3OH) was observed from the $[M + CH_3OH + H]^+$ ion signal for *tert*-butyl hydroperoxide, *tert*-butyl peroxyacetate, and peracetic acid. A neutral mass loss of 32 u as opposed to a mass loss of 33 u was expected since the PA for the three organic peroxides was higher than methanol (Table 6.2 and 6.3). Therefore, during MS/MS studies, the organic peroxide standards retained the proton (H^+) from the protonated methanol ion.

Contrastingly, product-ion analysis for the $[M + CH_3OH + H]^+$ ion signal observed during full scan analysis of di-*tert*-butyl peroxide, did not directly display a neutral mass loss of 32 u in the resultant MS/MS spectrum (Figure 7.11 (d)). The only ion signal observed in MS/MS spectrum was *m/z* 73. Previous full scans and product-ion scans of the molecular ion ($[M]^+$, *m/z* 146) for di-*tert*-butyl peroxide revealed that *m/z* 73 was a fragment ion signal attributed to the formed ion cleaving at the peroxy bond. Therefore, it was reasonable to assume that the $[M + 33]^+$ ion signal (*m/z* 179) was still related to di-*tert*-butyl peroxide being ionized with protonated methanol. Nevertheless, the product-ion scans acquired for the selected organic peroxide standards proved that the appearance of ions $[M + 33]^+$ was attributed to gas-phase ionization with protonated methanol.
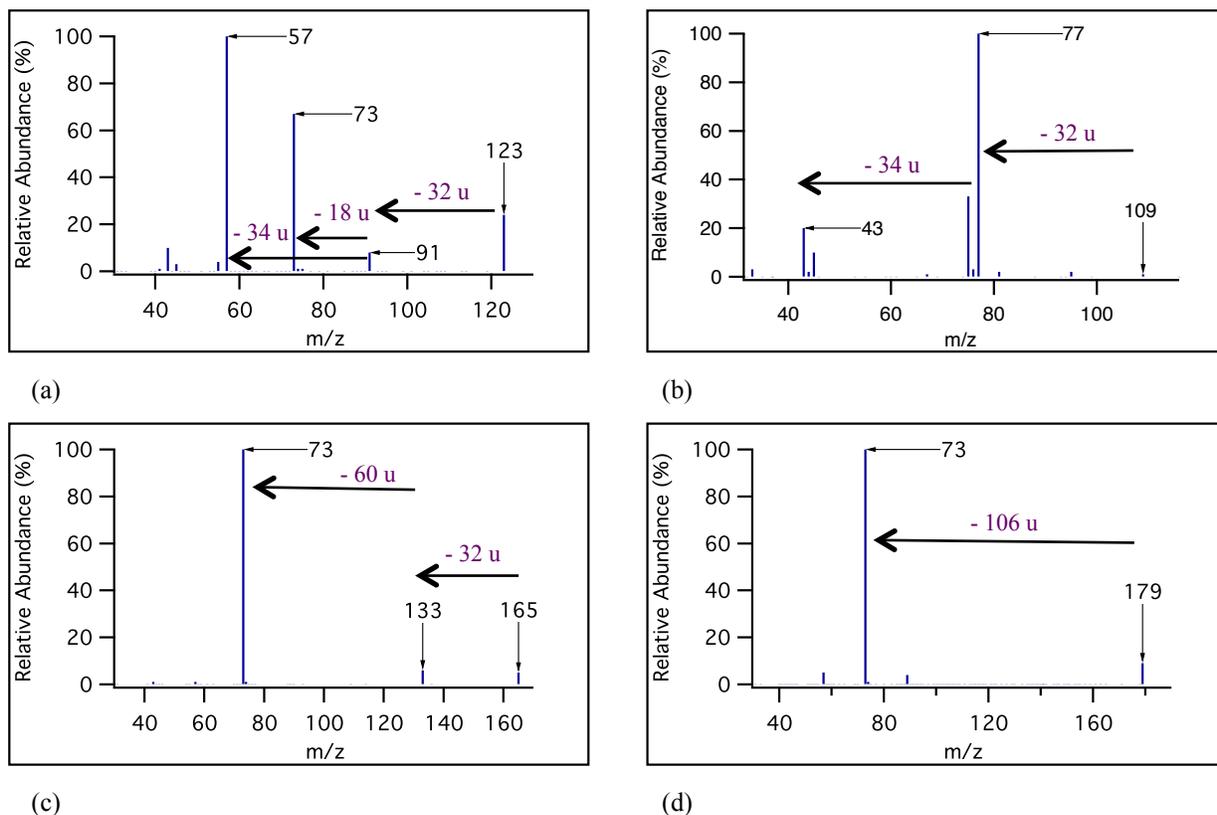
Figure 7.11: Product-ion mass spectra for organic peroxides standards using methanol as an ionization reagent. (a) Represents *tert*-butyl hydroperoxide, (b) *tert*-butyl peroxyacetate, (c) peracetic acid and (d) di-*tert*-butyl peroxide. Product-ion mass spectra were acquired at an APCI-MS/MS CE setting of 10 eV. Mass losses are shown in purple for clarity

7.1.2.2. Neutral-Loss Scan Analysis

During product-ion scan analysis of the $[M + CH_3OH + H]^+$ ion signal for *tert*-butyl hydroperoxide and peracetic acid, ion signals representing $[M + CH_3OH + H - 32]^+$ were apparent in their MS/MS spectra (Figure 7.11 (a) and (c)). Since the observed ion signal ($[M + CH_3OH + H - 32]^+$) for *tert*-butyl hydroperoxide and peracetic acid differed by 1 u from the molecular weight of the two organic peroxides standards analyzed respectively, it was assumed

that this ion signal represented the protonated precursor ion $[M + H]^+$. Given this assumption, NLS analysis was performed for *tert*-butyl hydroperoxide, peracetic acid and cumene hydroperoxide to determine a range of precursor ions capable of losing 34 u. Similar to previous NLS analysis using water as an ionization reagent, the intention was to determine if $[M + H]^+$ ions formed in the APCI ion source could be detected. Results for *tert*-butyl hydroperoxide and peracetic acid are portrayed in Figure 7.12 (a) and (b). Cumene hydroperoxide did not exhibit $[M + H]^+$ ion signal in its neutral-loss scan. This was consistent with the $[M + H]^+$ ion signal not present in previous full scan mass spectrum (Figure 7.5 (e)). Additionally, this observation was expected since it was postulated during early full scan analysis experiments that the PA of methanol might be larger than the PA for cumene hydroperoxide. On the other hand, neutral-loss mass spectrum for *tert*-butyl hydroperoxide and peracetic acid exhibited an easily observable ion signal at *m/z* 91 and *m/z* 77 respectively representing the $[M + H]^+$ ion signal. Similar to NLS analysis with protonated water, ionization with protonated methanol increased the sensitivity for the $[M + H]^+$ ion signal. However, a comparison of NLS scans for *tert*-butyl hydroperoxide revealed that detection of the $[M + H]^+$ ion signal was vastly improved using protonated methanol as opposed to protonated water as an ionization reagent (Figure 7.13).
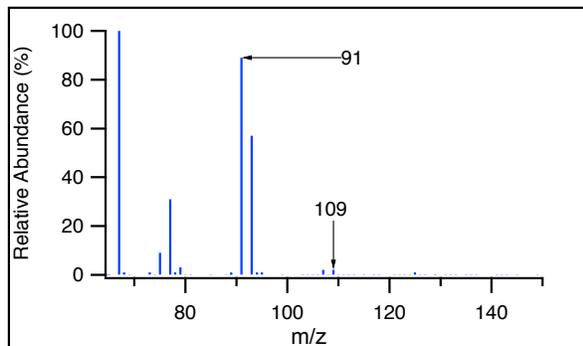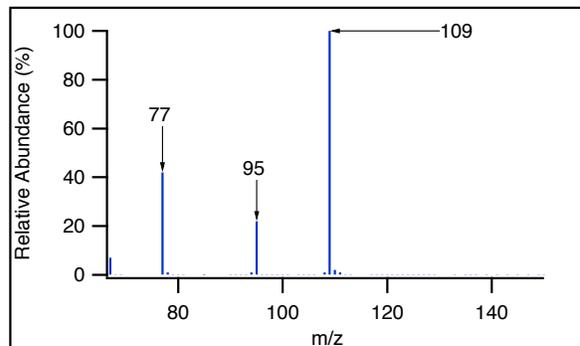
Figure 7.12: NLS mass spectra for 34 u mass loss. (a) Represents *tert*-butyl hydroperoxide and (b) peracetic acid. Protonated methanol was used the ionization reagent. NLS mass spectra were acquired at an APCI-MS/MS CE setting of 10 eV.
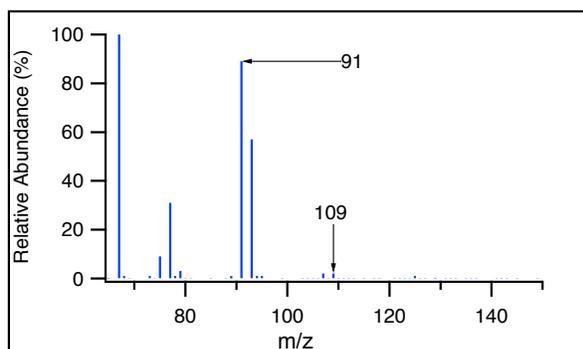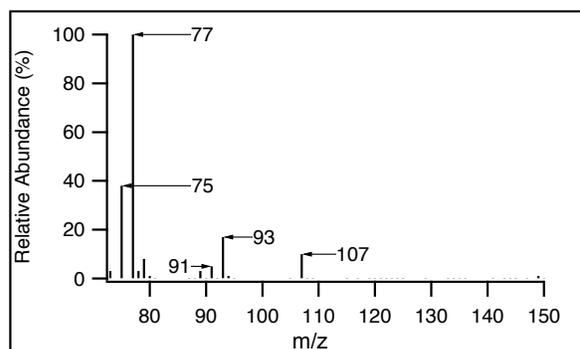
Figure 7.13: NLS mass spectra for 34 u mass loss using protonated methanol (a) or protonated water as an ionization reagent (b) during analysis of *tert*-butyl hydroperoxide. NLS mass spectra were acquired by setting the APCI-MS/MS CE to 10 eV

In the case of peracetic acid, the relative intensity for the *m/z* 77 ($[M + H]^+$) ion signal decreased when protonated methanol was used in comparison to the results obtained using protonated water. However, this relative decrease was caused by the appearance of the *m/z* 109 ($[M + CH_3OH + H]^+$) ion signal. Its presence in the neutral-loss mass spectrum meant that this ion lost 34 u from its structure during collision events. Moreover, this was validated by

77

previously acquired product-ion scans by the presence of *m/z* 75 ion signal ([M + CH$_3$OH + H −

34]$^+$) in the MS/MS spectrum (Figure 7.11 (b)). Although the primary focus of the project was

not to study the fragmentation pathway in great detail, some observations were made regarding

the possibility for a [M + CH$_3$OH + H]$^+$ ion's ability to lose 34 u. Figure 7.14 shows a

rudimentary diagram for adduct formation in the ion source. The portrayed schematic shows that

certain orientations of the protonated methanol ion coupled with hydrogen bonding between

oxygen and hydrogen could make this loss possible.
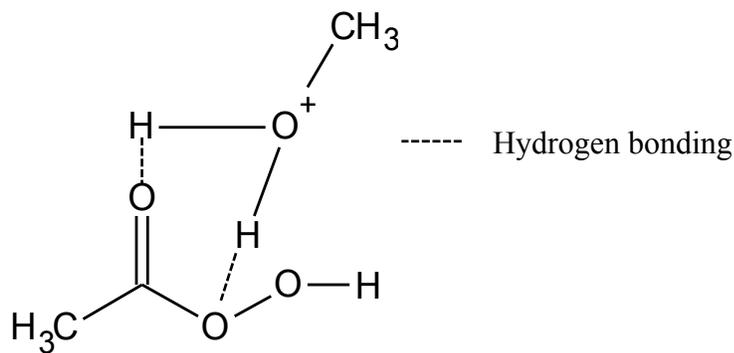
Figure 7.14: General schematic rationalizing the loss of 34 u from a protonated adduct with
methanol.

Regardless of the ionization reagent used, NLS analysis appeared to be a more selective

method for detecting organic peroxides containing a hydroperoxy moiety. The acquired MS/MS

spectra demonstrated the ability to simplify a range of *m/z* ions based on a characteristic neutral

fragment loss of 34 u. The advantage of this type of scan would continue to be useful during β-

pinene ozonolysis experiments where *m/z* ions relating to a specific neutral mass loss could be

ascertained and studied further. The applications of NLS analysis during ozonolysis experiments are discussed in detail in Section 8.0.

7.1.3. Methanol Introduced Directly into the Ion Source

In this experiment, methanol was introduced directly into the APCI ion source independent of standard introduction. This experimental design was described previously and was shown in Figure 6.3 (b). This was in contrast to the experiments conducted previously and described in Section 7.1.2 where methanol and standard were mixed, introduced into a purified airflow, and then transferred to the APCI ion source using the same transfer line (Figure 6.4). The intent was to validate the ion-molecule chemistry observed in the Section 7.1.2. Furthermore, general operation of the APCI-MS/MS involved ionization reagents being directly supplied to the source. Under those circumstances, experiments were conducted using the experimental design depicted in Figure 6.3 (b)

Results for this experiment are portrayed in Figure 7.15 (a) to (d). Experiments with cumene hydroperoxide were not conducted since previous experiments showed that cumene hydroperoxide could not be ionized using protonated methanol as an ionization reagent. Nevertheless, results were obtained by utilizing single ion monitoring analysis mode of the APCI-MS/MS to monitor the expected $[M + CH_3OH + H]^+$ ion signal for all organic peroxide standards pre- and post ionization with protonated methanol and its clusters. While the total acquisition time was 6 minutes for all experiments, the methanol syringe pump operated between 2 to 4 minutes to produce changes in the $[M + CH_3OH + H]^+$ ion signal.
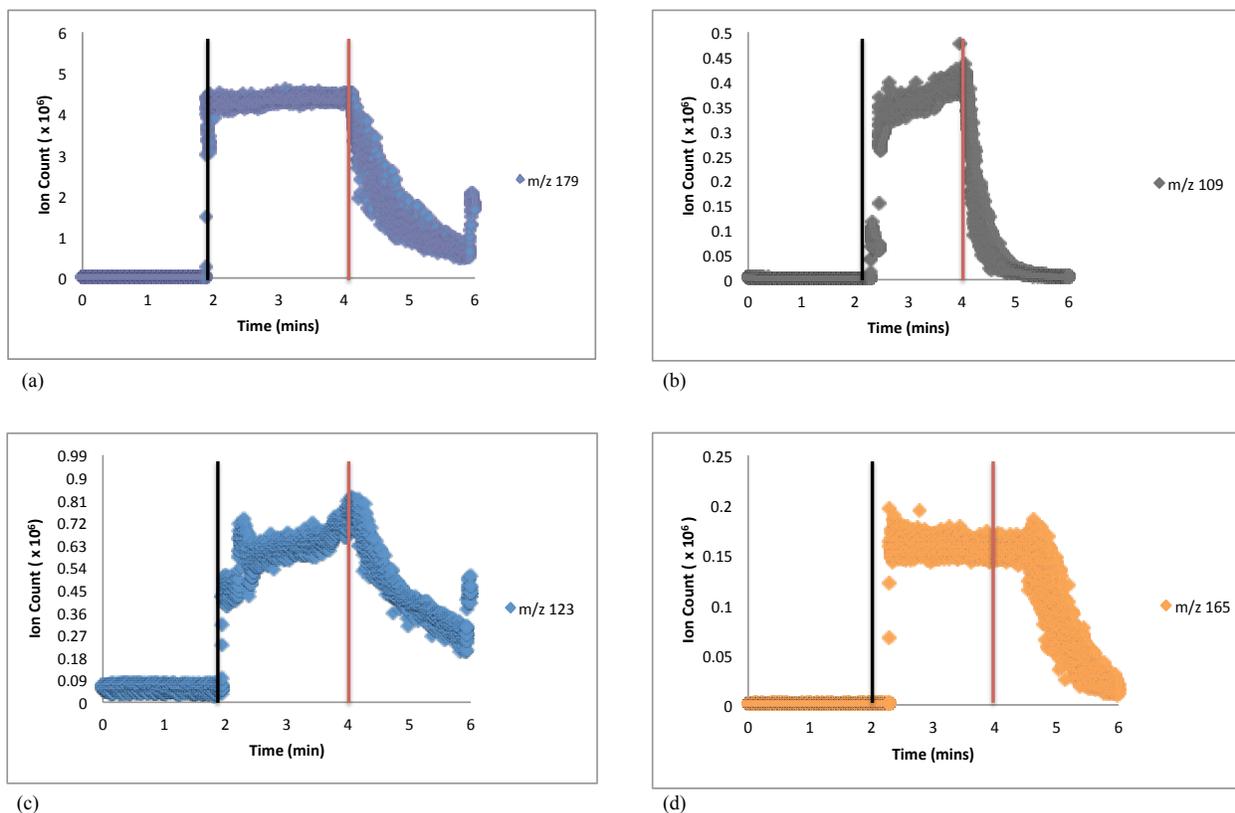
Figure 7.15: SIM analysis for the expected $[M + CH_3OH + H]^+$ ion for (a) di-*tert*-butyl peroxide, (b) *p*eracetic acid, (c) *tert*-butyl-hydroperoxide and (d) *tert*-butyl peroxyacetate. The vertical black line indicates when the methanol syringe pump was turned on while the vertical red line indicates when the methanol syringe pump was turned off.

The results portrayed in Figure 7.15 (a) to (d) showed that the $[M + CH_3OH + H]^+$ ion signal was not observed in mass spectra during the first and last 2 minutes of the experiment when the methanol syringe pump was not operating. Increases in the $[M + CH_3OH + H]^+$ ion signal was only observed when the methanol syringe pump was operating between 2 to 4 minutes. Between 4 to 6 minutes of the experiment Figure 7.15 (a) to (d) showed that the $[M + CH_3OH + H]^+$ ion signal slowly declined as the methanol syringe pump was no longer operating. This slow declined suggested the possibility that methanol was adsorbing onto the transfer line.

80

To test this notion, the effective residence time (τ) for methanol was calculated for all four organic peroxide standards and compared to the effective residence for purified air inside the transfer line. Calculations were based on the dimensions of the transfer line (60 centimeters in length and 0.125 inch inner diameter), a purified airflow of 5 L min^{-1} and assuming a first order loss rate. Equation 7.1 and 7.2 was used to calculate τ for both methanol and purified air, respectively. To determine the rate constant (k) in Equation 7.2, a plot of ln ($[M + CH_3OH + H]^+$ ion count) versus time was generated for each standard. This plot gave a straight line with the slope equal to $-k$ (Equation 7.3). The calculated τ for methanol ranged from 0.468 minutes to 1.97 minutes while τ for purified air was determined to be 9.50 x 10^{-4} minutes. The 3 to 4 orders of magnitude difference between the calculated τ for methanol and purified indicated that methanol adsorbed onto the transfers lines during the experiments.

$$\tau_{purified\ air} = \frac{\pi r^2 L}{airflow} \qquad\qquad \text{Equation 7.1}$$

$$\tau_{methanol} = \frac{1}{k} \qquad\qquad \text{Equation 7.2}$$

$$ln([M + CH_3OH + H]^+ ion)_t = -kt + ln([M + CH_3OH + H]^+)_0 \qquad\qquad \text{Equation 7.3}$$

In short, this aspect of the project validated the ion-molecule chemistry described by Reaction 6.7. Moreover, it showed that the $[M + CH_3OH + H]^+$ ion could be produced in the APCI ion source when methanol was supplied directly to the ion source independent to standard introduction (Figure 6.3 (b)). For this reason, it was concluded that methanol could be introduced directly to the ion source without prior contact or mixing with standards. Therefore, all future

smog chamber experiments could be conducted using the experimental set-up depicted in Figure 6.3 (b).

7.1.4. Comparison of Water and Methanol as an Ionization Reagent

For gas-phase protonation to occur, the PA of the neutral molecule must be higher than the PA of the ionization reagent. Although the PA for most of the organic peroxide standards used in this experiment satisfied this requirement (Table 6.3), the acquired full scan mass spectra yielded unexpected results. Generally, ionization using protonated water resulted in full scan mass spectra dominated by fragmented ions while ionization with protonated methanol resulted in a protonated adduct ion. This meant that the criterion of having a higher PA than the ionization reagent was not sufficient for developing a method to detect organic peroxides.

Given this, an evaluation of both ionization reagents was required. This was based on PA knowledge for both ionization reagents and acquired full scans, neutral-loss scans and product-ion scans for all standards. Collectively, these results showed that methanol was a more appropriate ionization reagent for the detection of organic peroxide standards. Although $[M + H]^+$ ions were not apparent, adduct ion signals $[M + CH_3OH + H]^+$ were observed during the analysis for four out of five organic peroxides tested. As described in Section 3.1.1, adduct ions form when the PA of a neutral molecule and ionization reagent are similar or the exothermicity ($-\Delta H^\circ_{reaction}$) of the overall proton transfer reaction is low.

A comparison of calculated $\Delta H^\circ_{reaction}$ for all organic peroxides with protonated methanol or water as an ionization reagent is portrayed in Table 7.1. The lower $\Delta H^\circ_{reaction}$ for methanol in comparison to water indicated that methanol can achieve a softer ionization for the organic

peroxide standards used in this project. As a result, intact adduct ions were observed since there was less excess energy available to facilitate the further fragmentation of any type of protonated parent molecules ($[M + H]^+$, $[M + H_2O + H]^+$, or $[M + CH_3OH + H]^+$). Contrastingly, the relatively larger $\Delta H°_{reaction}$ calculated for chemical ionization using protonated water resulted in more energy being transferred to the formed protonated molecule $[M + H]^+$. This caused the higher fragmentation observed during full scan analysis of organic peroxide standards.

Table 7.4: Enthalpy of the overall gas-phase protonation reaction ($\Delta H°_{reaction}$)

Compound	PA (kJ mol^{-1})	Water as Ionization Reagent	Methanol as Ionization Reagent
tert-butyl hydroperoxide	803	-107	-37
di-*tert*-butyl peroxide	790	-94	-24
cumene hydroperoxide	696 – 766*	-	-
peracetic acid	783	-87	-17
peroxyacetate	791	-95	-25

* This value was revised after data interpretation. The resultant value was reported as a range since PA for cumene hydroperoxide was not known. Its range was inferred from its reaction with protonated water and methanol ions in the ion source.

7.1.5. Optimal Ionization Reagent Flow

Since ionization with protonated methanol proved to be a more selective method for organic peroxide detection, the utility of this reagent was further investigated. Before conducting ozonolysis experiments, an optimum ionization reagent flow was established to maximize the [M

+ CH$_3$OH + H]$^+$ ion signal for organic peroxide standards. This was done using the direct method for ionization reagent introduction (Figure 6.3 (b)). To determine an optimal flow, the rate of the ionization reagent syringe pump was varied. The results for these experiments are depicted in Figure 7.16 (a) to (d). The observed graphs show that there was an initial increase for the [M + CH$_3$OH + H]$^+$ ion signal upon increasing the concentration of methanol used as an ionization reagent for *tert*-butyl hydroperoxide, di-*tert*-butyl peroxide, and peracetic acid (Figure 7.16 (a), (b) and (d)). However, increasing the concentration of methanol higher than 0.01 ppm resulted in a decrease in the [M + CH$_3$OH + H]$^+$ ion signal for *tert*-butyl hydroperoxide and peracetic acid (Figure 7.16 (a) and (d)). While the [M + CH$_3$OH + H]$^+$ ion signal for di-*tert*-butyl peroxide remained stable at methanol concentrations higher than 0.01 ppm, the [M + CH$_3$OH + H]$^+$ ion signal for *tert*-butyl peroxyacetate reached its maximum at the lowest methanol concentration output of 0.00334 ppm, declined, and stabilized at higher concentrations of methanol. Overall, it appeared that the [M + CH$_3$OH + H]$^+$ ion signal was optimized under low syringe pump settings. Based on the observed graphs, a syringe pump setting around 0.2 μL min^{-1} was selected for future experiments.
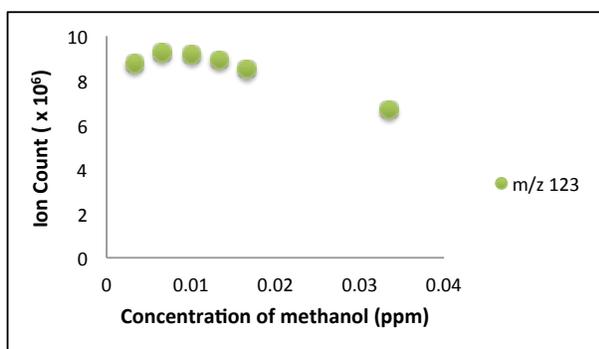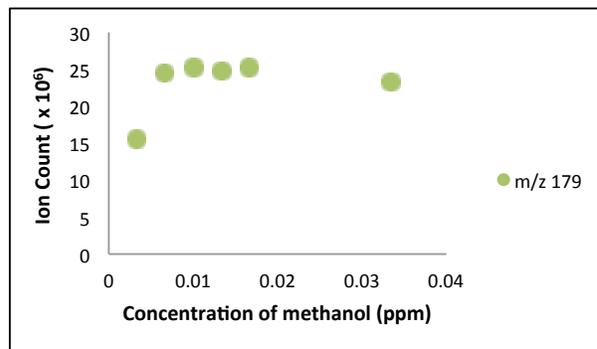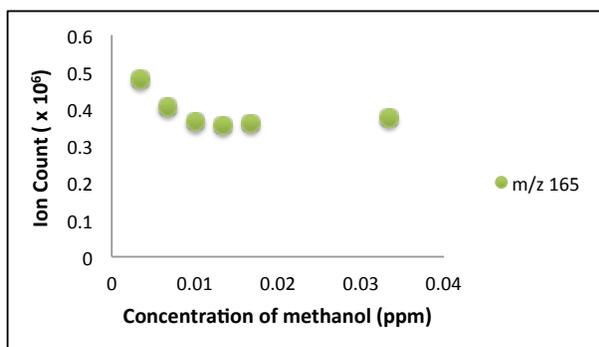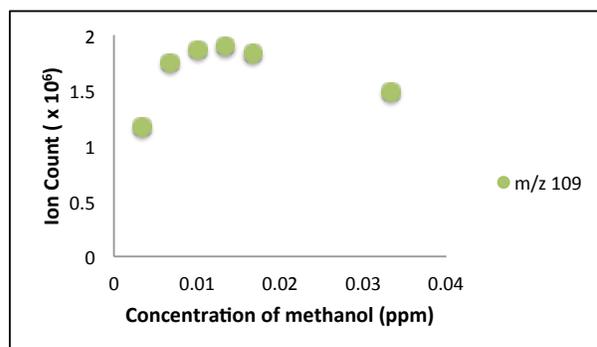
Figure 7.16: Graphs depicting the observed [M + CH₃OH + H]⁺ ion signal as a function of methanol concentration. (a) *tert*-butyl hydroperoxide, (b) di-*tert*-butyl peroxide, (c) *tert*-butyl peroxyacetate and (d) peracetic acid.

7.2. Summary for the Analysis of Commercially Available Organic Peroxide Standard by (+) APCI-MS/MS

Developing a method for organic peroxide detection required knowledge regarding its ion-molecule chemistry while using an (+) APCI-MS/MS. This was achieved by analyzing commercially available organic peroxide standards with the (+) APCI-MS/MS. The intention was to note commonalties such as similar mass losses during MS/MS experiments that would assist in developing a "fingerprint" analysis that could be applied to search for organic peroxide formation during β-pinene ozonolysis experiments.

Early experiments using protonated water for gas-phase ionization of selected standards resulted in full scan mass spectra dominated by fragmented ions. As a consequence, sufficient amount of intact ions ($[M + H]^+$ and $[M + H_2O + H]^+$) could not be observed or isolated by the APCI-MS/MS for further MS/MS experiments. Moreover, no common features could be ascertained from the resulting full scan mass spectra to develop a "fingerprint" for organic peroxide detection. Ionization with protonated water was determined to be unsuitable since the $\Delta H°_{reaction}$ was large enough to produce excess energy available to further fragment any intact ions produced in the ion source. Conversely, the $\Delta H°_{reaction}$ calculated for organic peroxide standards chemically ionized using protonated methanol was small enough to produce protonated stable adduct ions in full scan mass spectra. This proved to be more useful since the resultant stable protonated adduct ions could be isolated and fragmented to determine common mass losses to assist in developing a "fingerprint" methodology.

Collectively, the knowledge acquired from neutral-loss and product-ion scans along with gas-phase ionization using either protonated water or methanol was applied to establish a method for organic peroxide detection. It was determined that resultant products from ozonolysis experiments should be ionized using protonated methanol injected into the ion source at a flow rate of 0.2 μL min^{-1} using the direct syringe pump method. Since organic peroxides were the compounds of interest in this project NLS would be utilized to determine a range of *m/z* ions capable of losing 34 u.

8. Results and Discussion for β-pinene Ozonolysis Experiments

β-pinene/ozonolysis experiments were conducted using an 8 m^3 cylindrical smog chamber at York University. Ozonolysis products were detected on-line using (+) APCI-MS/MS. Smog chamber studies were undertaken to determine if the fingerprint method established during organic peroxide standard analysis could be successfully applied (Section 7.1.1.1 and 7.1.2.2). Similar to organic peroxide standard analysis, ozonolysis products were chemically ionized using either water or methanol in purified air as an ionization reagent.

8.1. Smog Chamber Products Ionized with Protonated Water

Full scan mass spectra for the reaction of β-pinene with O$_3$ were acquired using water as an ionization reagent inside the APCI ion source. An example of a full scan mass spectrum is portrayed in Figure 8.1 (a). The acquired full scan mass spectrum was dominated by odd-numbered m/z ions 139, 155, 277 and 293. The appearance of odd-numbered m/z ions were expected since it was assumed that ozonolysis products formed in the smog chamber would exclusively consist of carbon (C), hydrogen (H), and oxygen (O) in its resultant structure. Organic products with some variation of the structural formula $C_x H_y O_z$ have an even nominal mass since these elements together, form even number of covalent bonds. Therefore, the presence of odd-numbered m/z ion signals were a result of even-mass ozonolysis products being protonated at either the carbonyl or hydroxyl functional group region of the ozonolysis product to form an m/z ion signal that was 1 u higher than the nominal mass of the ozonolysis product.
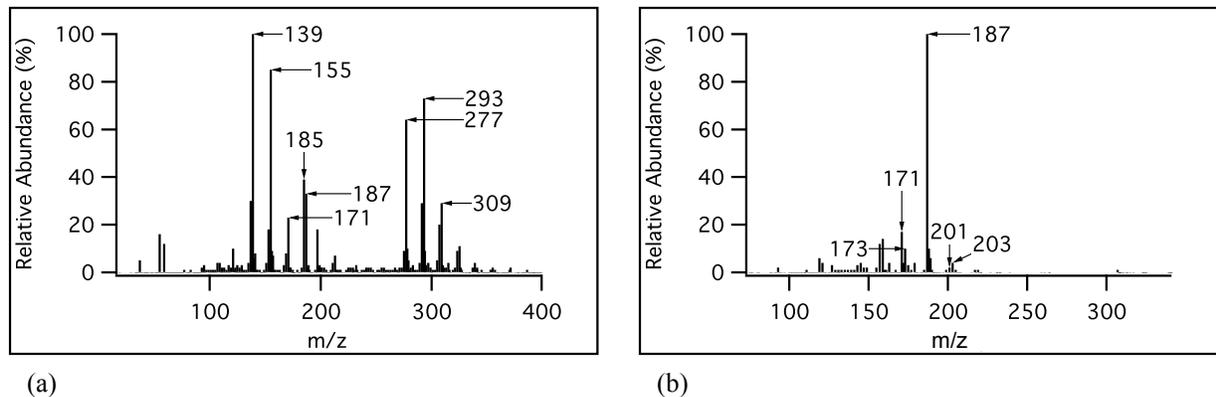
Figure 8.1: Mass spectra for β-pinene ozonolysis. (a) Represents a full scan mass spectrum while (b) represents a 34 u neutral-loss scan mass spectrum acquired an APCI-MS/MS CE setting of 10 eV.

Although the full scan mass spectrum shown in Figure 8.1 (a) revealed a range of *m/z* ions, this analysis mode does not provide structural information for the detected ion signals. Furthermore, this analysis mode is not as sensitive since Q_1 is focusing on a wide range of products over time (Section 4.1.4). Therefore, this analysis mode was not useful for organic peroxide detection. Enhanced sensitivity was achieved when oxidation products were analyzed using the NLS analysis mode of the APCI-MS/MS. Setting the APCI-MS/MS to only detect a range of *m/z* ions losing 34 u during collision events, greatly reduced the complexity observed in Figure 8.1 (a) to a handful of *m/z* ions displayed in Figure 8.1 (b). Since this project was only concerned with organic peroxide identification, this analysis mode revealed *m/z* ions that were possible organic hydroperoxide candidates. Similar to the organic peroxide standard analysis, a loss of 34 u was attributed to a loss of H_2O_2 from the $[M + H]^+$ ion signal during protonation followed by collisions with collision gas. Overall, the resultant NLS mass spectrum revealed five *m/z* ion signals of interest since they were capable of losing 34 u from its structure; *m/z* 171, 173, 187, 201, and 203.

8.1.1. Smog Chamber Products Ionized with Protonated Methanol

Early experiments with organic peroxide standards revealed that fragmented ions dominated the full scan mass spectrum when water was used as an ionization reagent. Since intact ions representing $[M + H]^+$ and $[M + H_2O + H]^+$ were not observed, this prevented conducting MS/MS experiments to confirm standard structures or ascertain common mass losses. Considering this, it was suspected that organic peroxides formed during ozonolysis experiments could exhibit similar behaviour during full scan analysis mode. Since protonation of organic peroxide standards using protonated methanol resulted in the appearance of protonated adduct ions $[M + CH_3OH + H]^+$ in full scan mass spectra and improved detection of $[M + H]^+$ ion signals during NLS analysis mode for 34 u mass loss, it was suspected that utilizing methanol as an ionization reagent could lead to improved organic peroxide identification during ozonolysis experiments.

Since chemical ionization using protonated methanol produces $[M + CH_3OH + H]^+$ ions in full scan analysis mode, a list of expected *m/z* ions was generated before smog chamber ozonolysis products were analyzed by APCI-MS/MS. The generated list was based on *m/z* ion signals ($[M + H]^+$) observed in full scan mass spectrum shown in Figure 8.1 (a) and *m/z* ions representing organic hydroperoxide candidates from NLS mass spectrum as shown in Figure 8.1 (b). The expected *m/z* ion signals are shown in Table 8.1. Once ozonolysis experiments were conducted, full scan and NLS mass spectra were acquired using (+) APCI-MS/MS. Figure 8.2 (a) shows an example of an acquired full scan mass spectrum for ozonolysis products chemically ionized using protonated methanol while Figure 8.2 (b) portrays a NLS mass spectrum for precursor *m/z* ions losing 34 u during collision events. Similar to the results discussed in Section 8.1, the full scan mass spectrum shown in Figure 8.2 (a) was dominated by a range of odd-

numbered *m/z* ions. These ion signals were a result of either proton transfer to form *m/z* ion signals representing $[M + H]^+$ or adduct ion formation to form $[M + CH_3OH + H]^+$ ion signals. Additionally, the full scan mass spectrum in Figure 8.2 (a) displayed similar *m/z* ion signals as Figure 8.1 (a). Like the full scan mass spectrum shown in Figure 8.1 (a), the observed full scan mass spectrum depicted in Figure 8.2 (a) did not give first-hand information regarding which observed *m/z* ion signals represented organic peroxides. However, the full scan mass spectrum shown in Figure 8.2 (a) revealed that three out of five expected *m/z* ions listed in Table 8.1 were apparent. A summary of the expected *m/z* ions observed in the full scan mass spectrum is shown in Table 8.2. Ozonolysis products having a nominal mass of 170, 172 and 186 g mol^{-1} formed a $[M + CH_3OH + H]^+$ ion signal upon chemical ionization with protonated methanol. Since these ozonolysis products formed a $[M + CH_3OH + H]^+$ ion signal, it was reasonable to assume that the PA of these compounds were close to or greater than the PA of methanol.

Table 8.1: List of expected *m/z* ion signals during chemical ionization with protonated methanol

Nominal Mass (g mol^{-1})	Expected m/z Ion Signal $[M + CH_3OH + H]^+$
170	203
172	205
186	219
200	233
202	235
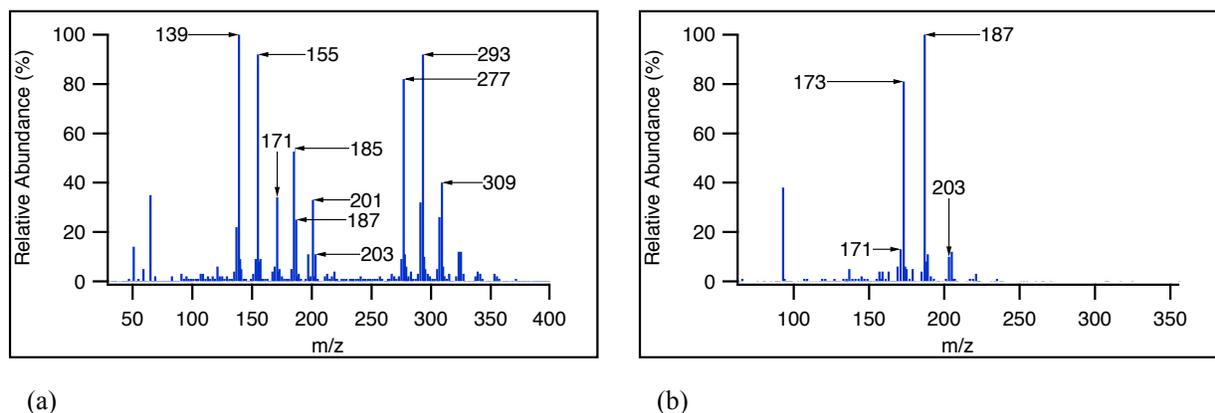
Figure 8.2: Mass spectra for β-pinene ozonolysis products chemically ionized with protonated methanol. (a) Represents a full scan mass spectrum while (b) represents a 34 u NLS mass spectrum acquired at an APCI-MS/MS CE setting of 10 eV.

Table 8.2: Summary of expected *m/z* ion signals observed in full scan mass spectrum

Nominal Mass (g mol^{-1})	Expected m/z Ion Signal [M + CH$_3$OH + H]$^+$	Observed Expected m/z Ion Signal [M + CH$_3$OH + H]$^+$
170	203	Yes
172	205	Yes
186	219	Yes
200	233	No
202	235	No

Similar to NLS analysis using protonated water as an ionization reagent (Figure 8.1 (b)), the full scan mass spectrum depicted in Figure 8.2 (a) was simplified by acquiring a NLS mass spectrum for a range of *m/z* ions capable of losing 34 u during collision events (Figure 8.2 (b)). During organic peroxide standard analysis using methanol as an ionization reagent, standards

containing a hydroperoxy group were easily detected as $[M + H]^+$ ions while utilizing the NLS analysis mode of the APCI-MS/MS to determine a range of *m/z* ions that lost 34 u during collision events (Ssection 7.1.2). Given these observations, smog chamber ozonolysis products were additionally analyzed using the NLS analysis mode to find additional organic hydroperoxide candidates, which were not apparent during initial NLS analysis described in Section 8.1. A comparison of NLS mass spectra for both ionization reagents is portrayed in Figure 8.3 (a) and (b). While Figure 8.3 (a) showed *m/z* ions 171, 173, 187, 201 and 203 as ions that lost 34 u during collision events, Figure 8.3 (b) showed *m/z* ions 171, 173, 187 and 203 as ions that exhibited a loss of 34 u. Consequently, 34 u NLS mass spectrum shown in Figure 8.3 (b) did not yield additional organic hydroperoxide candidates.

(a)   (b)
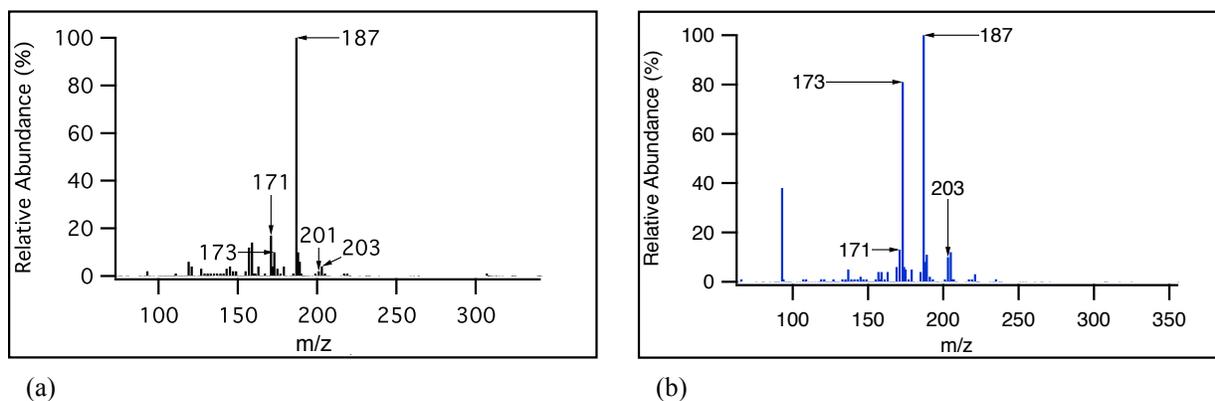
Figure 8.3: 34 u NLS mass spectra obtained by setting APCI-MS/MS CE to 10 eV. (a) Represents NLS mass spectrum using protonated water while whereas (b) was obtained using protonated methanol.

Overall, it was apparent that additional organic hydroperoxide candidates were not obtained using methanol as an ionization reagent. This was contrary to the results obtained

during organic peroxide standard analysis. Moreover, it was apparent that not all ozonolysis products were capable of forming a protonated adduct ion $[M + CH_3OH + H]^+$ in the APCI ion source. For instance of the five expected *m/z* ions listed in Table 8.1, only three were actually observed in the full scan mass spectrum (Figure 8.2 (a)). Collectively, the results summarized in Table 8.2 along with full scan and NLS mass spectra shown in Figure 8.2 (a) and (b) respectively, did not provide enough information to continue using methanol as an ionization reagent during smog chamber experiments. As a result, organic peroxide detection by the APCI-MS/MS continued by using water present in purified air as an ionization reagent.

8.2. Product-ion Scan Analysis for Smog Chamber Products

Since it was established in the previous section that chemical ionization using protonated methanol did not identify additional organic hydroperoxide candidates, APCI-MS/MS continued by using water from purified air as an ionization reagent. To confirm the loss of 34 u during collision events, ascertain additional common mass losses and ultimately suggest structures to represent the precursor molecule, product-ion scan analysis was conducted using the APCI-MS/MS. Product-ion scans for precursor ions *m/z* 171,173, 187, 201 and 203 are shown in Figure 8.4 (a) to (e) where a loss of 34 u was observed during MS/MS experiments of the precursor ions $[M + H]^+$. These ion signals were previously identified as organic hydroperoxide candidates in smog chamber experiments described in Section 8.1. For some precursor ions like *m/z* 171, 173, and 201 the loss of 34 u was minor in comparison to other losses displayed in their respective product-ion mass spectrum whereas *m/z* 187 and 203 showed a significant loss of 34 u in their product-ion mass spectrum. Regardless of the signal intensity representing a loss of 34 u [M + H

$- H_2O_2]^+$, the acquired product-ion mass spectra supported the results obtained initially through

NLS analysis described in Section 8.1.
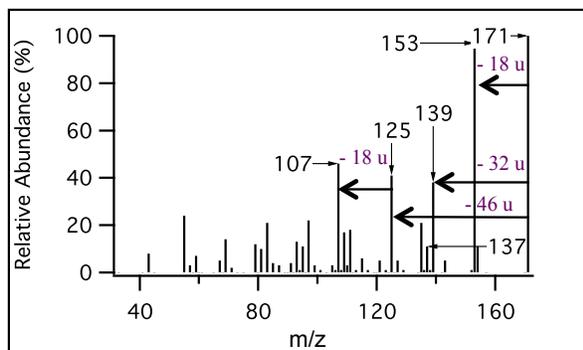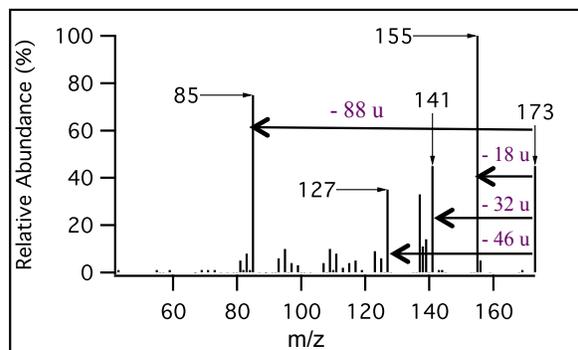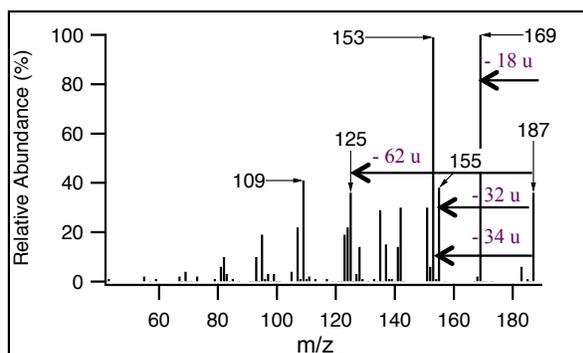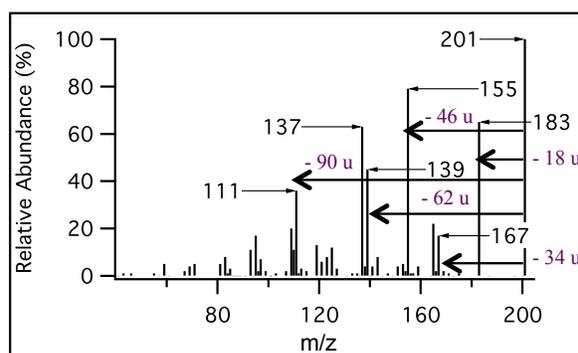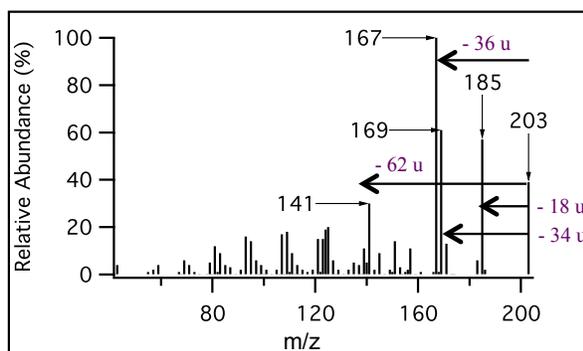
Figure 8.4: Product-ion mass spectra for *m/z* (a) 171, (b) 173, (c) 187, (d) 201 and (e) 203. Product-ion scans were acquired by setting the APCI-MS/MS CE to 10 eV. Selected precursor ions were organic hydroperoxide candidates based on NLS analysis for 34 u loss shown in Figure 8.1 (b). Mass losses are shown in purple for clarity.

Aside from an observed loss of 34 u, additional common mass losses were observed while comparing the product-ion mass spectra of all five selected m/z ions of interest. For instance, losses of 18 u (H_2O) from precursor ion signal $[M + H]^+$ indicated the presence of an alcohol (OH) functional group within the precursor ion structure. Other common mass losses like 32 u and 62 u were observed at various intensities for all five m/z ions of interest. Fragments representing a single neutral fragment loss of 32 u and 62 u are summarized in Table 8.3. These fragments were derived based on precursor ion's elemental composition of $C_x H_y O_z$. Most neutral mass losses listed in Table 8.3 can be explained from different combinations of smaller mass losses. For instance a mass loss of 32 u could arise from sequential losses of 18 u (H_2O) and 14 u (CH_2). However, a neutral loss of CH_2 is highly unlikely. However, a loss of 32 u was previously observed and rationalized during organic peroxide standard analysis of cumene hydroperoxide (Figure 7.2). During analysis of cumene hydroperoxide, protonation in the APCI ion source did not occur at the hydroperoxy functional group as expected. Protonation occurred within the ring of the molecule allowing the elimination of an O_2 molecule during MS/MS experiments. Therefore, the observed mass loss of 32 u during product-ion scan analysis was attributed to a loss of O_2. On the other hand, 62 u could reasonably be a result of a sequential neutral mass loss of 18 u (H_2O) and 44 u (CO_2) or 34 u (H_2O_2) and 28 (CO). This type of loss presented an interesting scenario to consider since it introduced the possibility that some of the observed oxidation products might be an organic peroxy acid (as shown in Figure 7.3) as opposed to an organic hydroperoxide (as shown in Figure 7.3). Total mass losses of 62 u were investigated further and will be discussed in Section 8.2.3. Regardless of the mass loss combination, it was apparent that a loss of 34 u was not the only mass loss common amongst the five selected m/z ions.

Table 8.3: Possible Neutral Loss Fragments during MS/MS Experiments

Molar Mass	Neutral Fragment	Exact Mass
18	H_2O	18.0153
32	O_2	31.9898
	CH_4O	32.0262
34	H_2O_2	34.0055
46	CH_2O_2	46.0054
	C_2H_6O	46.0419
62	CH_2O_3	62.0003
	$C_2H_6O_2$	62.0368

[Watson and Sparkman, 2007]

8.2.1. Additional NLS Analysis

Common mass losses of 32 and 62 u allowed for additional NLS analysis studies to be conducted. In the atmospheric science literature, other groups validated organic hydroperoxide formation by using mass losses of 34 u alone during MS/MS experiments (Baker et al., 2001 and Reinnig et al., 2007). However, losses of 32 and 62 u have never been considered or observed in the literature. Similar to NLS analysis of 34 u during ozonolysis experiments, the APCI-MS/MS was set to detect a range of *m/z* ions capable losing 32 or 62 u during MS/MS experiments. Resultant NLS mass spectra are shown in Figure 8.5 (a) and (b). Comparing the NLS mass spectra shown in Figure 8.5 (a) and (b) to the NLS mass spectrum for 34 u mass loss shown in Figure 8.1 (b), NLS analysis for 32 and 62 u mass losses displayed most of the *m/z* ions observed during 34 u NLS analysis under the same MS/MS conditions at various relative intensities. For instance, NLS for 32 u displayed *m/z* 171, 187, 201 and 203 ions in its resultant NLS mass

spectrum. The NLS mass spectrum for 62 u mass loss displayed very minor *m/z* 203 ion signals

whereas ion signals *m/z* 171, 173, 187, and 201 were apparent in the NLS mass spectrum.

(a)   (b)
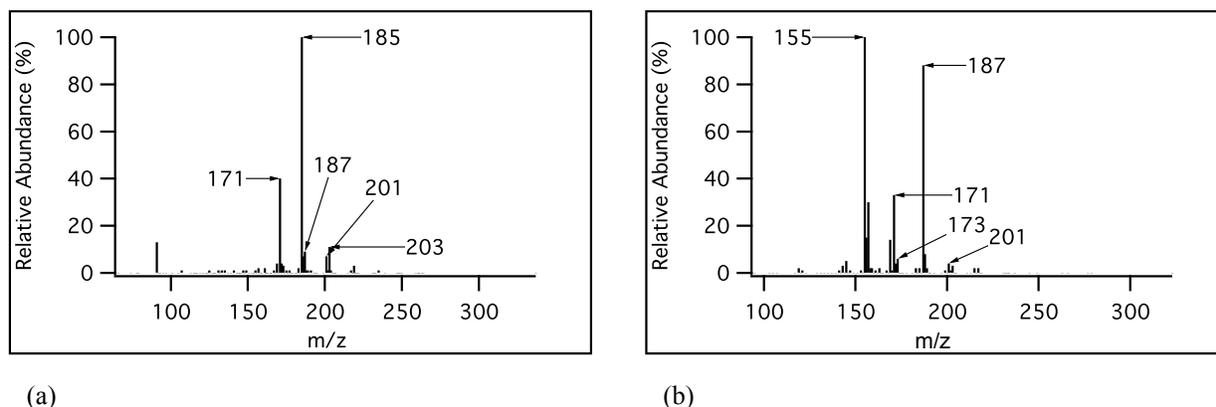
Figure 8.5: NLS analysis probing for mass losses of 32 and 62 u. (a) Represents the APCI-MS/MS detecting a range of *m/z* ions that lost 32 u whereas (b) depicts the APCI-MS/MS detecting mass losses of 62 u. Both scans were acquired by setting the collision energy to 10 CE.

Despite the differences between NLS mass spectra for 32, 34 and 62 u mass loss, the

obtained NLS mass spectra validated previously described product-ion scans for the five organic

hydroperoxide candidates (Figure 8.4). It appeared that mass losses of 32 and 62 or 32, 34 and

62 u may be unique to compounds that contain at least a hydroperoxy functional group.

8.2.2. Exclusivity of Mass Losses 32, 34 and 62 u to Organic Peroxide Structures

To confirm unique mass losses of 32, 34 and 62 u, product-ion mass spectra for other

known β-pinene/ozonolysis oxidation products were examined. Product-ion mass spectra

portrayed in the previous section were compared to product-ion mass spectra previously acquired

on 01/11/12 during photo-oxidation experiments of β-pinene conducted in the same York University smog chamber (Sarrafzadeh, 2012). Unlike the oxidation experiments conducted in this project, the experimental results used for comparative analysis were obtained by oxidizing β-pinene with hydroxyl radicals (HO) in the presence of 400 part-per-billion (ppb) NO. NOx chemistry through the two competing reactions described by Reaction 5.2 and 5.3 affects the formation of organic peroxides. As a result, it was assumed that organic peroxide formation would be minimal during the HO-initiated oxidation experiments. The photo-oxidation products used for comparative analysis are shown in Figure 8.6 (a) to (f). These structures were postulated and identified by Auld (2009) and Sarrafzadeh (2012) during photo-oxidation experiments. Notably, the postulated structures used for comparative analysis do not contain a hydroperoxy functional group. The product-ion mass spectra for $[M + H]^{+}$ ion signals for all six photo-oxidation products is shown in Figure 8.7 (a) to (f).
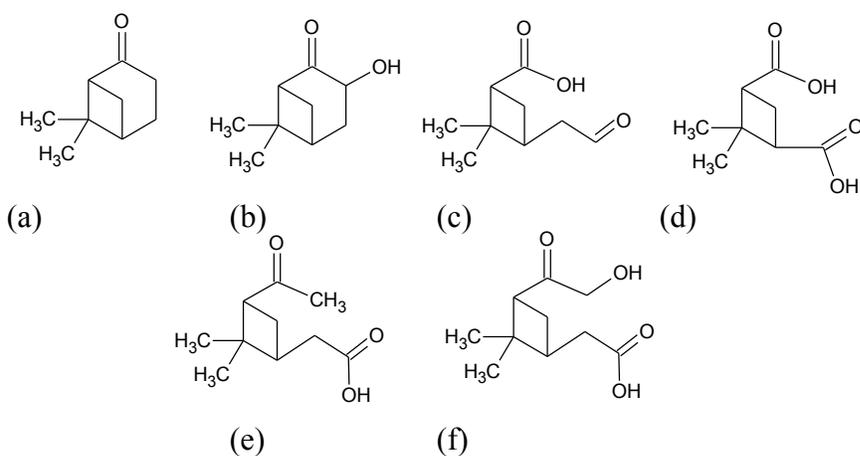
Figure 8.6: Postulated oxidation products for β-pinene photo-oxidation experiments. Oxidation products were postulated and identified previously by Auld (2009) and Sarrafzadeh (2012).
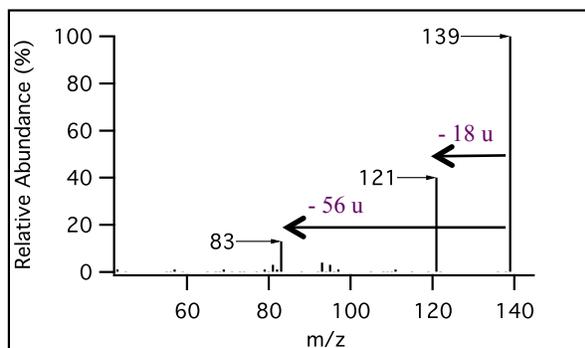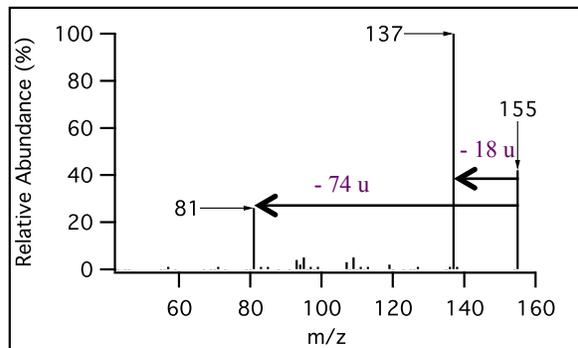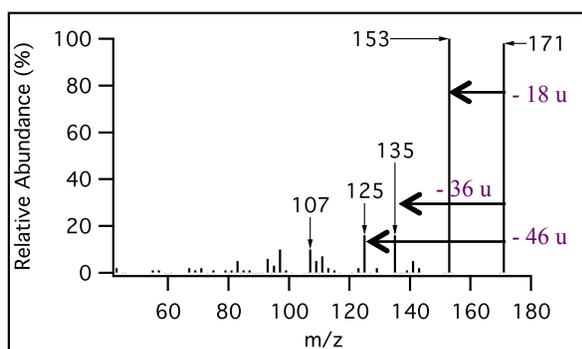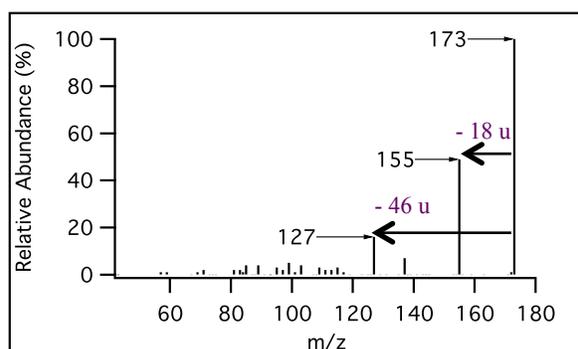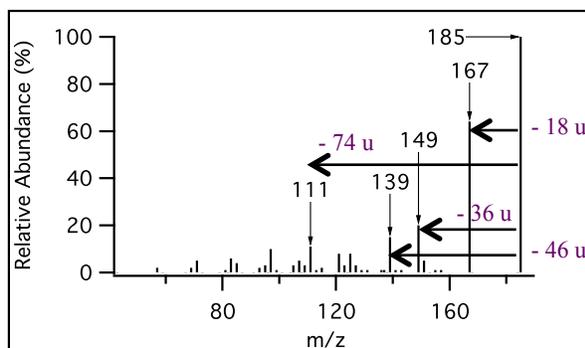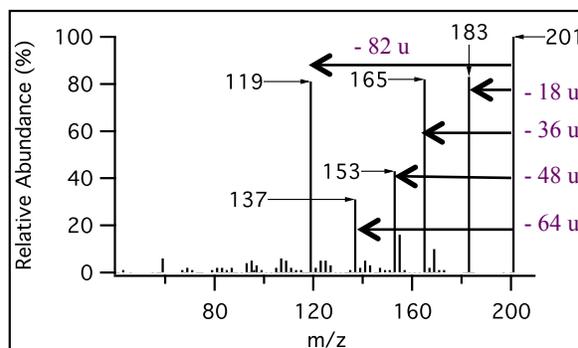
Figure 8.7: Product-ion mass spectra acquired 01/11/12 by Sarrafzadeh 2012. Product-ion mass spectra were acquired at a CE setting of 10 eV using (+) APCI-MS/MS. Product-ion mass spectrum shown in (a) represents the proposed structure shown in Figure 8.6 (a), while (b) to (f) represents proposed structures shown in Figure 8.6 (b) to (f) appropriately. Mass losses are shown in purple for clarity.

Product-ion mass spectra during photo-oxidation experiments revealed that mass losses of 32 and 34 u were unique to organic hydroperoxides since these mass losses were not observed in product-ion mass spectra for the six photo-oxidation products considered for comparative analysis. This was expected since mass losses of 32 and 34 u were possible if resultant oxidation products contained at the very least a peroxy moiety (O – O). Contrastingly mass losses of 18 (H_2O) and 46 u (H_2O and CO) were common between organic peroxides and carboxylic acids. Therefore, these losses were not unique enough to distinguish organic peroxide formation from carboxylic acids. Considering mass losses of 18 and 46 u would be problematic for m/z ion signals composed of a mixture of organic peroxides and carboxylic acids. Given this observation, mass losses of 32 and 34 u were essential at distinguishing the two oxidation products from one another.

Additionally, mass losses of 62 u were investigated further since its appearance in product-ion mass spectra during ozonolysis experiments revealed the possibility for organic peroxy acid formation (refer to Figure 7.3 for general structure). Similar to mass losses of 32 and 34 u, mass losses of 62 u were not observed in the product-ion mass spectra shown in Figure 8.7 (a) to (f). To validate the exclusivity of this mass loss to organic peroxy acids, 3-chloroperbenzoic acid (Sigma-Aldrich) (Figure 8.8) was purchased and analyzed using (+) APCI-MS/MS. This was the only organic peroxy acid standard commercially available. A portion of this standard was dissolved in methanol to achieve a concentration of 10% w/v and analyzed in the same manner as the 10% v/v organic peroxide standards described in Section 7.1.1.2. The resultant full scan mass spectrum and product-ion mass spectrum is portrayed in Figure 8.9 (a) and (b). Mass losses of 62 u dominated the product-ion mass spectrum while masses losses of 34 u were visible. Since an ion signal at m/z 155 (loss of 18 u) was absent,

losses of 62 u could not be justified through sequential losses of H_2O (18 u) and CO_2 (44 u). Instead, 62 u mass losses could be rationalized through a mass loss of 34 u (H_2O_2) and 28 u (CO). Overall, the product-ion mass spectrum demonstrated the possibility that 62 u mass losses observed during product-ion analysis could indicate the formation of organic peroxy acids. Moreover, this mass loss was deemed unique since it was not observed in product-ion mass spectra of photo-oxidation products considered in this project for comparative analysis.
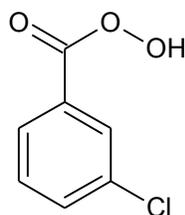
Figure 8.8: Structure for 3-chloroperbenzoic acid

(a)   (b)
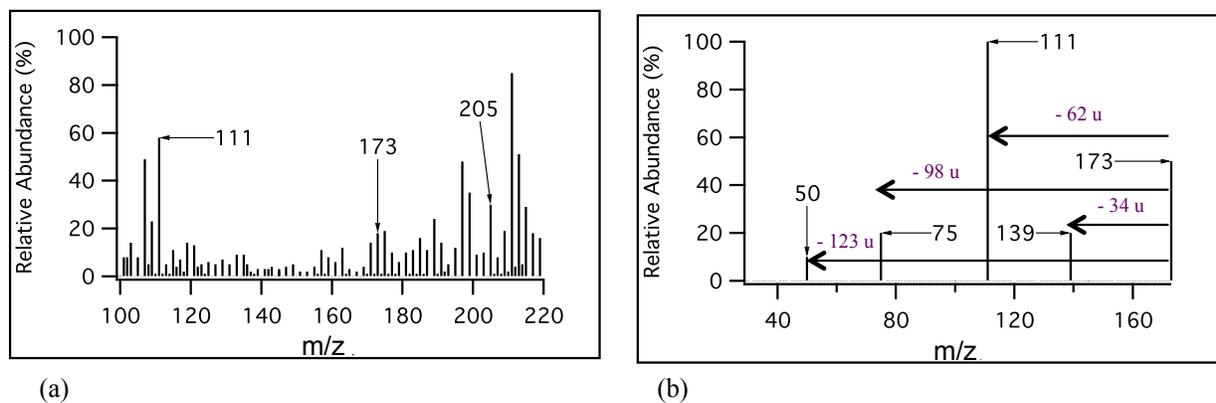
Figure 8.9: Analysis of 10% w/v 3-chloroperbenzoic acid. (a) Represents a full scan mass spectrum while (b) shows the product-ion mass spectrum obtained at a CE setting of 10 eV for the $[M + H]^+$ ion signal *m/z* 173. Mass losses are shown in purple for clarity.

8.3. Proposed Structures

Based on observed mass losses of 18, 32, 34, 46, and 62 u during β-pinene/ ozonolysis experiments, six possible structures representing organic peroxides are proposed based on a formula of C_x H_y O_z. Although in principle different empirical formulas can be suggested to explain ozonolysis products with molecular mass 170, 172, 186, 200 and 202 g mol^{-1}, it was assumed that the resultant empirical formula would not contain a carbon count higher than 9 (C_9). An empirical formula containing C_{10} was unlikely since β-pinene reaction with O_3 results in the elimination of an aldehyde/ketone (Figure 5.2). The six proposed structures along with probable fragmentation pathways to support the proposed structures are shown and described in later sections. Since APCI-MS/MS cannot distinguish between isobaric compounds and ozonolysis products were not separated prior to analysis, additional known β-pinene oxidation products were considered to rationalize MS/MS spectra. Lastly, although the focus of this work was not to describe the formation mechanism for the postulated structures, a credible reaction mechanism was proposed and is shown in Appendix G.

8.3.1. Proposed Structure Leading to Ion Signal at *m/z* 171

The [M+H]$^{+}$ ion signal *m/z* 171 was apparent during NLS scans for 32, 34 and 62 u mass loss. Additionally, mass losses of 18 and 46 u were observed during product-ion scan analysis. Collectively, these mass losses were used to determine the functional groups present in the neutral oxidation structure. Moreover, two empirical formulas, $C_8H_{10}O_4$ and $C_9H_{12}O_3$, were postulated for molar mass 170 using the observed mass losses. Although mass losses of 18 u (H_2O) indicated a hydroxyl functional group (OH), a hydroperoxy functional group was more likely given the observed mass loss of 34 u in product-ion mass spectrum. All plausible

structures representing molar mass 170 and an empirical formula of $C_9H_{14}O_3$ are depicted in Figure 8.10 (a) to (c). The only structure that includes the peroxy and hydroperoxy group is Figure 8.10 (a), which was observed by Heaton and coworkers (2007) during β-pinene/ozonolysis experiments. A conceivable loss mechanism for 18 and 34 u is portrayed in Figure 8.11 (a) and (b). Observed mass losses of 32 u representing O_2 were difficult to rationalize but still considered possible as long as mass losses of methanol (CH_3OH) were discounted and protonation in the APCI ion source occurred at the carbonyl moiety for the reasons discussed in Section 3.1.2.

(a)   (b)   (c)
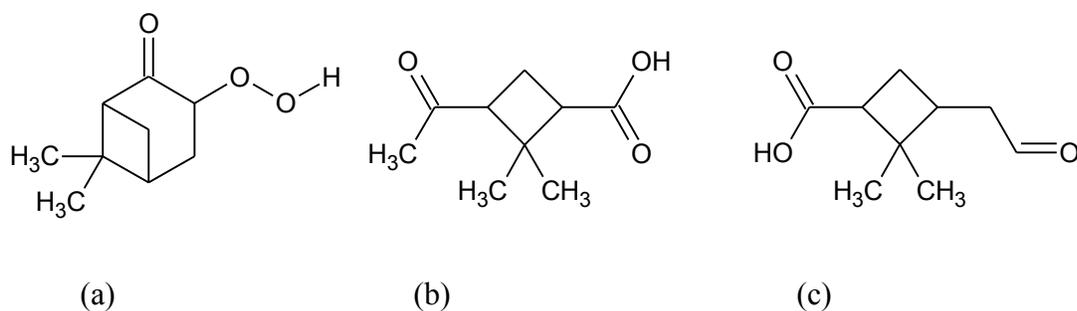
Figure 8.10: Postulated structures representing molar mass 170 g mol^{-1}

(a)

(b)
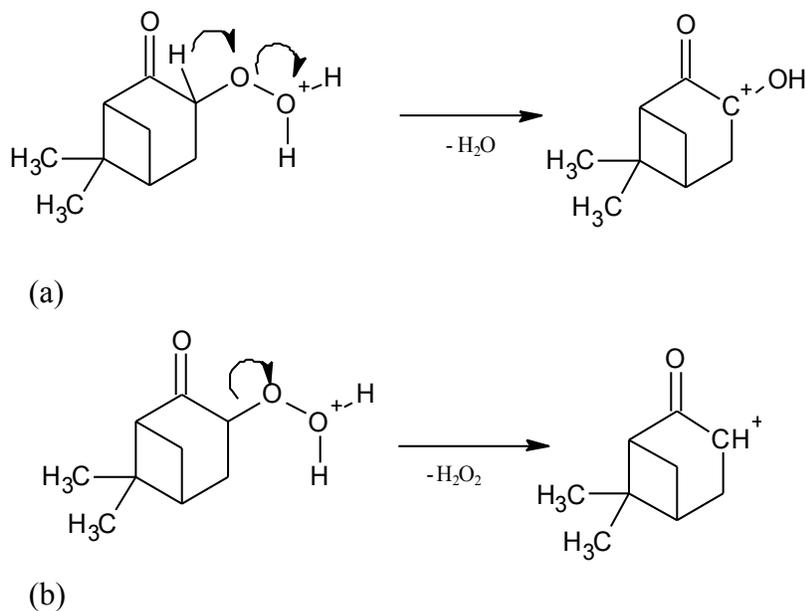
Figure 8.11: Postulated fragmentation pathway representing (a) losses of H_2O (18 u) and (b) losses of H_2O_2 (34 u)

Mass losses such as 46 and 62 u were harder to rationalize from the given structure shown in Figure 8.10 (a). This suggested that the resultant m/z 171 ion signal was a mixture of ozonolysis products with the same molar mass. However, it was understood that mass losses of 46 u represented a combined loss of CO (28 u) and H_2O (18 u) since these mass losses were observed during MS/MS experiments using (+) APCI-MS/MS for carboxylic acids (Sarrafzadeh, 2012) and organic peroxy acids (Heaton et al., 2007 and Reinnig et al., 2009). Combinations describing mass losses of 62 u were described in previous sections (Section 8.2.3). Furthermore, this mass loss was considered unique to structures resembling organic peroxy acids. Since the proposed structure did not match the product-ion mass spectrum for m/z 171 in its entirety, this indicated that the resultant m/z 171ion signal was a mixture of ozonolysis products with the same molar mass. This notion was valid since the isobaric oxidation product pinalic-3-acid (Figure

106

8.10 (b)) and the structure depicted in Figure 8.10 (c) have been proposed and observed during β-pinene oxidation experiments (Auld 2009, Heaton et al., 2007, and Jenkin, 2004). Lastly, losses of 62 u indicated that there was an additional undetermined structure capable of exhibiting this mass loss. Although this mass loss was unique to organic peroxy acids, a structure could not be established containing this functional group. However, combination of mass losses totalling 62 u could not be justified by the structures depicted in Figure 8.10 (b) and (c).

8.3.2. Proposed Structure Leading to Ion Signal at *m/z* 173

The *m/z* 173 ion signal was the only $[M + H]^+$ ion whose fragmentation pattern resulted in two postulated organic peroxide structures having the empirical formulas, $C_8H_{12}O_4$ or $C_9H_{16}O_3$. The two possibly credible structures are shown in Figure 8.12 (a) and (b) along with an isobaric structure identified previously by (Jenkin 2004, Auld 2009 and Sarrafzdeh 2012) (Figure 8.12(c)). Two organic peroxide structures were proposed since the observed mass losses in product-ion mass spectrum and the appearance of *m/z* 173 in 32, 34, and 62 u NLS mass spectra could not be rationalized considering one organic peroxide structure. The possible fragmentation pathways to give mass losses of 32, 34, 46 and 62 u are depicted in Figure 8.13 (a) to (d), while Figure 8.14 (a) and (b) describes fragmentation pathways to give mass losses of 32 and 34 u. Since *m/z* 173 was apparent in 34 u NLS mass spectrum, the resultant structure contained at least a hydroperoxy functional group. This functional group would validate mass losses of both 18 (H_2O) and 34 u (H_2O_2) observed in the product-ion mass spectrum (Figure 8.4 (b)). Additionally, the relatively minor appearance of *m/z* 173 in 32 u NLS mass spectrum indicated the presence of a peroxy bond (-O – O-) as long as losses of CH_3OH were discounted. A mass loss of 32 u can be rationalized by both structures shown in Figure 8.12 (a) and (b) but an additional mass loss

difference of 18 u (H₂O) between *m/z* 141 and *m/z* 123 fragment ions observed in the product-ion

mass spectrum shown in Figure 8.4 (b) can only be explained by the structure shown in Figure

8.12 (b) and fragmentation pattern depicted in Figure 8.14 (a) as long as protonation in the APCI

ion source took place at the hydroxyl functional group. For a structure like the one portrayed in

Figure 8.12 (a), mass losses of 32 u is reasonably explained in Figure 8.13 (a) since protonation

at a carbonyl functional group (C=O) was possible for the reasons discussed in Section 3.1.2.

(a)   (b)   (c)
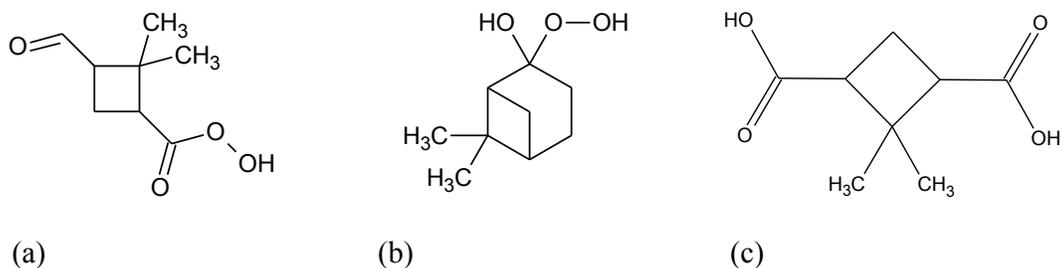
Figure 8.12: Postulated structure srepresenting molar mass 172 g mol⁻¹ (Auld 2009 and Heaton et al. 2007)
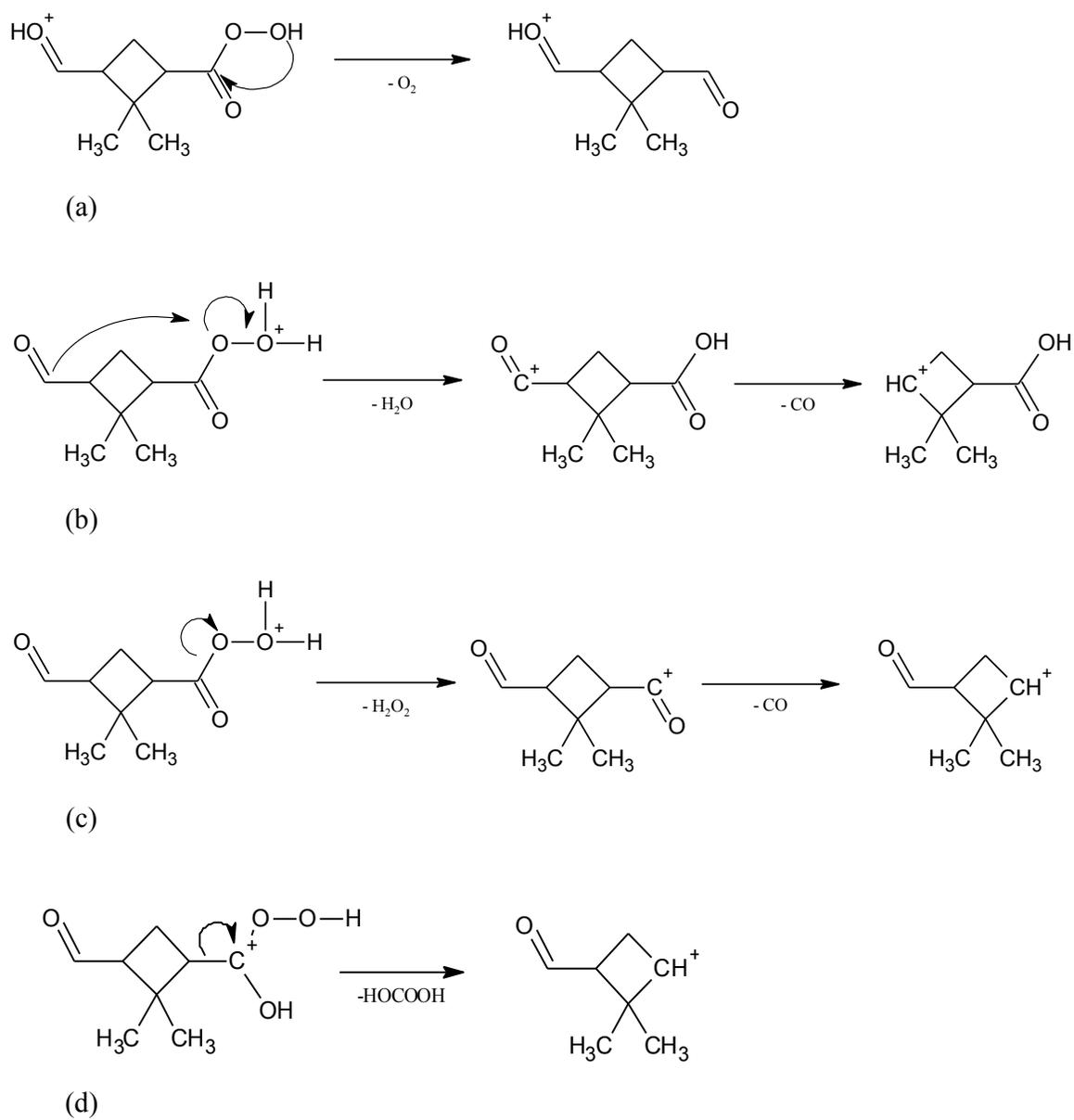
Figure 8.13: Possible fragmentation pathway for the protonated structure represented by Figure 8.12 (a)

(a)

(b)
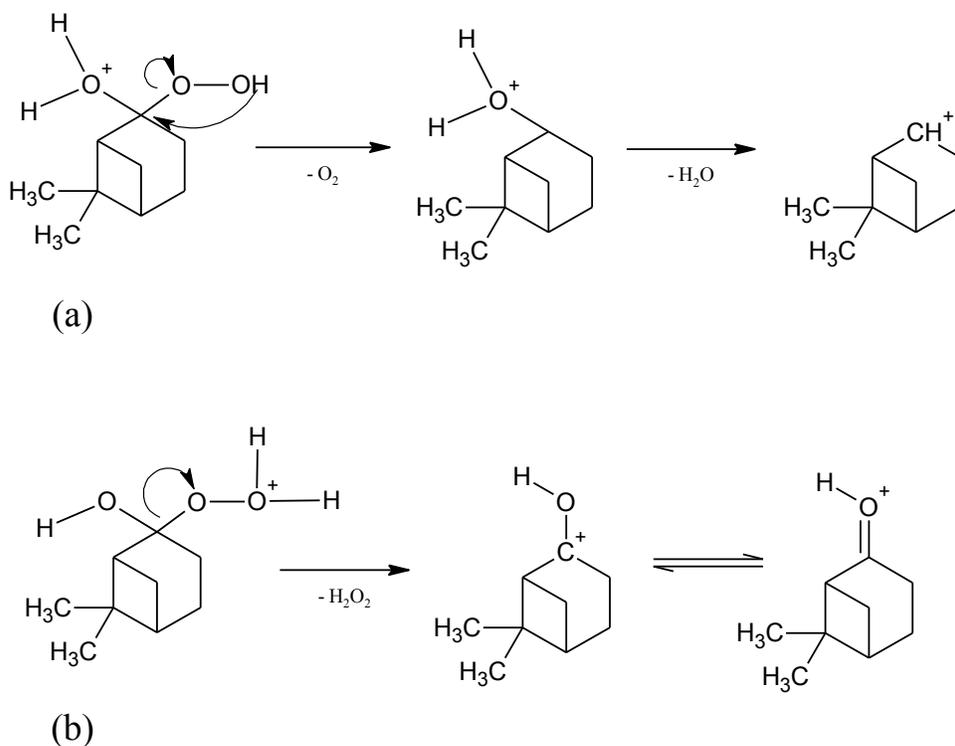
Figure 8.14: Possible fragmentation pathway for the protonated structure represented by Figure 8.12 (b)

Similar to *m/z* 171 fragmentation pathways, mass losses of 46 u were reasonable inferred through mass losses of H_2O (18 u) and CO (28 u). This mass loss can be rationalized by the structures shown in Figure 8.12 (b) and (c) after protonation in the APCI ion source. However, a fragmentation pathway leading to mass losses of 32, 34 and 62 u could not be realized from the structure shown in Figure 8.12 (c). As a result, the *m/z* 173 ion signal observed in full scan mass spectrum was assumed to be a mixture comprised of the protonated structure shown in Figure 8.12 (b) and (c) and an additional protonated structure shown in Figure 8.12 (a) that loses a 62 u fragment during MS/MS experiments. Two pathways were considered for rationalizing a mass loss of 62 u from the structure shown in Figure 8.12 (a). Figure 8.13 (d) portrays a fragmentation pathway where a single fragment totalling 62 u is lost from a protonated structure shown in

Figure 8.12 (a) whereas Figure 8.13 (c) describes a fragmentation pathway rationalizing a sequential mass loss totalling 62 u (loss of H_2O_2 and CO) as observed in product-ion mass spectrum. Although fragmentation pathways could easily be determined to rationalize mass losses of 62 u, the relative minor appearance of *m/z* 173 in 62 u NLS mass spectrum coupled with the dominant losses of H_2O and O_2 observed in the product-ion mass spectrum, suggested that the structure shown in Figure 8.12 (a) was a minor contributor to the overall *m/z* ion signal *m/z* 173 observed in full scan mass spectrum. Instead, the product-ion mass spectrum supported the organic peroxide structure shown in Figure 8.12 (b).

8.3.3. Proposed structure leading to ion signal at *m/z* 187 (Peroxypinalic acid)

Auld (2009) previously observed this ion signal during photo-oxidation experiments with β-pinene while its structure was described by Heaton and coworkers (2007), Docherty and coworkers (2006) and Jenkin (2009). The organic peroxy acid structure known as peroxypinalic acid, is depicted in Figure 8.15 (a) along with two known isobaric structures (Figure 8.15 (b) and (c)) (Heaton et al. 2007). While analyzing ozonolysis products by APCI-MS/MS, this ion signal was prominent during 34 and 62 u NLS analysis (Figure 8.2 (b) and Figure 8.5 (b)). Conversely, its signal was minor in 32 u neutral-loss mass spectrum (Figure 8.5 (a)). The proposed $C_9H_{14}O_4$ structure was supported by acquired product-ion mass spectrum portraying dominant mass losses of 18 u (H_2O) and 34 u (H_2O_2).

Figure 8.15: Proposed structures representing molar mass 186 g mol^{-1}

Figure 8.16 (a) to (d) shows peroxypinalic acid in its protonated form along with postulated fragmentation pathways. Minor mass losses of 32 u were possible as long as protonation occurred at the carbonyl functional group as opposed to the hydroperoxy functional group (Figure 8.16 (a)). Credible mass losses totalling 62 u (Figure 8.16 (c)) supported an organic peroxy acid structure (See Figure 7.3 for general structure) as opposed to an organic hydroperoxide structure (See Figure 7.3 for general structure). Similar to *m/z* 173 ion signal analysis, mass losses of 46 u during MS/MS experiments were attributed to losses of H_2O (18 u) and CO (28 u). Although the proposed structure shown in Figure 8.15 (a) could theoretically exhibit this mass loss, other known β-pinene ozonolysis products such as the ones proposed by Heaton et al., (2007) (Figure 8.15 (b) and (c)) could also exhibit this mass loss. However, by visual inspection, these isobaric ozonolysis products under the same experimental conditions are less likely to lose 62 u during MS/MS experiments. This inference was first established assuming that the neutral fragments portrayed in Table 8.3 can only explain mass losses of 62 u during MS/MS experiments. Lastly, the discussion of 62 u mass losses in Section 8.2.3 demonstrated that combined losses of H_2O_2 (34 u) and CO (28 u) were unique to structures containing a peroxy acid functional group. Oxidation products containing a carboxylic acid functional group as

shown in Figure 8.6 (c) to (f) do not exhibit combined losses of H_2O_2 (34 u) and CO (28 u) in their product-ion mass spectrum (Figure 8.7 (c) to (f)). Aside from this type of loss, product-ion mass spectra shown in Figure 8.7 (c) to (f) did not show a single fragment loss of 62 u. Since the isobaric structures shown in Figure 8.15 (b) and (c) contain carboxylic acid functional groups, it was valid to assume that mass losses of 62 u cannot be realized by these two oxidation products.

(a)

(b)

(c)

(d)
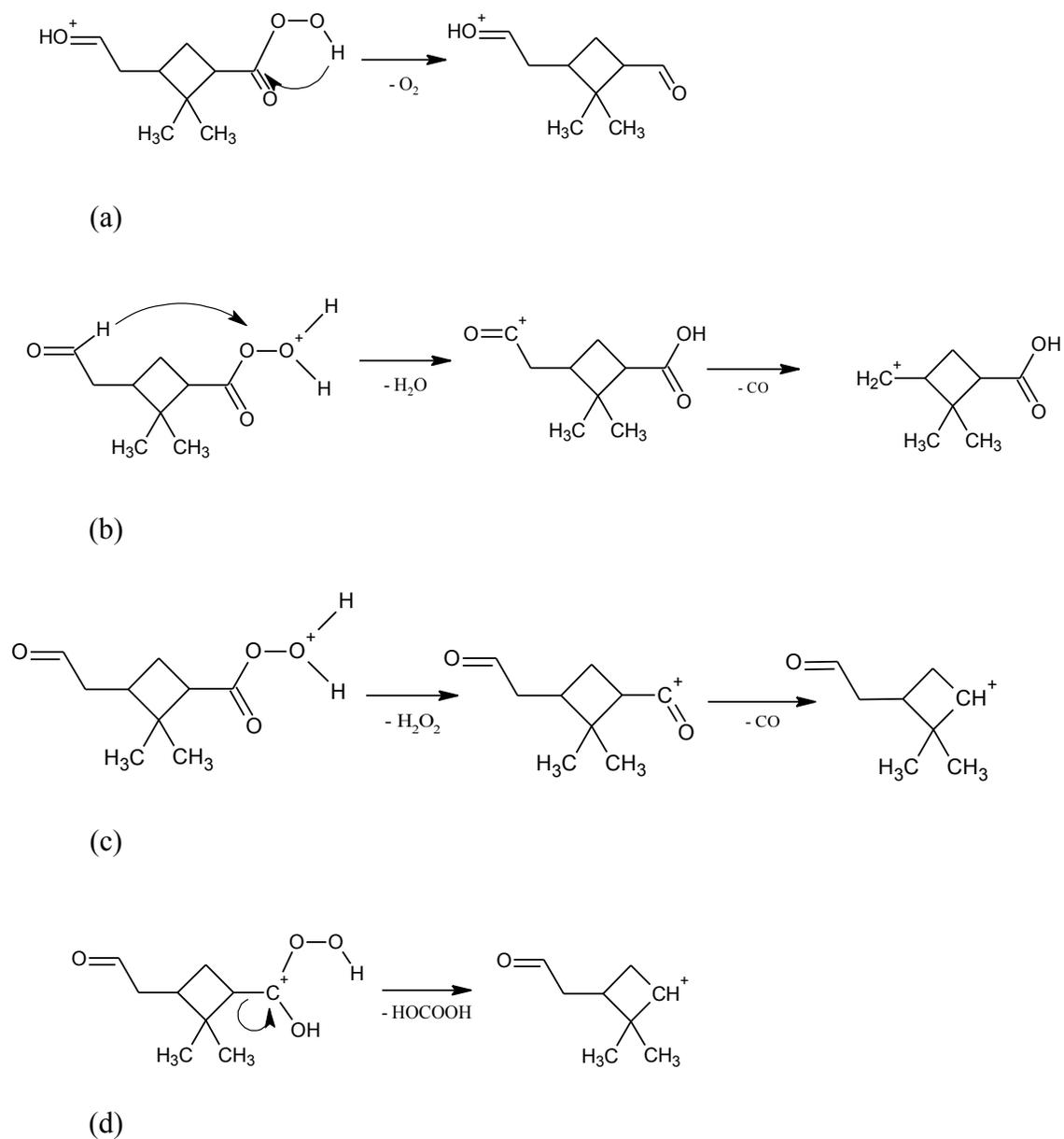
Figure 8.16: Conceivable fragmentation pathways for peroxypinalic acid

Overall, it was assumed that the m/z 187 ion signal in full scan mass spectrum was a mixture of all oxidation products displayed in Figure 8.15 (a) to (c) in the absence of any information that proved otherwise. However, observed mass losses of 32, 34 and 62 u in

product-ion mass spectrum indicated the formation of an organic peroxide compound during β-pinene ozonolysis.

8.3.4. Proposed Structure Leading to Ion Signal at *m/z* 201

This ion signal was not easily observable in the full scan mass spectrum. Although increased sensitivity was achieved during NLS analysis for 32, 34 and 62 u mass losses, the resultant ion signal was still minor in all three MS/MS spectra. One explanation for the minor ion signals at *m/z* 201 during full scan analysis was that the gas-phase concentration of the corresponding organic peroxide formed during ozonolysis was low compared to other ozonolysis products. Alternatively, the PA for the neutral structure could be lower compared to other β-pinene ozonolysis products resulting in a decrease in sensitivity for the *m/z* 201 ion in the APCI-MS/MS. Regardless of its minor appearance in full scan analysis or MS/MS experiments, its appearance in 34 u NLS mass spectrum indicated the presence of a hydroperoxy functional group within its structure. Based on 32, 34 and 62 u NLS mass spectra (Figure 8.1 (b), Figure 8.5 (a) and (b) correspondingly), product-ion mass spectrum (Figure 8.4 (d)) and findings published by Reinnig et al., (2009) and Heaton et al., (2007) two structures having formulas of $C_9H_{12}O_5$ and $C_{10}H_{16}O_4$ are shown in Figure 8.17 (a) and (b) and were good candidates to represent the observed ion signal. Aside from this project, Reinnig et al., (2009) was one of the only papers to describe an organic peroxide structure with molar mass 200 g mol^{-1}.
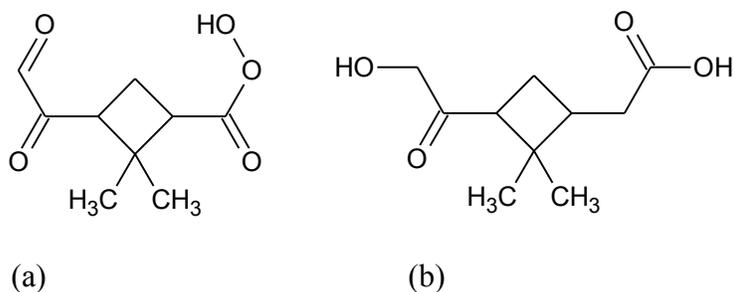
Figure 8.17: Proposed structures representing molar mass 200 g mol^{-1}. (a) Represents a molecular formula $C_9H_{12}O_5$ while (b) represents a molecular formula $C_{10}H_{16}O_4$

Credible fragmentation pathways are portrayed in Figure 8.18 (a) to (c) to rationalize mass losses of 32, 34 and 62 u. Mass losses of 32 u could be rationalized if protonation occurred at the hydroperoxy functional group as depicted in Figure 8.18 (a) or conceivably by protonation at the carbonyl functional group not associated with the hydroperoxy functional group. Both functional groups were considered basic sites for proton attachment as discussed in Section 3.1.2. Similar to the other ion signals representing organic peroxides, observed mass losses of 18 and 46 u could be justified by both structures depicted in Figure 8.17 (a) and (b). However, observed mass losses of 32, 34 and 62 u cannot be rationalized by the structure depicted in Figure 8.17 (b) for the same reasons discussed while realizing a structure to represent the ion signal *m/z* 186 (Section 8.3.3). Losses of H_2O_2 (34 u) and CO (28 u) were unique to structures containing a peroxy acid functional group. Since the isobaric structure shown in Figure 8.17 (b) is a di-carboxylic acid, this structure cannot lose H_2O_2 (34 u) and CO (28 u) from its [M + H]$^+$ structure during MS/MS experiments. This was further supported by MS/MS experiments conducted by Saraffzadeh (2012), which showed the product-ion mass spectrum of the [M + H]$^+$ ion signal for the isobaric structure shown in Figure 8.17 (b) losing H_2O (18 u) and HCOOH (46 u) fragments during MS/MS experiments (Figure 8.7 (f)). Similar to the other organic peroxides discussed in

this project, the *m/z* 201 ion signal was assumed to be a mixture of both structures portrayed in Figure 8.17 (a) and (b) since mass losses of 18 u ad 46 u could be realized by both structures portrayed in Figure 8.17 (a) and (b), but mass losses of 32, 34, and 62 u could only be described by the structure shown in Figure 8.17 (b).

(a)

(b)

(c)
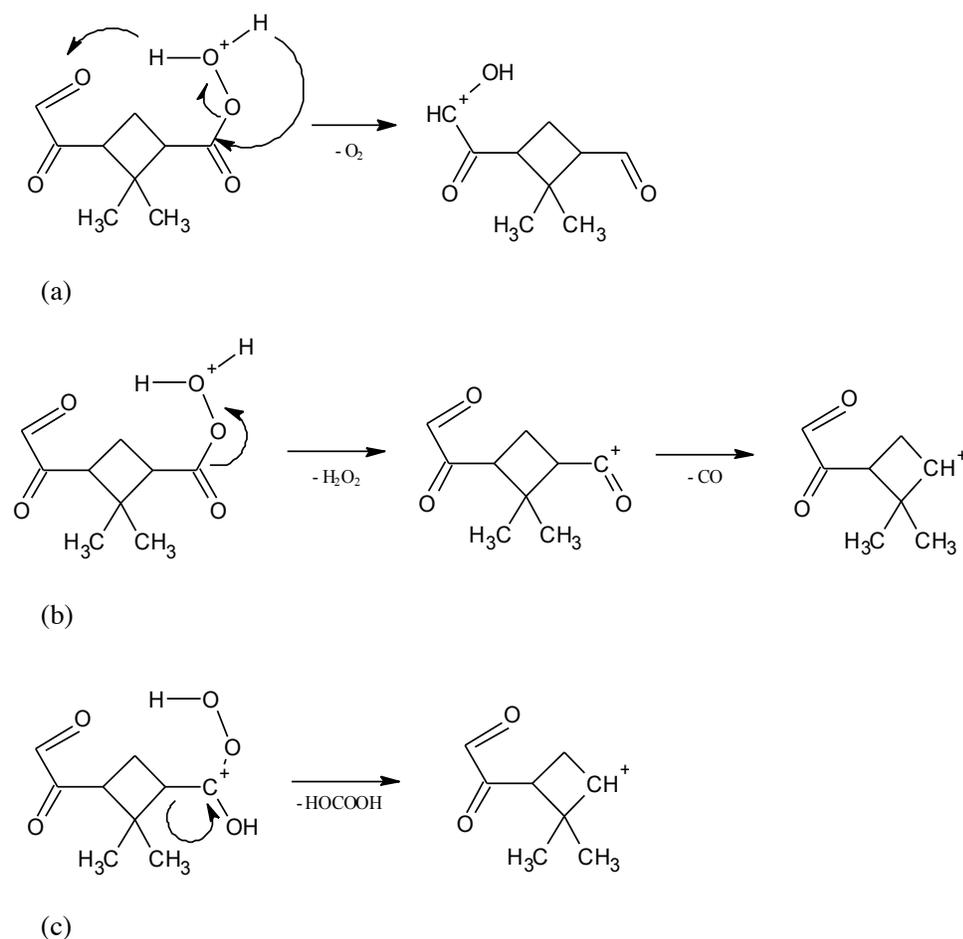
Figure 8.18: Postulated fragmentation pathway for the structure portrayed in Figure 35 (a) ($C_9H_{12}O_5$)

8.3.5. Proposed Structure Leading to Ion Signal at *m/z* 203

Similar to *m/z* 201, the *m/z* 203 ion signal was not easily observable during full scan analysis (Figure 8.1 (a)). Sensitivity for *m/z* 203 was first achieved during NLS analysis for mass losses of 34 u. Additionally; sensitivity for *m/z* 203 was enhanced in NLS mass spectrum for 32 u mass losses (Figure 8.5 (a)) while a small ion signal was observed in NLS mass spectrum from 62 u mass losses (Figure 8.5 (b)). Similar to *m/z* 201, *m/z* 203 relative abundance in full scan mass spectrum and all three NLS mass spectra was minor. This could be attributed to similar reasons discussed in the previous section for the minor appearance of *m/z* 201 during analysis. Moreover, Docherty et al., (2005), Heaton et al., 2007, and Reinnig et al., (2007) observed the corresponding organic peroxide ion signal, *m/z* 203, mainly in the particle phase as oppose to the gas phase. Therefore it was reasonable to obtain relatively low *m/z* 203 ion signals during gas phase analysis of β-pinene ozonolysis products in this project.
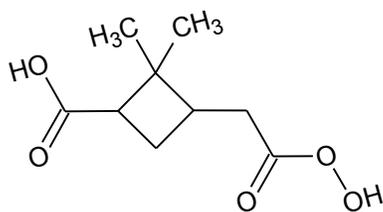
Figure 8.19: Proposed organic peroxy acid ($C_9H_{14}O_5$)

(a)

(b)

(c)

(d)
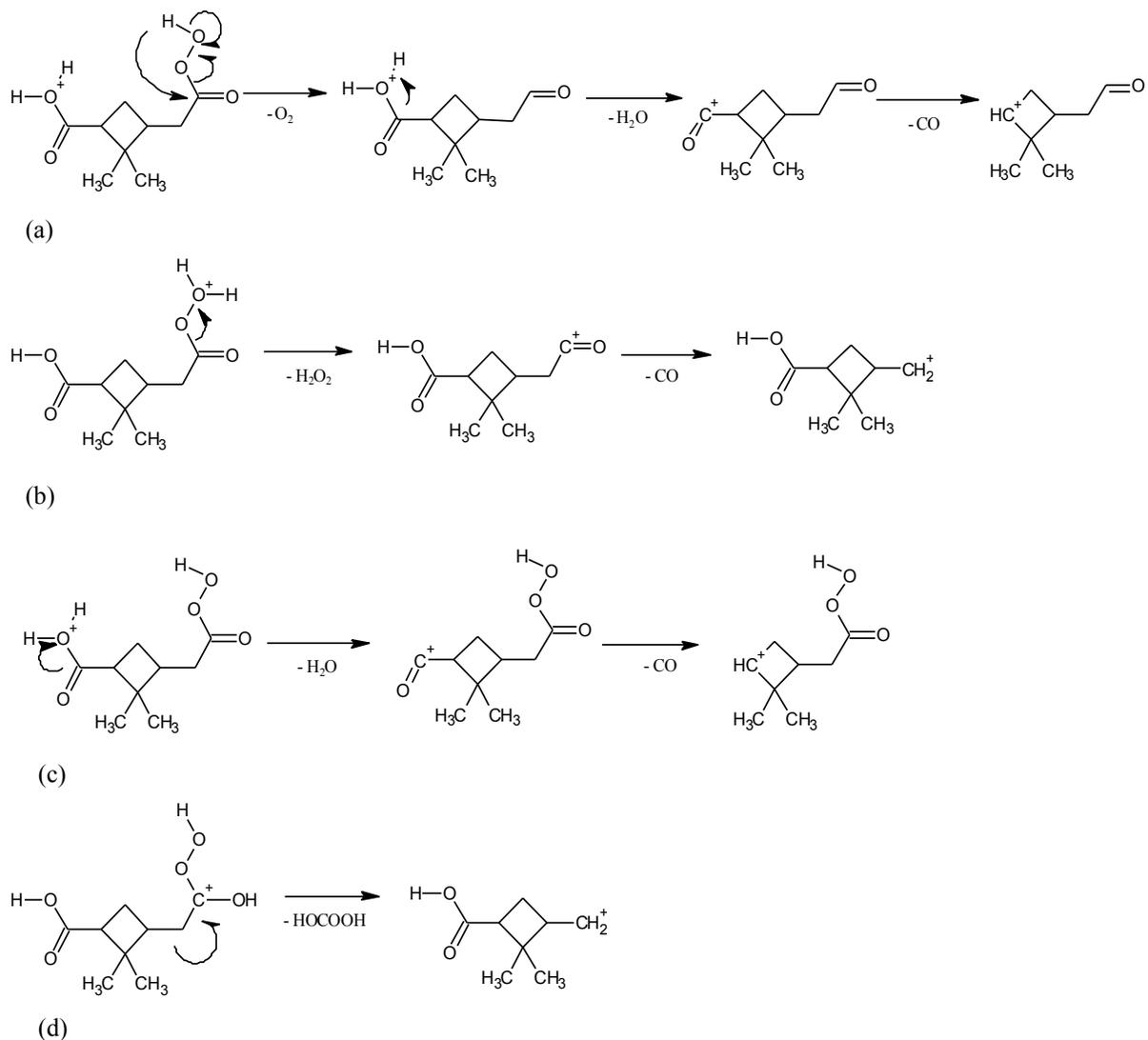
Figure 8.20: Postulated fragmentation pathways for molar mass 202 g mol^{-1} ($C_9H_{14}O_5$)

Based on product-ion mass spectrum, neutral-loss mass spectra and observations reported by Docherty et al., (2005) and Reinnig et al., (2007), an organic peroxide structure representing a molar mass of 202 g mol^{-1} ($C_9H_{14}O_5$) was ascertained along with credible fragmentation pathways. The neutral organic peroxide structure is shown in Figure 8.19 while the fragmentation pathways are depicted in Figure 8.20 (a) to (d). Although m/z 203 was relatively

minor during NLS analysis for 32 u mass losses, a credible fragmentation pathway was ascertained (Figure 8.20 (a)). Mass losses of 32 u were deemed possible if protonation occurred at the alcohol functional group of the neutral structure as opposed to the hydroperoxy functional group. Protonation at the hydroperoxy group as opposed to the alcohol group would promote losses of H_2O (18 u) and/or H_2O_2 (34 u) as observed in previous product-ion scan analysis. Although Figure 8.20 (a) shows a loss of 32 u (O_2) followed by a loss of 18 u (H_2O), the order at which m/z 203 losses these fragments could not be determined with certainty. This was because mass losses of 18 u followed by a loss of 32 u from m/z 203 would result in the appearance of fragment ions m/z 185 and m/z 153 correspondingly. These ion signals were apparent in the product-ion mass spectrum for m/z 203. On the other hand, a mass loss of 32 u followed by a loss of 18 u would result in the appearance of ion signals m/z 171 and m/z 153, respectively. These ion signals were also apparent during product-ion scan analysis for m/z 203. Regardless of the order of loss, the appearance of m/z 203 in 32 u NLS mass spectrum suggested the neutral structure with molar mass 202 g mol^{-1} had a peroxy bond in its structure.

A peroxy acid structure was assumed based on the ion signal's appearance in NLS mass spectra representing mass losses of 34 and 62 u. Mass losses of 34 u (H_2O_2) were possible as long as protonation occurred at the hydroperoxy moiety as shown in Figure 8.20 (b). Additionally, a loss of H_2O_2 (34 u) as described, would result in a subsequent loss of CO (28 u) from the $[M +H - 34]^+$ ion signal for a combined mass loss of 62 u. These mass losses were observed in product-ion mass spectrum of m/z 203 where ion signals m/z 169 ($[M + H - 34]^+$) and m/z 141 ($[M + H - 62]^+$) were apparent (Figure 8.4 (e)).

Equally important mass losses like 18 u (H_2O) were possible through the fragmentation pathway postulated in the first step of Figure 8.20 (c). However, dominate losses of 36 u

(2(H_2O)) shown by the appearance of m/z 167 in product-ion mass spectrum (Figure 8.4 (e)), suggested that the m/z 203 ion signal in full scan mass spectrum (Figure 8.1 (a)) was not purely attributed to an organic peroxide. Considering the organic peroxide structure shown in Figure 8.19, protonation at the alcohol or hydroperoxy functional group will not result in the loss of two H_2O molecules during collision events. Single losses of H_2O or H_2O_2 would be observed during collision events if protonation occurred at the alcohol or hydroperoxy functional group, respectively, based on early experiments and work by Sarrafzadeh (2012). As a result it was assumed that m/z 203 represented a $[M + H + H_2O]^+$ ion signal for a structure with molar mass 184 g mol^{-1}. An oxidation product with molar mass 184 was portrayed previously in Figure 8.6 (e). Based on this structure, losses of 2 H_2O molecules are possible if protonation occurred at the OH location of the carboxylic acid moiety and the PA for both water and the structure shown in Figure 8.6 (e) were similar enough to form an adduct $[M + H + H_2O]^+$.

8.4. Summary for Analyzing Organic Peroxides during Smog Chamber Experiments using (+) APCI-MS/MS

Since neutral mass losses of 34 u were imperative for detecting organic peroxides during standard analysis, this method was applied to detect organic peroxides during smog chamber studies of β-pinene ozonolysis. Although using methanol as an ionization reagent enhanced the ability to detect organic peroxide standards, this ionization reagent was not useful for detecting organic peroxides from β-pinene ozonolysis experiments. Therefore, organic hydroperoxide candidates from β-pinene ozonolysis were firstly detected using NLS analysis for mass losses of 34 u while using protonated water and its clusters as an ionization reagent.

Although full scan mass spectra showed a range of ozonolysis products formed during smog chamber experiments, NLS analysis simplified full scan mass spectra to five *m/z* ion signals capable of losing 34 u during collision events. Based on NLS mass spectrum for 34 u mass losses, *m/z* 171, 173, 187, 201, and 203 were determined as having a hydroperoxy functional group within their structure.

Additional product-ion mass spectra for these five *m/z* ions revealed other common mass losses such as 18 u (H_2O), 32 u (O_2), 46 u (H_2O and CO) and 62 u (H_2O_2 and CO). Although mass losses of 18 and 46 u were not considered unique due to its appearance in product-ion mass spectra of carboxylic acids, mass losses of 32 u were logical for structures containing a peroxy bond while mass losses of 62 u were considered exclusive to structures containing a peroxy acid functional group. As a result, NLS analysis for 32 and 62 u mass losses were useful for selective detection of organic peroxy acids in conjunction with NLS analysis for 34 u mass losses. Support for 32 and 62 u mass loss came from the fragmentation pattern observed in the full scan mass spectrum of cumene hydroperoxide and product-ion mass spectrum of 3-chloroperobenzoic acid.

Organic peroxide assignment and elucidation relied heavily on NLS analysis of 34 u mass losses. Standard analysis of *tert*-butyl hydroperoxide and peracetic acid coupled with published results from Baker et al., (2002) and Reinnig et al., (2009) supported the notion that mass losses of 34 u were exclusive to structures containing a hydroperoxy functional group. Ultimately, all observed mass losses were used to propose six organic peroxide structures along with credible fragmentation pathways.

9. Conclusion and Future Work

The aim of this project was to evaluate the ability of (+) APCI-MS/MS to detect organic peroxides formed during β-pinene/ozonolysis experiments. Despite their importance to SOA formation and composition, their detection is problematic given the thermally labile nature of these compounds. Most of the analytical methods employed for its detection are considered "off-line" and tend to be time consuming and require extensive sample treatment such as derivitization and separation. Moreover, they fail to provide information regarding the structure of organic peroxides.

In this project, (+) APCI-MS/MS did not require extensive sample treatment and provided fast on-line analysis for organic peroxides. After protonation in the APCI ion source, m/z ions of interest could be isolated and studied using various tandem mass spectrometry modes such as product-ion scan and neutral-loss scan analysis mode. The tandem mass spectrometry analysis modes allowed for the ability to determine common mass losses between all organic peroxide standards. During organic peroxide standard analysis, mass losses of 34 u were common to organic peroxide standards containing a hydroperoxy functional group. Given this observation, losses of 34 u were used as a criterion for detecting organic peroxides containing a hydroperoxy functional group. As a result, neutral-loss scan analysis for 34 u mass loss increased the sensitivity for $[M + H]^+$ ions during organic peroxide standard analysis.

Similar to organic peroxide standard analysis, organic peroxide detection during smog chamber experiments relied heavily on unique mass losses observed during tandem mass spectrometry analysis. For instance, organic peroxide candidates were first detected by utilizing neutral-loss scan analysis mode for 34 u mass losses. Based on organic peroxide standard

analysis and work by Baker et al., 2001 and Reinnig et al., 2009, mass losses of 34 u were considered exclusive to organic peroxides containing a hydroperoxy functional group. Additional product-ion scan analyses showed that mass losses of 32 u and 62 u could be used as a criteria for organic peroxide detection. While 32 u mass losses supported a hydroperoxy functional group, mass losses of 62 u were possible for organic peroxides containing a peroxy acid functional group. Exclusive mass losses of 32, 34 and 62 u were valid as long as smog chamber products were limited to carbon, hydrogen, and oxygen. Lastly, neutral-loss and product-ion scan analysis mode aided in the structural elucidation of six organic peroxide structures formed during β-pinene/ozonolysis experiments.

9.1. Future Work

9.1.1. The Influence of Experimental Conditions of Organic Peroxide Formation

During this study, it was clear that organic peroxide formation was enhanced under certain laboratory conditions. For example, comparisons of product-ion mass spectra acquired in this study to the product-ion mass spectra acquired by Sarrafzadeh (2012) suggested a higher organic peroxide formation during ozonolysis experiments than photo-oxidation experiments. One of the contributing factors to observed differences was due to the presence of NO_x during photo-oxidation experiments. Factors influencing the formation of organic peroxides during ozonolysis experiments were not investigated in great detail during this project. However, it is beneficial to understand what influences organic peroxide formation since it can be an important oxidizer of SO_2 when H_2O_2 is limited in the atmosphere and its role as a reservoir for odd-hydrogen radicals in the atmosphere (Lee et al., 2000). Prospective experiments can explore how changes to experimental conditions such as relative humidity, precursor and oxidant

concentration and NO_x chemistry affects the formation of organic peroxides during smog chamber studies. Findings from this study and atmospheric literature can be utilized to investigate changes to organic peroxide formation (Baker et al., 2000, Docherty et al., 2005, and Reinnig et al., 2008 and 2009). For instance changes to ion signals pertaining to organic hydroperoxides can be monitored in real time using SRM analysis mode of the (+) APCI-MS/MS. Ion-pairs formed due to unique mass losses of 34 u for organic hydroperoxides and peroxy acids can be monitored as changes to experimental conditions are implemented.

9.1.2. Quantitative Analysis

This project showed that selective detection for organic peroxides containing a hydroperoxy functional could be achieved. However, this type of analysis is qualitative and does not provide insight on the concentration of organic peroxides formed inside the smog chamber during β-pinene/ozonolysis experiments. Quantitative analyses were attempted by generating a calibration curve using commercially available organic peroxide standards. However, linear data could not be obtained. Previous (+) APCI-MS/MS calibration studies performed by Dobrusin (2012) indicated that linear calibration curves could be obtained by accounting for changes in the proton ion signal (m/z 37 and m/z 55) and plotting a relative signal rather than the raw ion count (IC) signal (Equation 9.1).

$$\frac{IC_{[M+H]^+}}{IC_{m/z\ 37} + IC_{m/z\ 55}} \qquad \text{Equation 9.1}$$

However, linear signal versus concentration relationships could still not be obtained. This was due to an unknown sampling problem during standard addition. Future experiments are required

to determine the nature of the sampling problem. Overall, a more effective method to obtain calibration curves for quantitative and sensitivity analysis needs to be explored.

Additionally, there were no suitable organic peroxide standards to assist in the quantification of formed organic peroxides during ozonolysis experiments. This was due to resultant ozonolysis products having more complex structures. The commercially available organic peroxide standards used in this study could not be used as a surrogate since it was highly unlikely to have the same sensitivity in the (+) APCI-MS/MS as organic peroxide structures formed during smog chamber studies. Therefore, future quantitation studies would require synthesizing standards that represent organic peroxides formed during smog chamber studies. Synthesized standards would have to be purified and standardized to determine the concentration organic peroxides formed during smog chamber studies.

9.1.3. Analysis of Higher Molecular Weight Products

During this study, the formation of higher molecular weight species (m/z values greater than 200) was apparent in full scan mass spectra for β-pinene ozonolysis experiments. High-range m/z values tend to correspond to the formation of dimers and higher order oligomers (Heaton et al. 2007) in the sample or produced in the ion source. Moreover, these ion signals are of great interest since Heaton et al., (2007) and Yasmeen et al., (2010) proposed that higher molecular weight organics are great candidates for particle nucleation during monoterpene ozonolysis experiments. Although these ion signals were not thoroughly investigated, brief analysis revealed that these ion signals were not apparent during NLS analysis for 18, 32, 34, 46 and 62 u mass losses. This indicated that losses of H_2O, H_2O_2, $C(O)OH$, and $C(O)OOH$ were not

dominant. During MS/MS experiments the resultant product-ion mass spectra were dominated by mid-range m/z values (m/z values between 100 and 200 u). For example, the product-ion mass spectra for m/z 277 and 291 revealed m/z 139 as the dominant fragment ion. It appeared that these larger m/z ions were fragmenting almost in half producing smaller mid-size fragment ions. Since this study was limited to organic compounds exhibiting smaller mass losses such as CO, O_2, H_2O, H_2O_2, etc., the identity of these higher-range m/z ions were not determined.

However, it has been suggested that organic peroxides can react further with other products to form higher molecular weight organics (dimers and oligomers) (Docherty et al., 2005, Heaton et al., 2007, Reinnig et al., 2009 and DePalma et al., 2013). Products formed through further reactions of organic peroxides include peroxy hemiacetals, peroxide esters, and secondary ozonides (Heaton et al., 2007 and Reinnig et al., 2009). A summary of how these higher molecular weight compounds are formed is shown in Figure 9.1. Essentially, dimers are formed between either a hydroperoxide or stabilized criegee intermediated (SCI) and a second species (Heaton et al., 2007). Formed products like peroxy hemiacetal in aerosol mass have been observed by Docherty et al., (2005) during ozonolysis experiments with 1-tetradecane. Heaton et al., (2007) suggested that peroxy hemiacetals and peroxide esters might break in the middle of the compound to form mid-range m/z values. Given this notion, it is possible that the higher-range m/z values observed in this study could represent the formation of these compounds. However, given the high pressure conditions in the ion source of the APCI-MS/MS, it is possible to form dimers. As a result, it is not possible to attribute any dimer or higher molecular weight oligomer formation to reactions occurring inside the smog chamber. Therefore, future investigation of these compounds would require utilizing a mass spectrometer where the ionization process is achieved at lower pressures.
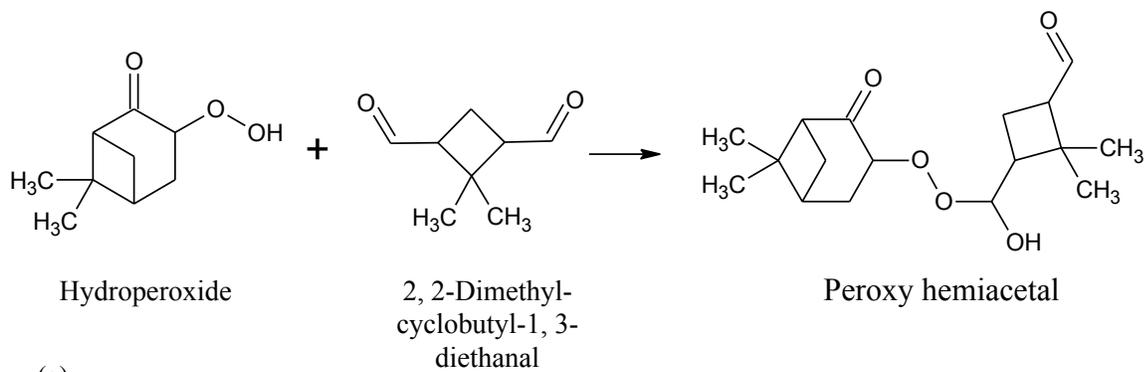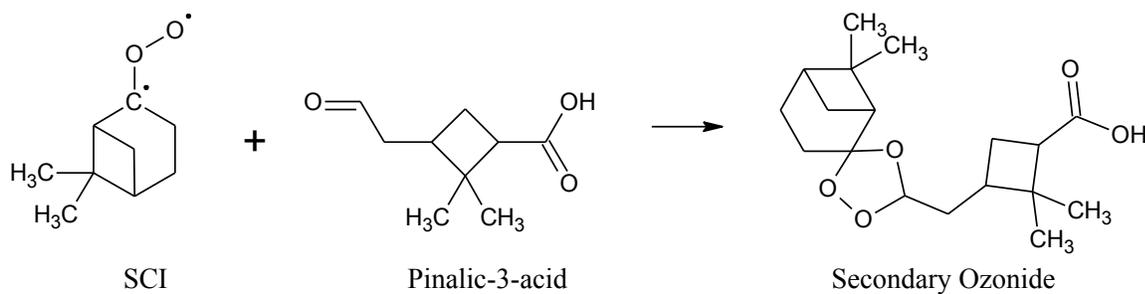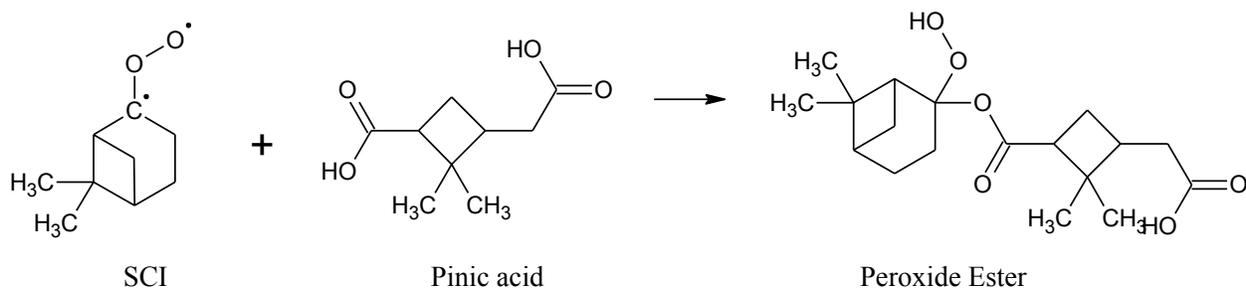
Figure 9.1: Example reaction mechanism for higher molecular weight formation adopted from Heaton et al., (2007)

Appendix A. Mass Filter Equations of Motion and Stability Diagram

The equations used to describe gas-phase ions motion inside a quadrupole fields is taken from Miller and Denton (1986). Within the quadrupole structure is a time-dependent electric field defined by the potential applied to the quadrupoles. The strength of this electric field is calculated by taking the partial derivative of the potential, Φ, as shown in Equations A.1 to A.3.

$$E_x = -\frac{\partial \Phi}{\partial x} = -[U + VCos(\omega t))]\frac{x}{r_0^2}$$ Equation A.1

$$E_y = -\frac{\partial \Phi}{\partial y} = [U + VCos(\omega t))]\frac{y}{r_0^2}$$ Equation A.2

$$E_z = -\frac{\partial \Phi}{\partial z} = 0$$ Equation A.3

Where

Φ = potential

U = magnitude of applied DC potential

V = magnitude of applied RF potential

ω = angular frequency of RF potential

t = time

x and y = distance along the axes

r_0 = distance of rods from z-axis

Using Newton's law of motion ($F = ma$), the force experienced by a gas-phase ion is given by Equation A.4 to A.6.

$$\frac{d^2x}{dt^2} + \frac{ex}{mr_0^2}[U + Vcos(\omega t)] = 0$$
Equation A.4

$$\frac{d^2y}{dt^2} - \frac{ey}{mr_0^2}[U + Vcos(\omega t)] = 0$$
Equation A.5

$$\frac{d^2z}{dt^2} = 0$$
Equation A.6

Where

e = electron charge (1.6×10^{-19} C)

m = mass of ion

Equation A.4 and A.5 can rewritten by defining a and q parameters as shown in Equation A.7 and A.8 to produce Equation A.9 and A.10. Note the separation of potentials in Equations A.7 and A.8, a is related to the DC potential while q is related to the RF potential.

$$a_u = a_x = -a_y = \frac{4eU}{m\omega^2 r_0^2}$$
Equation A.7

$$q_u = q_x = -q_y = \frac{2eV}{m\omega^2 r_0^2}$$
Equation A.8

$$\frac{d^2x}{dt^2} + \frac{\omega^2}{4}[a + 2qCos(\omega t))]x = 0$$
Equation A.9

$$\frac{d^2y}{dt^2} - \frac{\omega^2}{4}[a + 2qCos(\omega t))]y = 0$$
Equation A.10

Solutions of the differential equations will depend on the values of a and q. These values will determine whether a gas-phase ion trajectory is stable (bounded solution) or unstable (unbounded solution). Stability diagrams shown in Figure A.1 are created by plotting values of a and q to show regions of stability and instability. Overlaying the two stability diagrams in Figure A.1 generates Figure A.2.

(a)   (b)
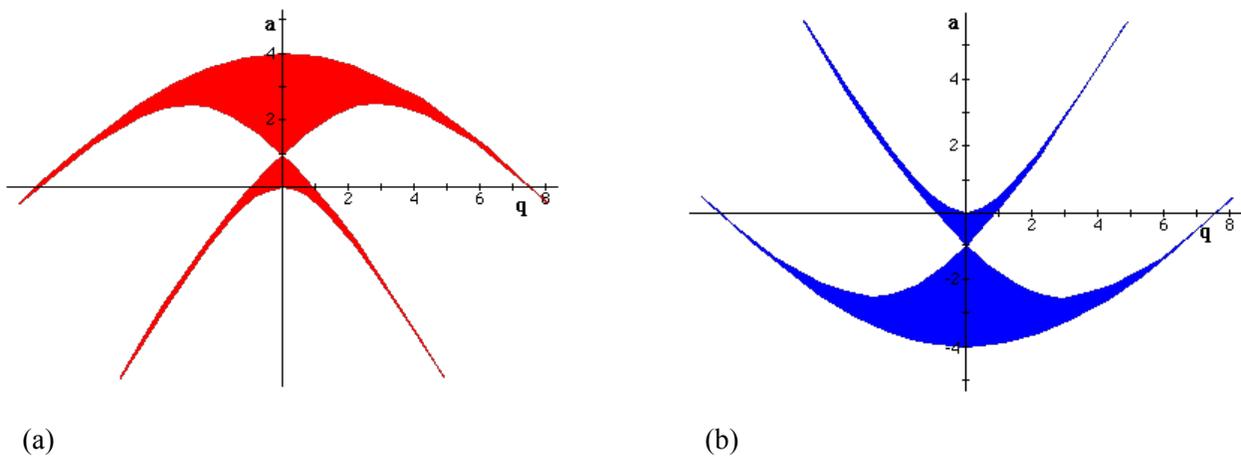
Figure A.1: Stability diagrams showing values of a and q that result in stable or unstable solutions for Equations A.9 and A.10. (a) Represents stability in the x-direction while (b) represents ion stability in the y-direction. The areas that are shaded indicate regions of stability. Figure was adopted from University of Richmond (1998).
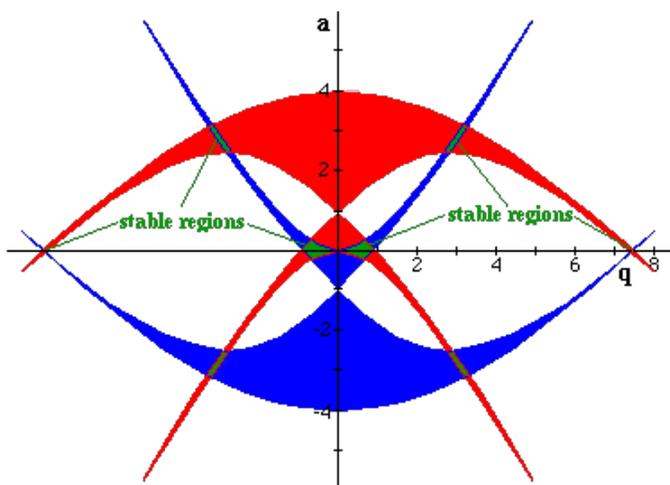
Figure A.2: Overlay of the two stability diagrams illustrated in Figure A.1. The regions that overlap indicate values of *a* and *q* where there are stable solutions in both x- and y-direction. In these regions (shown in green), an ion can travel through the mass analyzers without making contact with the quadrupoles. Figure was adopted from University of Richmond (1998).

Appendix B. Collisions in Tandem Mass Spectrometry

Potential Energy and Kinetic Energy

Gas-phase ions are accelerated into q_2 (collision cell) by a potential difference between Q_1 and q_2. As a result, the ions gain kinetic energy as given by Equation B.1

$$\frac{1}{2}mv^2 = zeV$$

Equation B.1

m = mass of ion

v = ion velocity

z = number of charges on ion

e = electron charge (1.6 x 10^{-19} C)

V = accelerating potential

Collision Events in q_2

Collisions between a gas-phase ion and an inert gas are inelastic since a portion of the kinetic energy is converted to internal energy. Collision events are visualized and modelled using a center of mass (CM) reference frame (Douglas 1998). Equation B.2 describes the amount of kinetic energy that can be converted to internal energy (E_{CM}).

$$E_{CM} = E_{lab}\left(\frac{m_c}{m_c + m_i}\right)$$

Equation B.2

E_{CM} = Amount of energy converted to internal energy

E_{lab} = kinetic energy of precursor ion

m_c = mass of inert gas

m_i = mass of precursor ion

By visual inspection of Equation B.2, increasing the amount of internal energy to drive precursor-ion decomposition can be caused by increasing E_{lab}. Since E_{lab} is the kinetic energy of the precursor-ion, increasing or decreasing the collision energy (CE) setting of the APCI-MS/MS can change the value of E_{lab}.

Appendix C. Equations for Calculating Maximum Syringe Pump Output

Vapour Pressure Calculations

Parameters

Temperature = (T + 273.15 K)

Gas Constant = 0.0821 L atm mol^{-1} K^{-1}

Vapour Pressure of Methanol = 0.167 atm (at 25°C)

Vapour Pressure of Water = 0.0313 atm (at 25°)

$$Concentration\ (M) = \frac{Pressure\ (atm)}{(T + 273.15\ K)(0.0821\ L\ atm\ mol^{-1}\ K^{-1})}$$

Vapour Pressure Syringe Pump Limit

Parameters

Molecular weight of methanol = 32.04 g mol^{-1}

Molecular weight of water = 18.015 g mol^{-1}

Density (ρ) of methanol (at 25°C) = 0.7915 g mL^{-1}

Density (ρ) of water (at 25°C) = 0.9973 g mL^{-1}

$$[Solvent]\ (mol\ min^{-1}) = \frac{Syringe\ pump\ flow\ (mL\ min^{-1})\ x\ \rho(g\ mL^{-1})}{Molecular\ Weight\ (\ g\ mol^{-1})}$$

$$[Solvent]\ (M) = \frac{[Solvent](mol\ min^{-1})}{Purified\ airflow\ (L\ min^{-1})}$$

If the [Solvent](M) is less than the calculated concentration based on vapour pressure, then there are no liquid droplets forming in the ion source.

Appendix D. Operating Parameters for (+) APCI-MS/MS

Table D.1: Summary of the APCI-MS/MS General Operating Parameters for Various MS/MS modes

Analysis Mode	Needle Current (kV)	De-clustering Potential (V)	Curtain Gas	Collision Energy (V)	Acquisition time (minutes)
Full scan	+ 2	10	8	-	30
Product-ion scan	+ 2	10	8	5 to 30	10
Neutral-loss scan	+ 2	10	8	5 to 30	10
Single reaction monitoring	+ 2	10	8	5 to 30	30

During this project, the APCI-MS/MS was set to unit resolution. This allowed for a mass resolution of +/- 0.1 u.

Appendix E. Calculations for β-pinene Ozonolysis Experiments

Parameters Used

Temperature: 273.15 K

Pressure: 1 atm

Chamber volume ($V_{chamber}$) : 8000 L

Gas constant (R): 0.0821 L atm mol^{-1} K^{-1}

Avogadro's number (AN): 6.022 x 10^{23} molecules mol^{-1}

Beta pinene molar mass: 136.23 g mol^{-1}

Beta pinene density ($\rho_{Beta-pinene}$) = 0.87 g cm^{-3}

Desired beta pinene concentration = 0.4 ppm

Number density of air (N_{air}) (molecules cm^{-3})

$$N_{air} = \frac{P}{R\,T} \times 10^{-3} \times AN$$

Number density of Beta pinene ($N_{Beta\ pinene}$) (molecules cm^{-3})

$$N_{Beta\ pinene} = 0.4 \times N_{air} \times 10^{-6}$$

Volume to inject ($V_{Beta\ pinene}$) (mL)

$$V_{Beta\ pinene} = N_{Beta\ pinene} \times V_{chamber} \times \frac{1}{AN} \times molar\ mass \times \frac{1}{\rho} \times 10^{3}$$

Ozone Generator Operating Parameters and Ozone Concentration Calculation

Volume of the Chamber ($V_{chamber}$) = 8000 L

Air flow (F): 10 standard cubic feet per hour (SCFH)

0.472195 L min^{-1} = 1 SCFH

Percent output (O): 25 %

O_3 efficiency at 100% output (E_{100}): 3%

$$Actual\ output\ of\ O_3\ (O_{actual}) = \frac{E_{100}}{100} \times O$$

$$Volume\ Required\ for\ 1\ ppm\ O_3\ (V_{req}) = V_{chamber} \times 10^6$$

$$F_{L/min} = F \times 0.472195\ L\ min^{-1}$$

$$Ozone\ generator\ operation\ time = \frac{1}{F_{L/min}} \times \frac{100}{O_{actual}} \times V_{req}$$

Appendix F. Summary of Experimental Conditions for Smog Chamber Studies

Table F.1: Smog Chamber Experimental Conditions

Experiment Date (M/D/Y)	Ozone Concentration (ppm)	β-Pinene Concentration[a] (ppm)	Relative humidity (%)	Temperature °C
01/30/14	1.2	0.4	0.3	25.9
02/05/14	1.1	0.4	0.4	25.9
02/08/14	0.9	0.4	1.4	25.0
02/13/14	5.6[b]	0.4	1.7	25.8
02/21/14	1.3	0.4	1.6	25.4

[a] Concentration of β-pinene was based on the amount injected into the chamber

[b] Ozone generator operated beyond calculated time for desired ozone concentration. However, results were still deemed valid since smog chamber results were only used for qualitative purposes.

Appendix G. Postulated Mechanism for β-pinene Ozonolysis
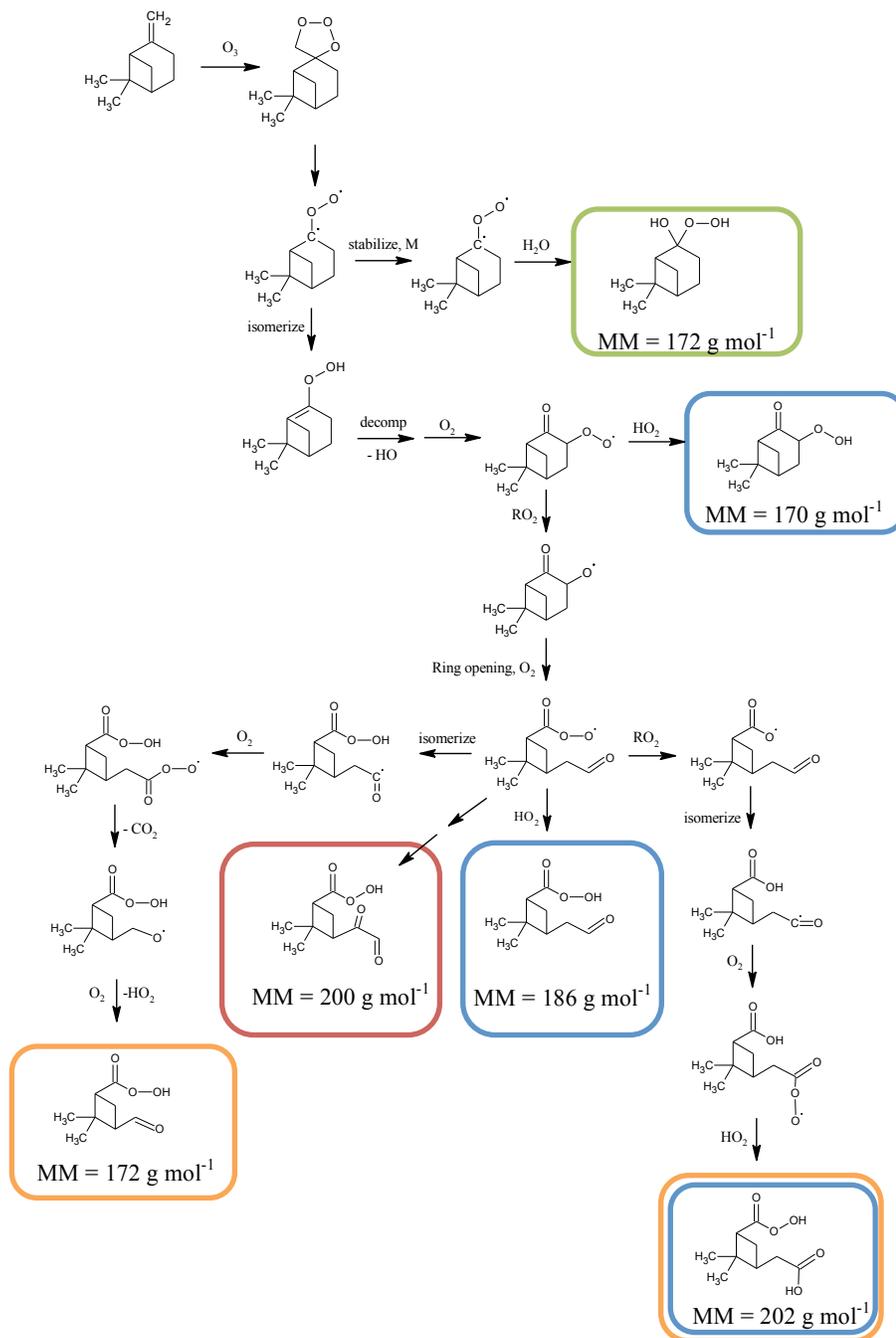
Figure G.1: Portrayed mechanism was adopted from Jenkin et al., 2004, Docherty et al., 2005, and Reinning et al., 2009. Products outlined in green were proposed by Jenkin et al., 2004. Products outlined in blue and orange were proposed and rationalized by Docherty et al., 2005 and Reinnig et al., 2009, respectively. Lastly, Reinnig et al., 2009, proposed products outlined in red however; its formation mechanism could not be ascertained. The acronym MM represents molar mass.

References

Amad, M.H., Cech, N.B., Jackson, G.S., and Enke, C.G. (2000). Importance of gas-phase proton affinities in determining the electrospray ionization response for analytes and solvents. *Journal of Mass Spectrometry, 35, 784 – 789*.

Auld, J. (2009). A smog chamber study of mechanisms for beta-pinene oxidation by hydroxy radicals. Ph.D., York University.

Baker, J., Aschmann, S.M., Arey, J., and Atkinson, R. (2002). Reactions of stabilized criegee intermediates from the gas-phase reactions of O_3 with selected alkenes. *Journal of Chemical Kinetics, 34, 73 – 85*. Doi: 10.1002/kin.10022.

Bernstein, E.R. *Chemical reactions in clusters*. (1996). New York: Oxford University Press.

Bouchoux, G. (2007). Gas-phase basicities of polyfunctional molecules. Part 1: Theory and Methods. *Mass Spectrometry Review, 26, 775 – 835*.

Crounse, J.D. McKinney, K.A., Kwan, A.J., Wennberg, P.O. (2006). Measurement of gas-phase hydroperoxides by chemical ionization mass spectrometry. *Analytical Chemistry, 78, 6726 – 6732*.

de Hoffmann. (1996). Tandem mass spectrometry: a primer. *Journal of Mass Spectrometry, 3, 129 – 137*.

de Hoffmann, E. and Stroobant, V. (2007). *Mass spectrometry: Principles and applications* (3rd ed). West Sussex, England: John Wiley and Sons Ltd.

DePalma, J.W., Horan, A.J., Hall, W.A., and Johnston, M.V. (2013). Thermodynamics of oligomer formation: implications for secondary organic aerosols formation and reactivity. *Physical Chemistry Chemical Physics, 15, 6935 – 6944*.

Dobrusin, Z. (2012). Quantitative methods for the analysis of hydrocarbon oxidation products: A smog chamber study. M Sc., York University.

Docherty, K.S., Wu, W., Lim, Y.B., and Ziemann, P.J. (2005). Contributions of organic peroxides to secondary organic aerosols formed from reactions of monoterpenes with O_3. *Environmental Science and Technology, 39, 4049 – 4059.*

Douglas, D.J. (1998). Application of collision dynamics in quadrupole mass spectrometry. *Journal of the American Society for Mass Spectrometry, 9, 101 – 113*. Doi: 10.1016/S1044-0305(97)00246-8

Dron, J., Eyglunent, G., Temime-Roussel, B., Marchand, N., and Wortham, H. (2007). Carboxylic acid functional group analysis using constant neutral loss scanning-mass spectrometry. *Journal of Analytica Chimica Acta, 605, 61 – 69*. Doi: 10.1016/j.aca.2007.10.020

Finlayson-Pitts, B. and Pitts Jr., J.N. (1999). *Upper and lower atmosphere*. San Diego, California: Academic Press.

Hastie, D.R., Gray, J., Langford, V.S., Maclagan, R., Milligan, D.B., and McEwan, M.J. (2010). Real-time measurement of peroxyacetyl nitrate using selected ion flow tube mass spectrometry. *Journal of Rapid Communications in Mass Spectrometry, 24, 343 – 348*. Doi: 10.1002/rcm.4400.

Hatakeyama, S., Lai, H., and Murano, K. (1995). Formation of 2-hydroxyethyl hydroperoxide in an OH-initiated reaction of ethylene in air in the absence of NO. *Environmental Science and Technology, 29, 833 – 835.*

Heaton, K.J., Dreyfus, M.A., Wang, S., and Johnston, M.V. (2007). Oligomers in the early stage of biogenic secondary organic aerosol formation and growth. *Environmental Science and Technology, 41, 6129 – 6136.*

Hellpointer,E. and Gab, S. (1989). Detection of methyl, hydroxymethyl and hydroxyethyl hydroperoxides in air and precipitation. *Nature, 337, 631 – 634.*

Hunter, E.P.L. and Lias, S.G. Evaluated gas-phase basicities and proton affinities of molecules.: An update. (1998). *Journal of Physical and Chemical Reference Data, 27, 413 - 656.*

Jacob, P. (1999). *Introduction to atmospheric chemistry*. Princeton, New Jersey: Princeton University Press.

Jacob, P. and Klockow, D. (1992). Hydrogen peroxide measurements in the marine atmosphere. *Journal of Atmospheric Chemistry, 15, 353 – 360.*

Jenkin, M.E. (2004). Modelling the formation and composition of secondary organic aerosol from α- and β- pinene ozonolysis using MCM v3. *Journal of Atmospheric Chemistry and Physics, 4, 1741 – 1757*

Jenkin, M.E., Shallcross, D.E., and Harvey, J.N. (2000). Development and application of a possible mechanism of cis-pinic acid from the ozonolysis of α- and β- pinene. *Atmospheric Environment, 34, 2837 – 2850.*

Kawai, Y., Yamaguchi, S., Okada, Y., Takeuchi, K., Yamuchi, Y., Ozawa, S., and Nakai, H. (2003). Reactions of protonated water clusters $H^+(H_2O)_n$ (n= 1-6) with dimethylsulfoxide in a guided ion beam apparatus. *Journal of Chemistry and Physics Letters, 377, 69 – 73.*

Kok, G.L., Holler, T.P., Lopez, M.L., Nachtrieb, H.A., and Yuan, M. (1978). Chemiluminescent method for determination of hydrogen peroxide in the ambient atmosphere. *Environmental Science and Technology, 12, 1077 – 1080.*

Kok, G.L., McLaren, S.E., and Staffelbach, T.A. (1994). HPLC determination of atmospheric organic hydroperoxides. *Journal of Atmospheric and Oceanic Technology, 12, 282 – 289.*

Kroll, H.J. and Seinfeld J.H. (2008). Chemistry of secondary organic aerosol: Formation and evolution of low-volatility organics in the atmosphere. *Journal of Atmospheric Environment, 42, 3593 – 3624.* Doi: 10.1016/j.atmosenv.2008.01.003.

Lazrus, A.L., Kok, G.L., Lind, J.A., Gitlin, S.N., Heikes, B.G., and Shetter, R.E. (1986). Automated fluorometric method for hydrogen peroxide in air. *Analytical Chemistry, 58, 594 – 597.*

Lee, A., Goldstein, A.H., Keywood, M.D., Gao, S., Varuntida, V., Bahreini, R., Ng, N.L., Flagan, R.C., and Seinfeld, J.H. (2006). Gas-phase products and secondary aerosol yields from the ozonolysis of ten different terpenes. *Journal of Geophysical Research, 111, DO7302.* Doi: 10.1029/2005JD006437.

Lee, M., Heikes, B.G., and O'Sullivan, D.W. (2000). Hydrogen peroxide and organic hydroperoxide in the troposphere: a review. *Atmospheric Environment, 34, 3475 – 3494.*

Mackay, G.I., Mayne, L.K., and Schiff, H.I. (1990). Measurement of H_2O_2 and HCHO by tunable diode laser absorption spectroscopy during 1986 carbonaceous species methods comparison study in Glendora, California. *Journal of Aerosol Science and Technology, 12, 56 – 63.*

Miller, P.E. and Denton, M.B. (1986). The quadrupole mass filter: Basic operating concepts. *Journal of Chemical Education, 63, 617 – 622.*

Proctor, C.J. and Todd, F.J. (1983). Atmospheric pressure ionization mass spectrometry. *Organic Mass Spectrometry, 18, 509 – 516.*

Purcell, T.C. and Cohen, I.R. (1967). Microdetermination of peroxides by kinetic colorimetry. *Environmental Science and Technology, 5, 431 – 433*. Doi: 0.1021/es60005a010

Reeves, C.E. and Penkett, S.A. (2003). Measurements of peroxides and what they tell us. *Chemistry Review, 103, 5199 – 5218*. Doi: 10.1021/cr0205053.

Reinning, M.C., Warnke, J., and Hoffmann, T. (2009). Identification of organic hydroperoxides and hydroperoxy acids in secondary organic aerosols formed during the ozonolysis of different monoterpenes and sesquiterpenes by on-line analysis using atmospheric pressure chemical ionization ion trap mass spectrometry. *Journal of Rapid Communications in Mass Spectrometry, 23, 1735 – 1741*. Doi: 10.1002/rcm.4065.

Reinning, M.C., Muller, L., Warnke, J., and Hoffmann, T. (2008). Characterization of selected organic compound classes in secondary organic aerosol from biogenic VOCs by HPLC/MS[n]. *Journal of Analytical and Bioanalytical Chemistry, 391, 171 – 182*. Doi: 10.1007/s00216-008-1964-5.

Rondeau, D., Vogel, R., and Tabet, J.C. (2003). Unusual atmospheric pressure chemical ionization conditions for detection of organic peroxides. *Journal of Mass Spectrometry, 38, 931 – 940.* Doi: 10.1002/jms.501.

Sarrafzadeh, M. (2012). A chamber study of the aging of reaction products formed by photo-oxidation of beta-pinene. Ph.D. Annual Research Evaluation Report., York University.

University of Richmond. (1998). *Equations of motion in a QMA*. Retrieved September 24, 2014, from
http://chemistry.clemson.edu/chemdocs/marcusgroup/software/CONCEPT/QMA/fma/fmaqma/fmaqma.htm

Watson, J.T. and Sparkman, O.D. (2007). *Introduction to mass spectrometry* (4th ed). West Sussex, England: Wiley.

Warscheid, B. and Hoffmann, T. (2002). Direct analysis of highly oxidized organic aerosol constituents by on-line ion trap mass spectrometry in the negative-ion mode. *Rapid Communications in Mass Spectrometry, 16, 496 – 504*. Doi: 10.1002/rcm.602.

Williams, T.T.J and Perreault, H. (2000). Selective detection of nitrated polycyclic aromatic hydrocarbons by electrospray ionization mass spectrometry and constant neutral loss scanning. *Rapid Communication in Mass Spectrometry, 14, 1474 – 1481.*

Yasmeen, F., Vermeylen, R., Szmigielski, R., Iinuma, Y., Böge, O., Herrmann, H., Maenhaut, W., and Claeys, M. (2010). Terpenylic acid and related compounds: precursor for dimers in secondary organic aerosol from the ozonolysis of α- and β-pinene. *Atmospheric Chemistry and Physics, 10, 9383 – 9392*. Doi: 10.519/acp-10-9383-2010.

Yu, J., Cocker III, D.R., Griffin, R.J., Flagan, R.C., and Seinfeld, J.H. (1999). Gas-phase ozone oxidation of monoterpenes: Gaseous and particulate products. *Journal of Atmospheric Chemistry, 34, 207 – 258.*